34355

National Library of Canada
Bibliothèque nationale du Canada

CANADIAN THESES ON MICROFICHE

THÈSES CANADIENNES SUR MICROFICHE

NAME OF AUTHOR/*NOM DE L'AUTEUR* BARRY CAMERON GREEN

TITLE OF THESIS/*TITRE DE LA THÈSE* An Investigation of Thermal Fields and Secondary Circulations in the Canadian Western Arctic

UNIVERSITY/*UNIVERSITÉ* Alberta

DEGREE FOR WHICH THESIS WAS PRESENTED/*GRADE POUR LEQUEL CETTE THÈSE FUT PRÉSENTÉE* M. Sc.

YEAR THIS DEGREE CONFERRED/*ANNÉE D'OBTENTION DE CE GRADE* 1977

NAME OF SUPERVISOR/*NOM DU DIRECTEUR DE THÈSE* Dr. E. R. Reinelt

Permission is hereby granted to the NATIONAL LIBRARY OF CANADA to microfilm this thesis and to lend or sell copies of the film.

The author reserves other publication rights, and neither the thesis nor extensive extracts from it may be printed or otherwise reproduced without the author's written permission.

L'autorisation est, par la présente, accordée à la BIBLIOTHÈQUE NATIONALE DU CANADA de microfilmer cette thèse et de prêter ou de vendre des exemplaires du film.

L'auteur se réserve les autres droits de publication; ni la thèse ni de longs extraits de celle-ci ne doivent être imprimés ou autrement reproduits sans l'autorisation écrite de l'auteur.

DATED/*DATÉ* October 12/77 SIGNED/*SIGNÉ* Barry Green

PERMANENT ADDRESS/*RÉSIDENCE FIXE*
211 - 10127 - 121 ST
Edmonton, Alberta
T5N 3X1

NL-91 (3-74)

National Library of Canada

Cataloguing Branch
Canadian Theses Division

Ottawa, Canada
K1A 0N4

NOTICE

The quality of this microfiche is heavily dependent upon the quality of the original thesis submitted for microfilming. Every effort has been made to ensure the highest quality of reproduction possible.

If pages are missing, contact the university which granted the degree.

Some pages may have indistinct print especially if the original pages were typed with a poor typewriter ribbon or if the university sent us a poor photocopy.

Previously copyrighted materials (journal articles, published tests, etc.) are not filmed.

Reproduction in full or in part of this film is governed by the Canadian Copyright Act, R.S.C. 1970, c. C-30. Please read the authorization forms which accompany this thesis.

THIS DISSERTATION
HAS BEEN MICROFILMED
EXACTLY AS RECEIVED

Bibliothèque nationale du Canada

Direction du catalogage
Division des thèses canadiennes

AVIS

La qualité de cette microfiche dépend grandement de la qualité de la thèse soumise au microfilmage. Nous avons tout fait pour assurer une qualité supérieure de reproduction.

S'il manque des pages, veuillez communiquer avec l'université qui a conféré le grade.

La qualité d'impression de certaines pages peut laisser à désirer, surtout si les pages originales ont été dactylographiées à l'aide d'un ruban usé ou si l'université nous a fait parvenir une photocopie de mauvaise qualité.

Les documents qui font déjà l'objet d'un droit d'auteur (articles de revue, examens publiés, etc.) ne sont pas microfilmés.

La reproduction, même partielle, de ce microfilm est soumise à la Loi canadienne sur le droit d'auteur, SRC 1970, c. C-30. Veuillez prendre connaissance des formules d'autorisation qui accompagnent cette thèse.

LA THÈSE A ÉTÉ
MICROFILMÉE TELLE QUE
NOUS L'AVONS REÇUE

NL-339 (3/77)

THE UNIVERSITY OF ALBERTA

AN INVESTIGATION OF THERMAL FIELDS AND SECONDARY CIRCULATIONS IN THE CANADIAN WESTERN ARCTIC

by

© BARRY CAMERON GREEN

A THESIS

SUBMITTED TO THE FACULTY OF GRADUATE STUDIES AND RESEARCH

IN PARTIAL FULFILMENT OF THE REQUIREMENTS FOR THE DEGREE

OF MASTER OF SCIENCE

IN

METEOROLOGY

DEPARTMENT OF GEOGRAPHY

EDMONTON, ALBERTA

FALL, 1977

THE UNIVERSITY OF ALBERTA

FACULTY OF GRADUATE STUDIES AND RESEARCH

The undersigned certify that they have read, and recommend to the Faculty of Graduate Studies and Research, for acceptance, a thesis entitled "An Investigation of Thermal Fields and Secondary Circulations in the Canadian Western Arctic", submitted by Barry Cameron Green in partial fulfilment of the requirements for the degree of Master of Science in Meteorology.

E R Reinelt

Supervisor

Keith D. Hage

Keith [illegible]

Date 4 October 1977

DEDICATION

To my Mother and Father,
whose love and support have made
everything possible

ABSTRACT

APT satellite imagery in the infra-red (IR) is used to investigate the thermal characteristics of the lower levels of the atmosphere in the Western Arctic contiguous to the Beaufort Sea. A complex temperature structure is shown to exist at the surface which gives rise to a variety of meteorological phenomena in summer, such as the rapid development of small synoptic-scale depressions in the southern shallows of the Beaufort Sea, inversions, and local circulations of the Arctic islands.

A summary of synoptic-scale circulation patterns in summer is provided. The mean circulation is described on the basis of climatological data collected by investigators in the 1950's. Mean-sea-level pressure maps and 500-mb charts are used to summarize the synoptic-scale circulation for the months of July and August, 1976, when predominantly high pressure existed over the Beaufort Sea.

A brief survey is included of inversions observed in July, August and September, 1976, at five stations in the Western Arctic. Inversions between the surface and the 700-mb level are classified according to their intensity. Inversion conditions existed nearly 100 percent of the time at Point Barrow and other stations adjacent to the Beaufort Sea. The inversions observed at the coastal stations were generally intense and much more persistent than at inland stations.

A qualitative assessment of the low level thermal field in the study area was carried out by means of image enhancement and slicing. The gray-shade display of IR images so obtained were used to provide quick overviews of synoptic conditions. The limiting factor in gray-scale displays is the inability of the eye to distinguish between more than about six or seven shades of gray.

A second, more quantitative approach made use of the IR data in digitized form. The digital data were processed by means of a modified version of the algorithm introduced by Madden and Parsons (1973). The IR data are arranged in scan lines with a superimposed grid of latitude and longitude lines.

An isotherm analysis of the data yielded realistic representations of the strong baroclinic zones between the land masses and the large bodies of water. However, little success was achieved detecting inversions with the satellite imagery.

Three small, synoptic-scale depressions were observed to form over land near the northern Alaskan coast. In the course of some eighteen hours these disturbances first moved eastward, out over the Beaufort Sea, then tended to stall and drift northeastward, toward Banks Island. All three systems were shallow structures, confined almost certainly to levels below 700 mb. They seemed to derive support from the strong, but shallow baroclinic zone "bound" to the coast of the Beaufort Sea in summer. On crossing this zone, the systems underwent growth and intensification, followed by rapid decay a few hours later.

Various secondary circulations developed as a result of local circulations set up over the Arctic islands. The IR satellite imagery showed that Banks and Victoria islands in summer act as heat islands in a frigid sea. Convergence of air from the cool surrounding ice and water surface toward the interior of the heated islands occurred during the day. Evidence of this was provided by the presence of convective cloud over the islands. The existence of a sea breeze at Sachs Harbour on Banks Island also demonstrated the prevailing on-shore convergence.

The sources of the satellite data were the polar orbiting NOAA-4 and NOAA-5 spacecraft. Image processing was done by the APT Satellite Laboratory at the University of Alberta, Edmonton, Alberta.

ACKNOWLEDGEMENTS

I wish to express my sincere appreciation to my departmental supervisor, Professor Erhard R. Reinelt, for suggesting the topic of this study, for contributing his time and editorial skill, and for offering his most welcome advice and encouragement during the preparation of this work. I wish to thank the examining committee members, Professor Reinelt, Professor Keith D. Hage, and Professor K.W. Smillie, for reading the thesis and making helpful suggestions.

I am grateful to Mr. Peter Hof and the staff of the University of Alberta Satellite Laboratory for their ready assistance. Special thanks goes to Mr. Dennis Oracheski for sharing his invaluable knowledge of satellite operations and computing, and to Mr. Jerry Broszkowski for his work on gridding satellite imagery.

I am indebted to Laura Smith for her patience and expertise in typing the final draft. Many of the figures were produced with the aid of the technical staff of the Department of Geography to whom I am grateful.

This work was done while on educational leave from the Atmospheric Environment Service. I wish to acknowledge the cooperation I received from Mr. D. B. Fraser and his staff of the Arctic Weather Centre. I especially appreciate the assistance of Mr. W. Prusak and Mr. H. Turchanski of the climatology section.

TABLE OF CONTENTS

Page

DEDICATION iv

ABSTRACT v

ACKNOWLEDGEMENTS viii

TABLE OF CONTENTS ix

LIST OF TABLES xi

LIST OF FIGURES xii

CHAPTER

1 SOME ASPECTS OF SATELLITE METEOROLOGY APPLIED TO THE CANADIAN ARCTIC 1

1.1 Introduction 1

1.2 The Use of Satellite Imagery in Arctic Studies 2

2 A SUMMARY OF ARCTIC CIRCULATION IN SUMMER 14

2.1 Normal Circulation Patterns 14

2.2 Circulation Observed in the Summer of 1976 21

3 THE ARCTIC INVERSION 39

3.1 Introduction 39

CHAPTER Page

3.2 Climatology of the Arctic Inversion 41

3.3 Inversions Observed in Summer 1976 49

4 THE USE OF SATELLITE IMAGERY TO OBSERVE THE TEMPERATURE STRUCTURE NEAR THE EARTH''S SURFACE . . 58

4.1 Introduction 58

4.2 Temperature Structure in Gray Shades 59

4.3 Quantitative Analysis of the IR Imagery . . . 77

4.4 Temperature Structure from Quantitative Analysis of IR Imagery 84

5 SECONDARY AND TERTIARY CIRCULATIONS 92

5.1 Introduction 92

5.2 Three Case Studies Involving Small Synoptic-Scale Lows 93

5.3 Local Circulations Over Heated Islands . . . 111

6 SUMMARY AND CONCLUSIONS 121

6.1 Outline 121

6.2 Thermal Structure from IR Satellite Imagery 122

6.3 Secondary Circulations 123

6.4 Suggestions for Future Work 125

REFERENCES 126

APPENDIX A 129

APPENDIX B 133

APPENDIX C 159

LIST OF TABLES

Table		Page
3.1	Frequency of Occurrence of Inversion Classes in July	53
3.2	Frequency of Occurrence of Inversion Classes in August	54
3.3	Frequency of Occurrence of Inversion Classes in September	55
3.4	Overall Frequency of Occurrence of Inversion Classes 1, 2, or 3	56
5.1	July 12, 1976 Wind Record	117
A.1	Inversion Classes Observed during July, August and September, 1976	130
B.1	Listing of Computer Program	148
C.1	Wind Records for Arctic Stations	160

LIST OF FIGURES

Figure		Page
1.1	Map of Study Area	3
1.2	Visible Range Image July 14, 1976	5
1.3	IR Image July 14, 1976	6
1.4	Scanning Radiometer View of the Earth's Surface	7
2.1	July Mean Pressure Distribution	17
2.2	August Mean Pressure Distribution	18
2.3	September Mean Pressure Distribution	18
2.4	July-September Percentage Frequency of Cyclone Centres	19
2.5	June-August Percentage Frequency of Frontal Systems	20
2.6	500-mb Contours, 0000 GMT July 1, 1976	23
2.7	500-mb Contours, 0000 GMT July 5, 1976	23
2.8	Surface Map, 0000 GMT July 4, 1976	24
2.9	Surface Map, 0000 GMT July 9, 1976	24
2.10	Surface Map, 0000 GMT July 15, 1976	26
2.11	Surface Map, 0000 GMT July 23, 1976	26
2.12	500-mb Contours, 0000 GMT July 20, 1976	27
2.13	500-mb Contours, 0000 GMT July 27, 1976	27
2.14	500-mb Contours, 0000 GMT July 30, 1976	29
2.15	500-mb Contours, 0000 GMT August 1, 1976	29
2.16	500-mb Contours, 1200 GMT August 5, 1976	30

Figure		Page
2.17	Surface Map, 0000 GMT August 4, 1976	30
2.18	Surface Map, 0000 GMT August 9, 1976	31
2.19	500-mb Contours, 1200 GMT August 12, 1976	31
2.20	500-mb Contours, 1200 GMT August 16, 1976	33
2.21	500-mb Contours, 0000 GMT August 19, 1976	33
2.22	500-mb Contours, 0000 GMT August 23, 1976	34
2.23	Surface Map, 0000 GMT August 22, 1976	34
2.24	500-mb Contours, 0000 GMT August 28, 1976	36
2.25	Surface Map, 0000 GMT August 26, 1976	36
2.26	Surface Map, 0000 GMT August 28, 1976	37
2.27	Surface Map, 0000 GMT August 29, 1976	37
3.1	Types of Temperature Inversions	39
3.2	Frequency Distribution of Inversions	43
3.3	Area Distribution of the Frequency of Surface-based Inversions in Winter	44
3.4	Vertical Temperature Gradient Between the Surface and the 850-mb Level in Summer	45
3.5	Percentage Frequencies of Ground-based Inversions	46
3.6	Intensity of Surface-based Inversions	48
4.1	Tephigrams for 0000 GMT July 23, 1976	61
4.2	Visible-range Image July 22, 1976	63
4.3	IR Image July 22, 1976	64
4.4	Tephigrams for 0000 GMT August 15, 1976	67
4.5	Visible-range Image August 14, 1976	68
4.6	IR Image August 14, 1976	69
4.7	Tephigrams for 0000 GMT August 28, 1976	70

Figure Page
4.8 Visible-range Image August 27, 1976 71
4.9 IR Image August 27, 1976 72
4.10 Tephigrams for 0000 GMT August 29, 1976 73
4.11 Visible-range Image August 28, 1976 74
4.12 IR Image August 28, 1976 75
4.13 Computer Output from SRGRID-2 79
4.14 Temperature Calibration Curve for IR Signal 81
4.15 Isotherm Analysis for July 22, 1976 85
4.16 IR Image June 17, 1977 88
4.17 Isotherm Analysis of Banks Island and Surrounding Region June 17, 1977 89
4.18 Isotherm Analysis of Great Bear Lake Region and Victoria Island June 17, 1977 91
5.1 BAB Surface Map, 0900 GMT July 30, 1976 95
5.2 BAB Surface Map, 1200 GMT July 30, 1976 95
5.3 BAB Surface Map, 1800 GMT July 30, 1976 95
5.4 BAB Surface Map, 0000 GMT July 31, 1976 95
5.5 Visible Range Image July 30, 1976 97
5.6 IR Image July 30, 1976 98
5.7 BAB Surface Map, 0300 GMT August 16, 1976 101
5.8 BAB Surface Map, 0600 GMT August 16, 1976 101
5.9 BAB Surface Map, 1200 GMT August 16, 1976 101
5.10 BAB Surface Map, 1500 GMT August 16, 1976 101
5.11 BAB Surface Map, 2100 GMT August 16, 1976 102
5.12 BAB Surface Map, 0300 GMT August 17, 1976 102
5.13 Visible Range Image August 16, 1976 103
5.14 IR Image August 16, 1976 104

Figure		Page
5.15	BAB Surface Map, 1200 GMT August 18, 1976	106
5.16	BAB Surface Map, 1500 GMT August 18, 1976	106
5.17	BAB Surface Map, 1800 GMT August 18, 1976	106
5.18	BAB Surface Map, 2100 GMT August 18, 1976	106
5.19	Visible-range Image August 18, 1976	109
5.20	IR Image August 18, 1976	110
5.21	Map of Sachs Harbour Area	115
B.1	Inclination of Satellite in Polar Orbit	137
B.2	Geometry of Satellite Horizon	138
B.3	Westward Shift of Equator Crossings	141
B.4	Geometry of Trans-polar Orbit	143

CHAPTER 1

SOME ASPECTS OF SATELLITE METEOROLOGY APPLIED TO THE CANADIAN ARCTIC

1.1 Introduction

Recently, because of drilling programmes and proposed northern pipelines, a great deal of interest and concern has been expressed in the Arctic environment. From a meteorological viewpoint, a study of the Arctic offers a unique opportunity to observe situations which are encountered nowhere else in the world. Even in the warmest season of the year, when the Arctic is subjected to considerable insolation, permanent fields of snow and ice prevail against the ceaseless rays of the noon and midnight sun. This results in a contrasting and complicated thermal structure in the atmosphere, which has a profound influence on the weather of the Arctic Basin.

Until relatively recent times (post-World War II) little detailed knowledge of Arctic weather was available. Matters had improved somewhat by the early Fifties with the establishment of a small number of permanent weather reporting stations in the High Arctic. More recently still, since the launching of the first meteorological satellite TIROS I in April 1960, satellite imagery of the Arctic has become available in the infra-red (IR) and visible range of the spectrum, on a daily and routine basis.

This study makes use of APT (automatic picture transmission) satellite information, the IR data in particular, to investigate the thermal structure of the atmosphere in the Arctic and to suggest how some summer circulation patterns may be influenced by the observed temperature regimes. The investigation is restricted to the lower levels of the atmosphere, primarily below 700 mb (70 kPa), as far as detailed temperature analysis is concerned. The circulations which are examined include small, synoptic-scale and near mesoscale lows, thermal lows and seabreezes.

The geographical area of concern for this study is the Canadian Arctic contiguous to the Beaufort Sea, as shown in Figure 1.1. The case studies are based on surface and upper-air data for July, August and September 1976, obtained through the facilities of the Arctic Weather Centre in Edmonton, Alberta, and the Beaufort Advance Base at Tuktoyuktuk. The satellite imagery was received and processed by the University of Alberta Satellite Laboratory.

1.2 The Use of Satellite Imagery in Arctic Studies

Data collection by conventional weather stations located in remote, sparsely-populated regions such as the Arctic is always costly, and the economics of adequate coverage is such as to all but rule it out in practice. For this reason, satellite imagery provides a valuable, supplemental source of information. Satellite data from the Arctic are becoming more readily available with the establishment of

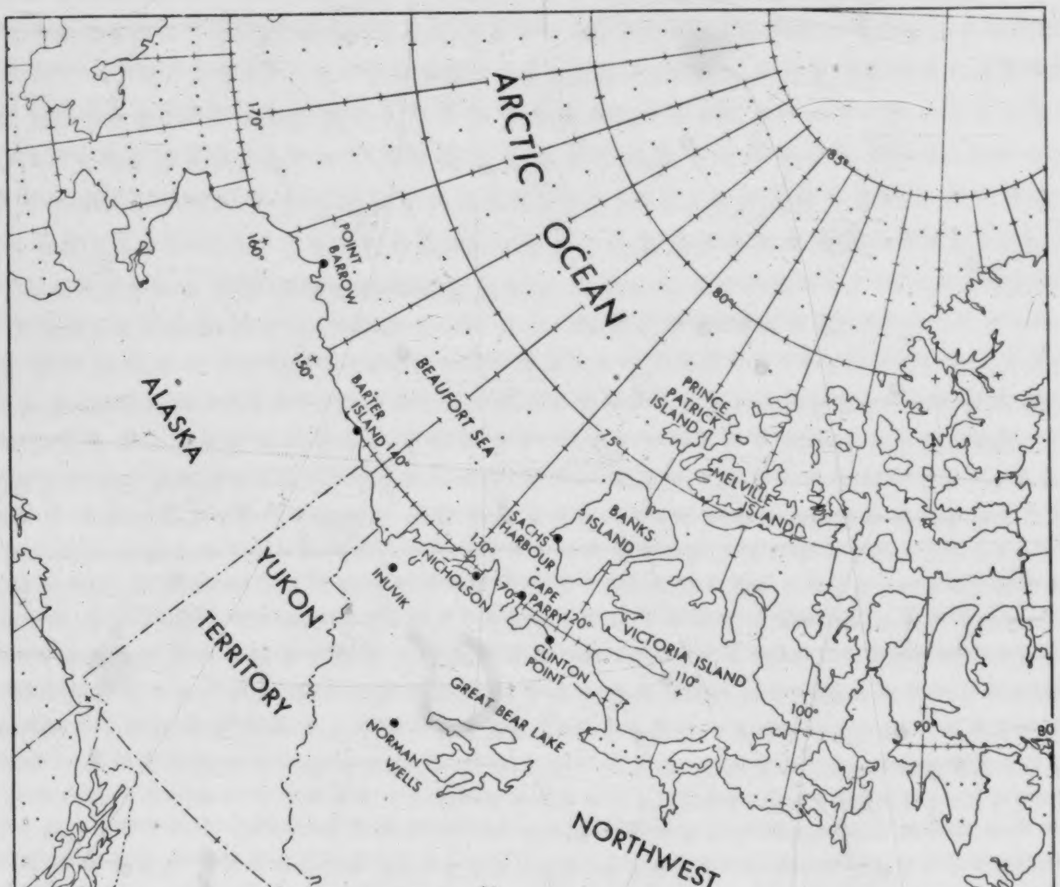
ARCTIC OCEAN
BEAUFORT SEA
ALASKA
YUKON TERRITORY
NORTHWEST TERRITORIES
POINT BARROW
BARTER ISLAND
INUVIK
NICHOLSON
CAPE PARRY
CLINTON POINT
SACHS HARBOUR
BANKS ISLAND
PRINCE PATRICK ISLAND
MELVILLE ISLAND
VICTORIA ISLAND
GREAT BEAR LAKE
NORMAN WELLS
170°
160°
150°
140°
130°
120°
110°
100°
90°
80
85°
80°
75°
70°
60°
50°

POLAR STEREOGRAPHIC PROJECTION. SCALE 1:10,000,000 TRUE AT 60° N
PROJECTION STEREOGRAPHIQUE POLAIRE, ECHELLE 1:10,000,000 CONFORME À 60°N

Figure 1.1: Map of Study Area

receiving stations in more northerly latitudes, such as the APT station at the University of Alberta. With proper interpretation techniques, satellite imagery becomes an important aid to forecasting and research.

In winter, the long Arctic night somewhat curtails the usefulness of satellite imagery. Because of the lack of sunlight, only the IR image is available, and the relative homogeneity of winter temperatures makes interpretation often difficult. In summer, both visible and IR data are available for analysis. The combination of the two makes it possible to differentiate between features such as high and low cloud, ice, open water, and land. Examples of imagery showing these features in the visible and infra-red range of the spectrum are given, respectively, in Figures 1.2 and 1.3.

There are numerous publications devoted to satellite photo interpretation. One of the most exhaustive studies can be found in W.M.O. Technical Note No. 124 (Anderson, 1973). However, there are relatively few published articles dealing specifically with satellite imagery of the Arctic, due in part, perhaps, to the difficulties encountered in the analysis of winter data. Another reason may be that there are only a small number of receiving stations in suitable locations, i.e., at high enough latitudes to ensure regular coverage of the Arctic regions. In this regard, the satellite laboratory at the University of Alberta, situated in Edmonton, Alberta (53° 25' N, 113° 33' W) is in a favourable position for the acquisition of satellite data from the western Canadian Arctic.

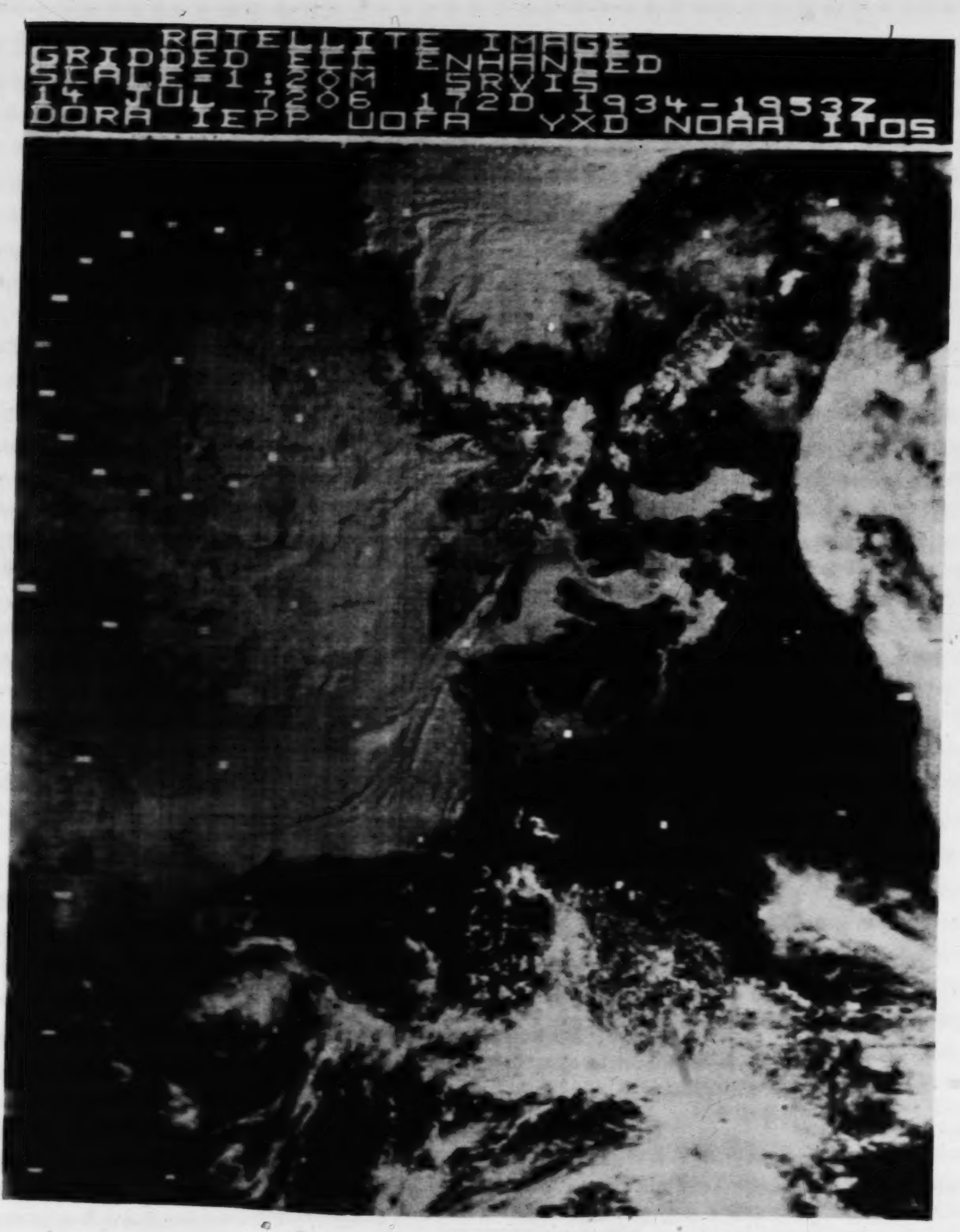
RATELLITE IMAGE
GRIDDED ELC ENHANCED
SCALE=1:20M SRVIS
14 JUL 7206 172D 1934-1953Z
DORA IEPP UOFA YXD NOAA ITOS

Figure 1.2: Visible Range Image July 14, 1976, Orbit 7602 1934-1953 GMT. Examples of high and low cloud, land, open water and ice.

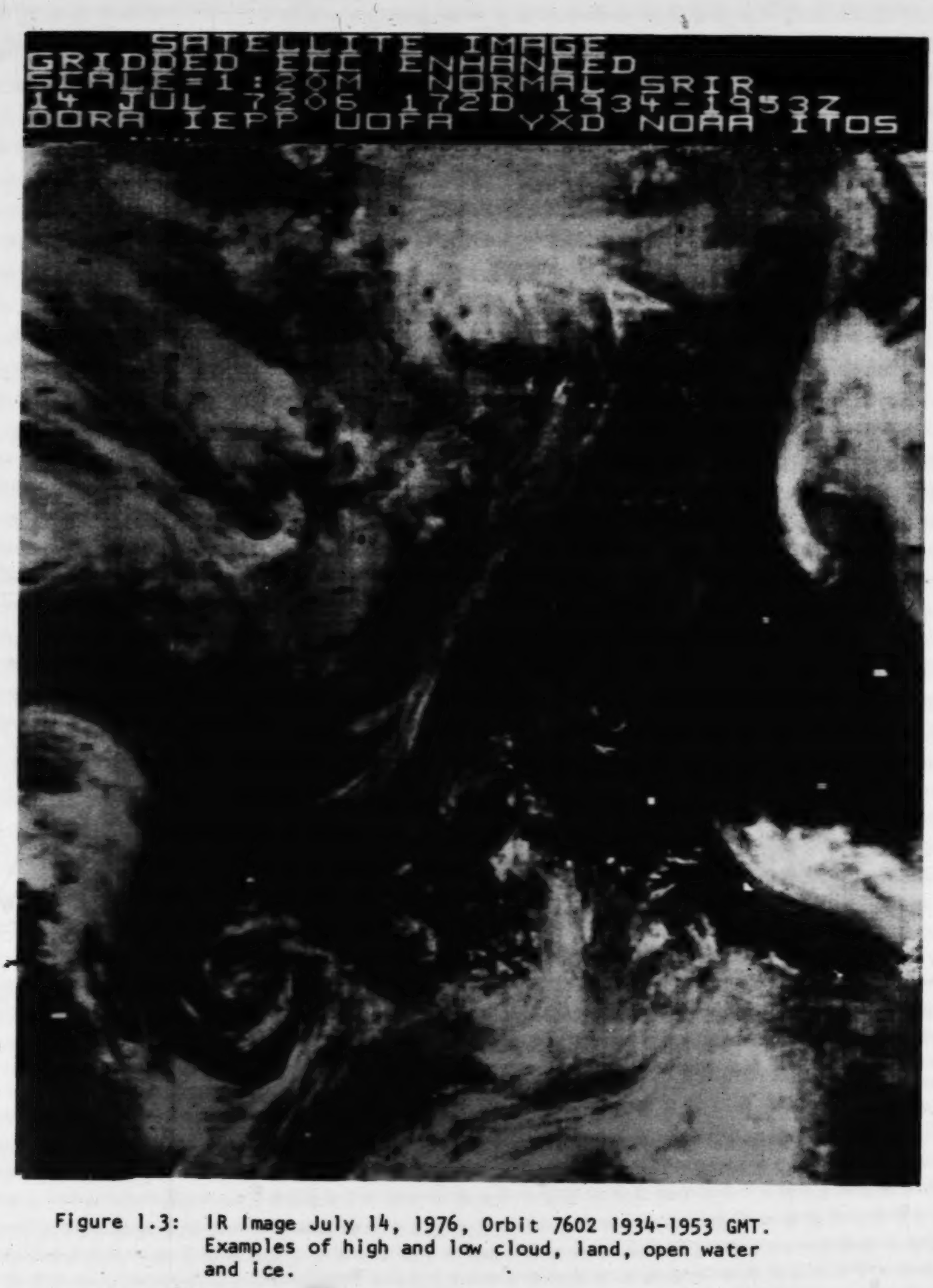
SATELLITE IMAGE
GRIDDED ECC ENHANCED
SCALE=1:20M NORMAL SRIR
14 JUL 7206 172D 1934-1953Z
DORA IEPP UOFA YXD NOAA ITOS

Figure 1.3: IR Image July 14, 1976, Orbit 7602 1934-1953 GMT. Examples of high and low cloud, land, open water and ice.

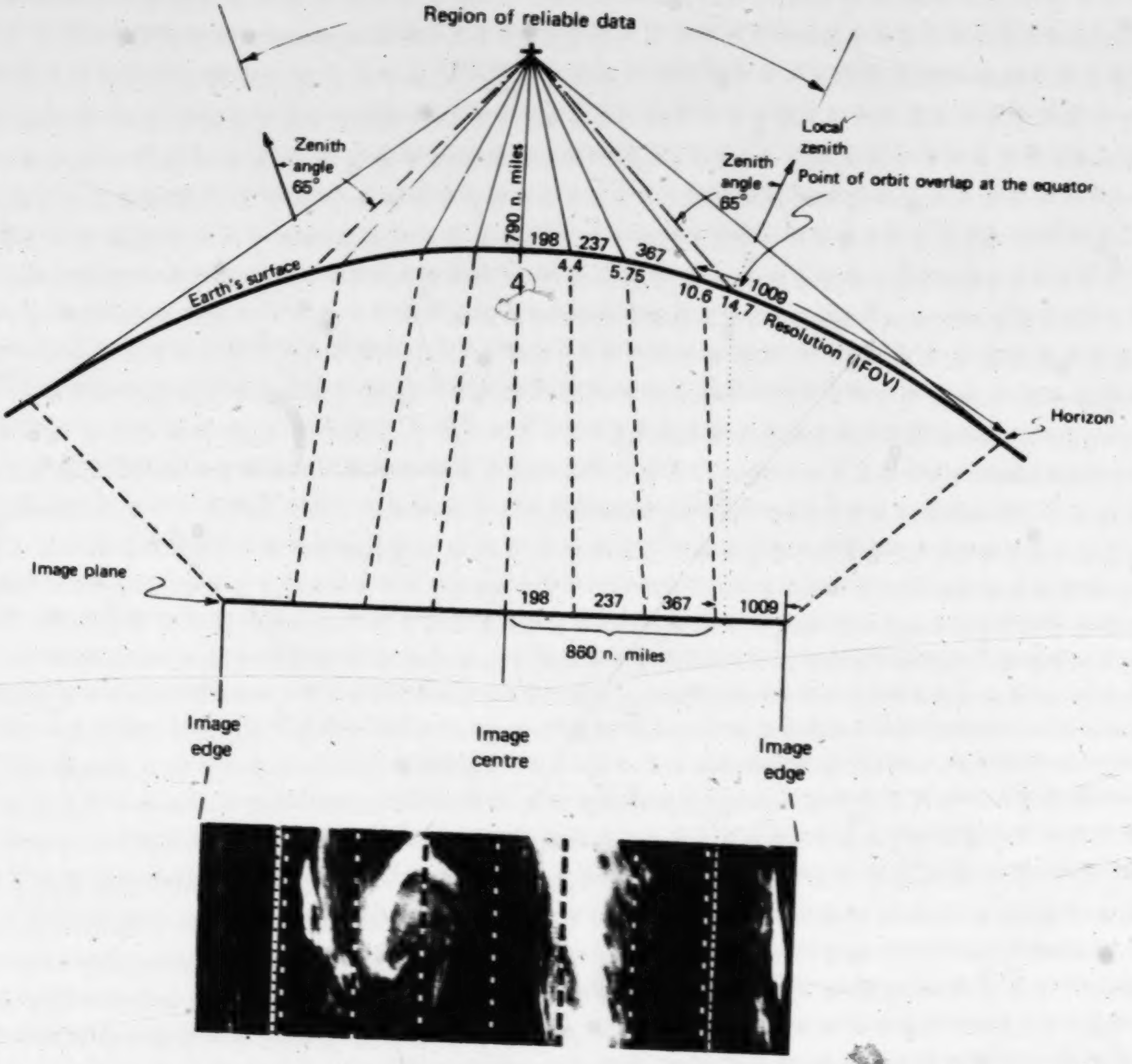
Region of reliable data
Zenith angle 65°
790 n. miles
Local zenith
Zenith angle 65°
Point of orbit overlap at the equator
Earth's surface
198
237
367
4
4.4
5.75
10.6
14.7
1009
Resolution (IFOV)
Horizon
Image plane
198
237
367
1009
860 n. miles
Image edge
Image centre
Image edge

Figure 1.4: Scanning Radiometer view of the Earth's surface, displayed on the flat plane of an IR imaging device. In this diagram, the image plane is divided into eight equal segments. The number above each segment of the image plane is the length in nautical miles (n.m.) of the arc of the Earth's surface displayed in that segment. These numbers show the rate at which foreshortening increases toward the edge of an IR display. The numbers below the curved line representing the Earth's surface are the size of the instrument field of view. It is 4 n.m. (7.4 km) wide at the satellite subpoint and increases to 14.7 n.m. (27.2 km) where the zenith angle is 65°. Beyond this point, resolution decreases markedly, and location errors increase because of foreshortening. The reliable data region is restricted to the inner 860 n.m. (1594 km) of the scan. At the Equator these regions are contiguous from pass to pass; poleward they overlap. This diagram applies to satellites of the NOAA/ITOS series, orbiting at altitudes of 790 n.m. (1464 km). (After Anderson and Smith, 1971)

The University of Alberta satellite laboratory processes APT visible and IR imagery. The recent NOAA satellites employ a scanning radiometer (SR) for observing visible and IR radiation directed at the spacecraft from the Earth. The SR is a two-channel scanning instrument sensitive to energy in the visible spectrum (0.5 to 0.7 μm) and in the infrared window region (10.5 to 12.5 μm). The spacecraft instrumentation is described in detail by Schwalb (1972). The SR contains a mirror rotating at a rate of 1.25 sec. per revolution which sweeps the Earth from horizon to horizon, and perpendicular to the track of the satellite. Maximum spatial resolution of the SR occurs on the Earth's surface directly below the satellite, along the subpoint track. For the IR sensor, the resolution is four nautical miles, and for the visible sensor, two nautical miles. Because of the geometry of the sweep, resolution decreases greatly near the horizon, so that only the more central portions of the scan are useful. For example, an IR scan at a zenith angle of 65° limits the resolution to 14.7 nautical miles. Details of the radiometer scan geometry are shown in Figure 1.4.

For the purpose of converting the measured IR radiation into temperature, the surfaces of the Earth and cloud are treated as blackbody radiators. Before launching, the SR is calibrated against a blackbody, and a curve is obtained which gives the temperature corresponding to a measured radiance. Once in orbit, the calibration curve is used to obtain equivalent blackbody temperatures from the IR data. The temperatures are subject to errors introduced by noise in the system, as well as by fluctuations in the response of the instrument. Part of the satellite signal to Earth is used for recalibrating the instrument while in flight. The temperature error will vary from approximately ±2°C at the warm end of the range (300°K) to about ±8°C at the cold end (185°K), (Schwalb, 1972).

The IR and visible measurements are transmitted from the spacecraft to Earth as an analog signal. This signal can be converted directly into an image using gray shades, or it can be put into digital form and processed by computer before it is displayed. The computer is used to make the data more presentable and easier to interpret. Some of the more common operations performed on the data include:

1. Gray Scale Enhancement:

This is used to improve the contrast of the image, but the transition between gray shades remains quasi-continuous.

2. Slicing:

The data may be "sliced" into discrete levels so that the transition between gray shades occurs in distinct steps. On IR imagery these levels can be made to correspond to isotherms.

3. Earth Curvature Correction:

Correction for the curvature of the Earth removes image foreshortening near the horizons.

4. Geodetic Grid and Boundary Display:

The image can be referenced and located with respect to the Earth by either superimposing latitude and longitude lines or their intersections, or by using geographical and political boundaries.

Once the satellite data are digitized and compatible with the computer system to be used for further processing, there are many techniques available to display the data. The digitized IR values can be converted into temperatures and then, by a slicing operation, the SR image can be contoured to produce equivalent isotherms. The display is not restricted to gray-shades only. It is sometimes difficult to differentiate between the various levels of gray once the number of shades becomes greater than six or seven. Alternative methods of displaying the quantitative SR data are available when detailed information is desired, such as folding or "wrapping", where the normal order of shades in the gray scale is interrupted, inverted or modified in some desirable way.

Whether visible or IR data (or a combination of both) are used, the processing and method of display all depend on the part of the imagery being examined and the information that is desired from it. For most operational purposes, e.g., weather analysis and forecasting, it is usually only necessary to focus attention on synoptic-scale features such as cloud patterns associated with frontal systems. Both IR and visible imagery are useful.

As previously noted, the Arctic winter restricts the use of satellite imagery. The lack of sunlight severely limits visible information north of the Arctic Circle. Also, the snow, ice and clouds are often very nearly at the same temperature, and so become practically indistinguishable in an IR image. However, illumination and contrast conditions become much more favourable in summer. As solar radiation increases, the snow and ice begin to melt, especially on the land masses. As the snow disappears from the land, more solar radiation is absorbed at the surface, and more IR radiation is emitted. Land masses become easier to see in both the IR and visible range of the spectrum. The albedo of open water is less than that of the ice packs. The open water and ice pack, with pools of water on the surface, both radiate at temperatures close to $0^{\circ}C$ and thus appear as much the same shades of gray on IR pictures. However, with lower albedo, the open water will appear darker than ice on a visible-range image. Figures 1.2 and 1.3 show open water along the southern shore of the Beaufort Sea, and along the west coast of Banks Island. It is, therefore, possible to use satellite images to advantage in ice reconnaissance. This is certainly much more efficient than mapping ice movements by aircraft. Some of the applications of satellite data in sea ice monitoring are described by McClain (1972), Struebing (1972) and Gerson (1975).

The IR satellite imagery can be useful for determining the height of cloud. High and low cloud will appear to be similar in the visible range of the spectrum. However, since high cloud is usually colder than low cloud, the IR image will show correspondingly different shades of gray. Referring again to Figures 1.2 and 1.3, the high cloud visible in the lower right of both images is very bright, while low cloud, such as stratus (which covers much of the Beaufort Sea) appears much darker, particularly in the IR image.

In addition, if a temperature can be assigned to the cloud, and the upper air temperatures are known from radiosonde data, the height of the cloud can be estimated. IR data have been used by Rao

(1970) to estimate cloud height in the tropics, but the method seems to have found little application elsewhere.

The procedure is made more difficult in the Arctic by the presence of complicated upper-air temperature structures associated with inversion conditions. Since inversions are a common occurrence in the Arctic, it is useful to know their horizontal and vertical extent for forecasting purposes. In an area where radiosonde data are not available, satellite information can be valuable for mapping inversions.

As mentioned earlier, low stratiform cloud may indicate the presence of an inversion. In a satellite picture of gray shades, low cloud in an inversion will appear darker than the Earth's surface in adjacent clear areas. In the absence of low cloud, inversion conditions are more difficult to detect. IR radiation is emitted by the Earth and received by the spacecraft radiometer. However, the radiation is "adulterated" along the way to the spacecraft. Water vapour and carbon dioxide in the atmosphere will absorb and re-emit some of the IR radiation at temperatures different from the Earth's surface. As a result, the spectral content of the original beam of radiation is altered, and the IR radiometer will not "see" a pure image of the underlying surface. This effect is called limb-darkening because it is most pronounced for rays grazing the limb of the Earth which delimits the spacecraft's horizon.

When the cloud is very thin or altogether absent, it may still be possible to find evidence of inversions in IR imagery, provided that the concentration of water vapour is fairly high, and the increase of temperature with height is large. This question will be examined later.

On the vast, data-sparse, open oceans, sea-surface temperatures have been mapped successfully by the use of IR satellite data. In this application Smith et al., (1970) attempted to estimate water temperatures with as little error as possible by allowing for atmospheric absorption of radiation, and by calibrating the instrumentation as accurately as possible. This method is readily adapted to the Arctic, a huge area beset by observational problems akin to those of the oceans.

The few weather reporting stations north of the Arctic Circle are all situated on or near the Arctic coast and on the shores of islands. This means in practice that only a handful of conventional weather reports are received from large, landlocked regions, and next to none are available from the shifting ice of the Arctic Ocean. Under such conditions, polar-orbiting satellites come truly into their own, and can be utilized to provide much useful (and often the only) information about cloud patterns and temperature structure.

In situations where it is difficult to obtain true absolute temperatures, it is often still possible to estimate relative temperature relationships from the IR data. In meteorological practice, the range and rate of temperature variation are usually more significant than the precise value of the actual temperatures. In the Arctic, where surface albedo is variable from dark land to reflective ice, large temperature contrasts develop which profoundly affect the circulation on every conceivable scale.

CHAPTER 2

A SUMMARY OF ARCTIC CIRCULATION IN SUMMER

2.1 Normal Circulation Patterns

The determination of the mean circulation of the Arctic is more difficult and uncertain than for other, more settled, areas having reliable, long-term records. Regular weather observations from the Arctic have become available only since the end of World War II. Prior to that time, weather information was sketchy and sporadic, provided mainly by a small number of northern outposts, and the occasional polar expedition. Shortly after the War, the United States and the Soviet Union set up meteorological stations on large "ice islands" adrift in the Arctic Basin. At about the same time reconnaissance flights over the Arctic were increased. By 1950, Canada and the U.S. had established jointly five first-order reporting stations in the High Arctic, at Resolute, Eureka, Mould Bay, Isachsen and Alert. Thus meteorological data from the Arctic became available on a routine basis only in the early 1950's.

In the absence of an adequate data base the early theories about the Arctic circulation tended to oversimplify the true synoptic situation. The German physicist, von Helmholtz, visualized a large dome of cold air sitting over the polar regions, creating a permanent anticyclone in the central Arctic. This theory, first proposed in 1888, could not be properly tested until fairly recent times, when sufficient data had been accumulated. In fact, for much of the first half of this century, synoptic maps were analyzed with von Helmholtz's theory in mind. As a result, all studies based on these early maps were subject to this bias. Petterssen (1950), used forty years of U.S. Weather Bureau Maps (1899 to 1939) to construct charts showing the distribution of cyclonic and anticyclonic activity in the Northern Hemisphere. Petterssen's charts show the Arctic to be an area with a predominantly anticyclonic circulation. However, as more information accumulated during the 1950's, evidence began to mount which contradicted von Helmholtz's theory. Klein (1956) investigated cyclone tracks in the Northern Hemisphere and found a secondary storm track north of Siberia, extending in some months to a position north of Alaska. Keegan (1958) used data collected in the winter months of 1952-1956. He found the Arctic to be an area of significant cyclonic activity, even in winter. Similarly, Kunkel (1959) looked at the Arctic summers of 1952-1956. His charts of cyclonic and anticyclonic distribution differ markedly from those produced by Petterssen, based on the old series of maps. Kunkel showed the Arctic Basin to be characterized by a high frequency of cyclonic activity. Storm tracks were found further to the north than had been considered before. Although the observations were taken during a period of only five years, they are thought to be representative of longer periods, since they do not seem to contradict the evidence provided by reports from the early polar explorers.

Analyses based on more recent data have been used to identify the normal summer circulation. Kunkel (1959) considered the months of July, August and September as representative of the Arctic summer situation.

The mean surface pressure over the Arctic is high during the winter months. By July a depression has formed near the Pole and a high-pressure cell has become established over the Canadian Mainland, as shown in Figure 2.1. The polar low fills gradually during August. (See Figure 2.2.) By September (Figure 2.3), the main features are high pressure over Canada and deepening low pressure near Iceland.

Cyclonic activity seems to reach a peak in July and tail off during August and September. The favoured area for the occurrence of low pressure centres is the Arctic Basin between Alaska and the Pole. Most of these lows originate in Siberia, but some are old Icelandic lows. Figure 2.4 from Kunkel shows the percentage frequency of occurrence of cyclonic centres in the period July-September. The Beaufort Sea is depicted as an area of minimum cyclonic activity. In fact, charts showing the distribution of anticyclonic centres over the summer indicate a circumpolar belt of high pressure at about 75°N latitude. The Canadian Archipelago is shown as one of the principal areas frequented by anticyclones. Kunkel also identifies the Beaufort Sea as an area undergoing but little variation from the predominantly high pressure.

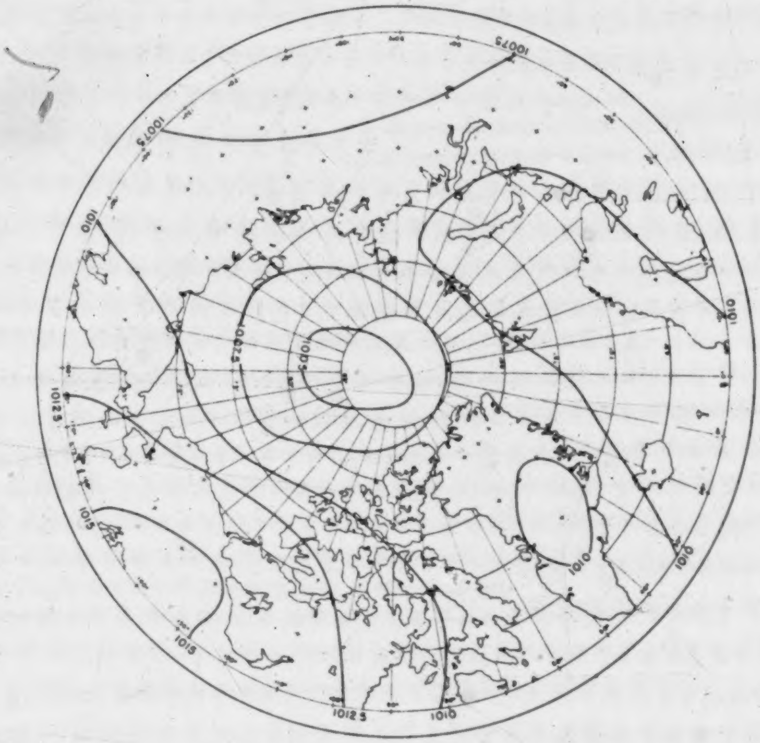
1007.5
1007.5
1010
1010
1005
1012.5
1012.5
1015
1015
1010
1010
1012.5
1010

Figure 2.1: Mean Pressure Distribution in July
(After Kunkel, 1959)

The Arctic front in summer tends to extend from central Siberia, through Alaska and into Canada, skirting the Arctic Basin, as indicated in Figure 2.5. This front can be thought of as defining a storm track, and also as marking the line between snow-free land and the ice packs of the ocean.

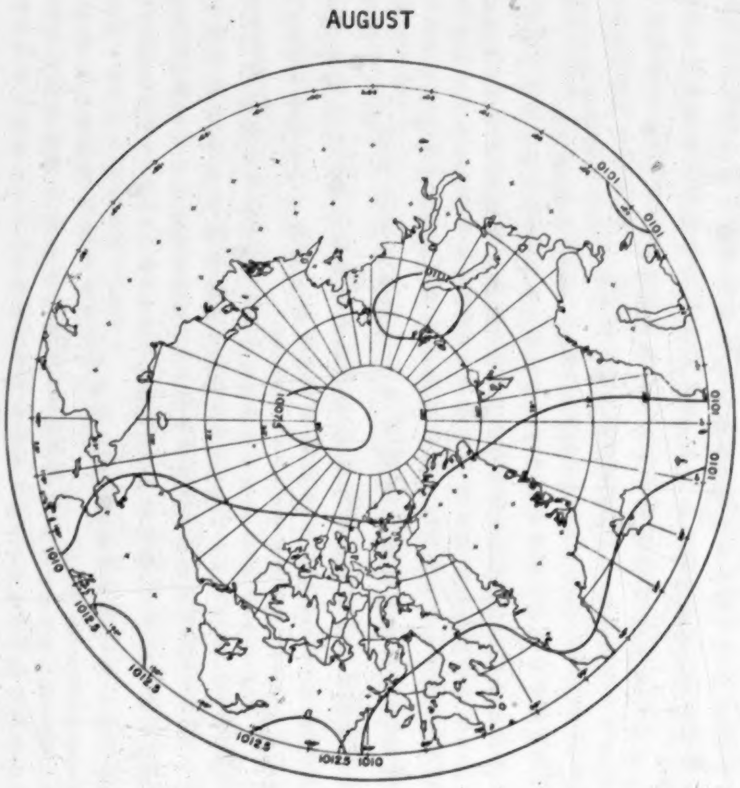
AUGUST
1010
1007.5
1012.5
1010
1012.5
1012.5
1012.5
1010

Figure 2.2: Mean Pressure Distribution in August (After Kunkel, 1959)

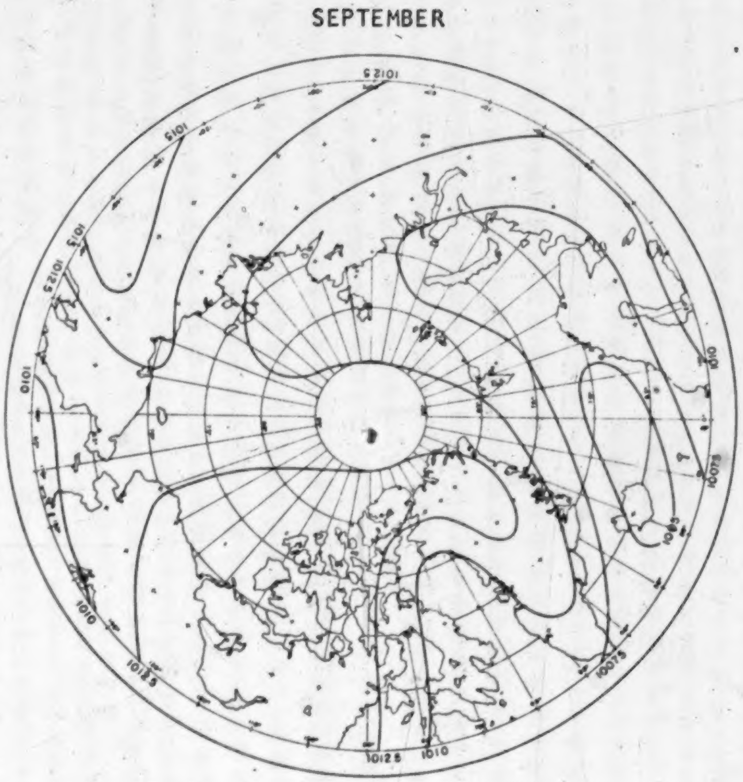
SEPTEMBER
1012.5
1015
1015
1012.5
1010
1010
1007.5
1012.5
1007.5
1012.5
1010

Figure 2.3: Mean Pressure Distribution in September (After Kunkel, 1959)

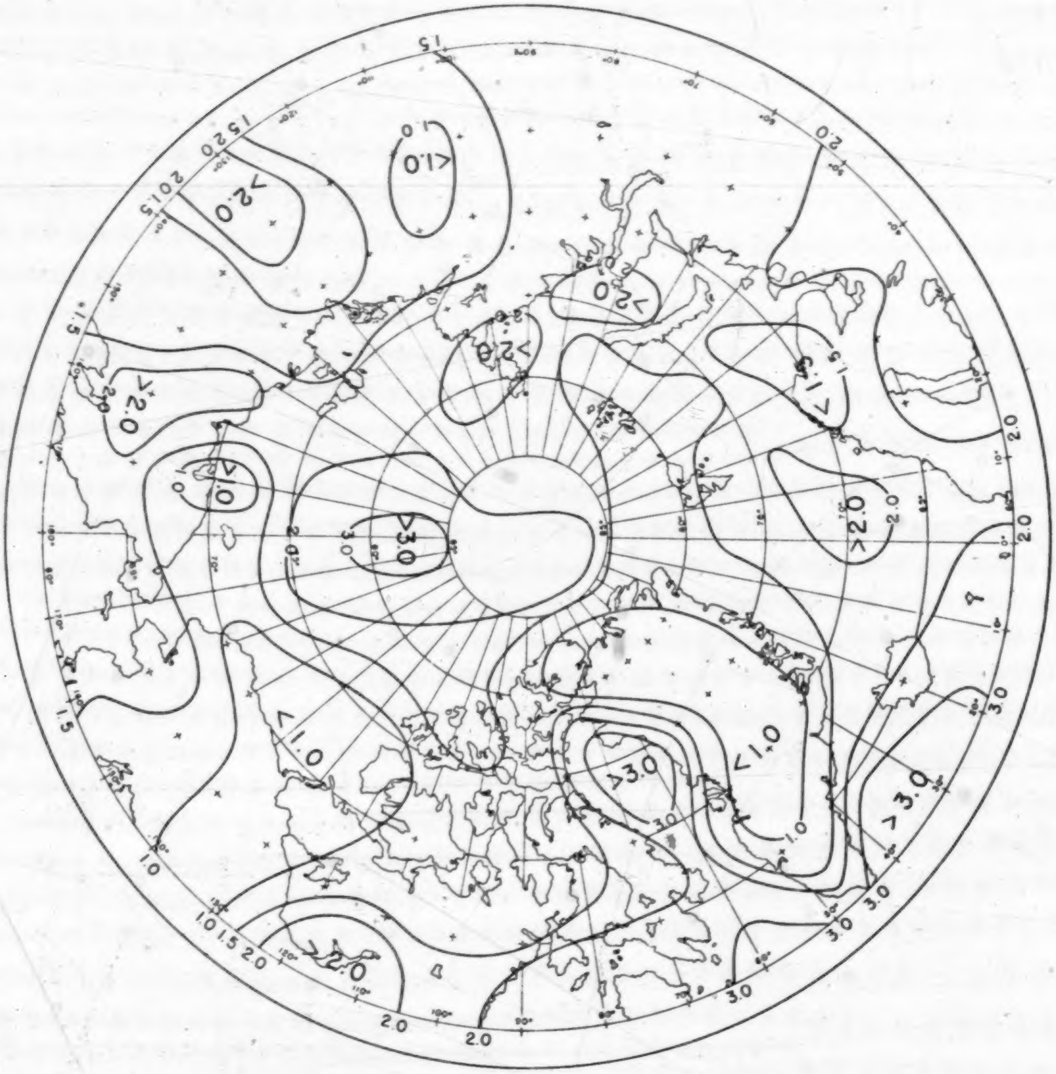
>2.0
<1.0
1.5
2.0
>2.0
<1.0
>3.0
3.0
<1.5
>2.0
2.0
<1.0
>3.0
<1.0
1.0
>3.0
3.0
1.0
>2.0
1.5
2.0

Figure 2.4: July-September Percentage Frequency of Cyclone Centres in Squares of 100,000 km^2 (After Kunkel, 1959)

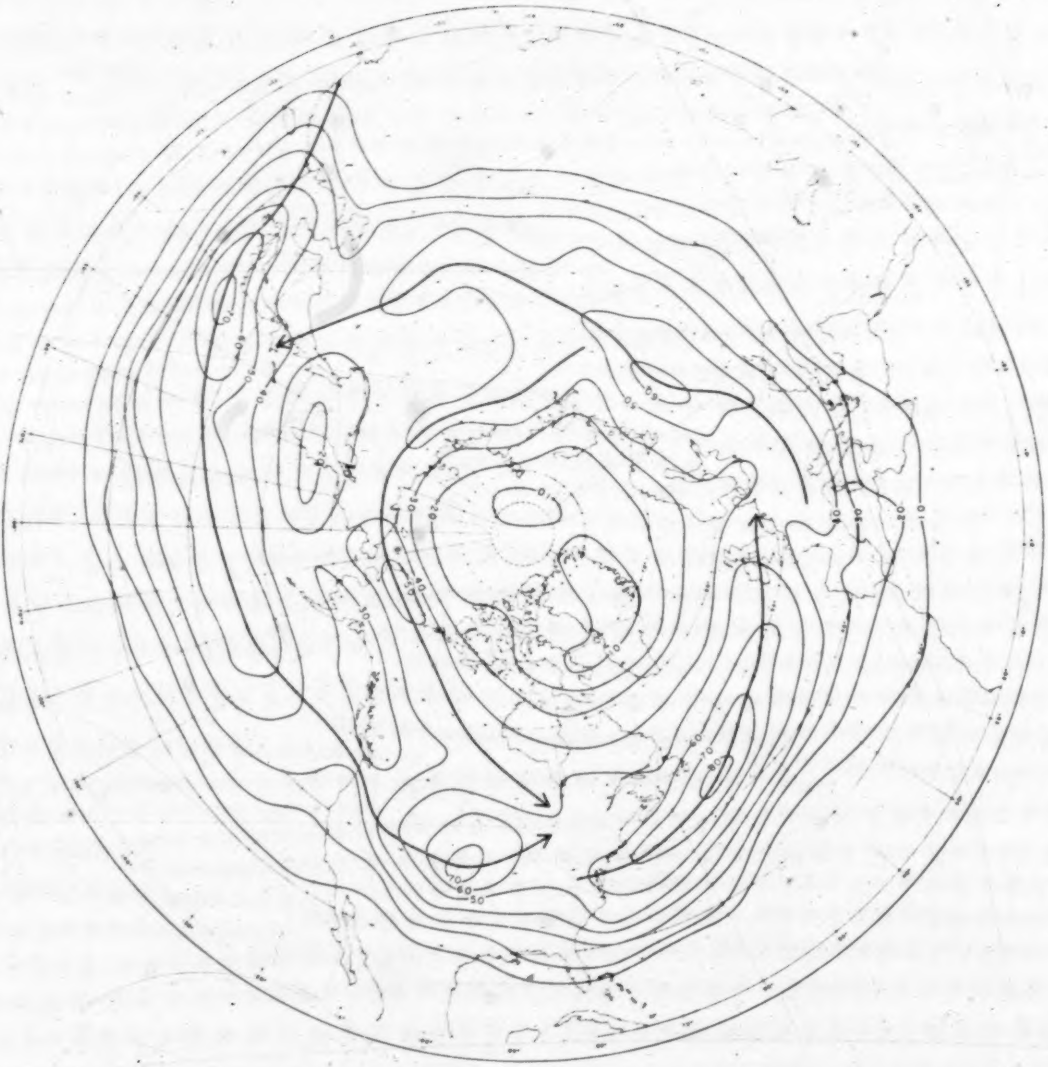
70
60
50
80
10
20
30

Figure 2.5: Percentage Frequency of Fronts in Squares of 400,000 km^2 (After Kunkel, 1959)

Kunkel comments on the increased latitudinal temperature gradient that is observed to exist at approximately 70°N along the north coasts of Siberia, Alaska and Canada. This large temperature gradient is in essence equivalent to a baroclinic zone. Disturbances should form and deepen, tending to move to the northeast, much in the manner of cyclonic developments initiated by baroclinic zones in middle latitudes. Fraser (1973) identifies the Mackenzie Delta as a region conducive to the formation of thermal lows which, on occasion, acquire frontal characteristics. This type of low can also be associated with the strong temperature gradient along the coast.

2.2 Circulation Observed in the Summer of 1976

The collection and description of July and August, 1976, maps given below is not meant to be a definitive assessment of the Arctic circulation. It is intended to serve only as a summary of the synoptic-scale patterns observed in summer, largely to provide a background for some specific situations on a smaller scale. Moreover, the summary is mainly concerned with the western Canadian Arctic and, in particular, with the regions contiguous to the Beaufort Sea.

Surface and 500-mb charts for July and August, 1976, are used to display the most important features of the summer circulation. These charts were analyzed by forecasters at the Arctic Weather Centre in Edmonton. No attempt was made to re-analyze them for this study. Further detail was provided by surface maps analyzed by forecasters working at the Beaufort Advance Base at Tuktoyaktuk, which operated from July to October, 1976. No vorticity analyses were available for the 500-mb charts used.

July and August, 1976, differed markedly in the way that the circulation pattern seemed to develop. Except for the beginning and end of the month, July proved to have little cyclonic activity in the Arctic Basin, with mainly high pressure over the Canadian Archipelago and the Beaufort Sea. The flow at the 500-mb level was generally light, with predominantly ridge conditions over the western Canadian Arctic. In August, on the other hand, the 500-mb flow was strong and zonal in nature for much of the month. Short waves moved rapidly and frequently in the strong upper flow. A series of disturbances moved west to east, closely following the coast-line of Alaska and Canada, criss-crossing the northern reaches of the continent and the waters of the Beaufort Sea.

The first week of July had more synoptic-scale activity than what was average for the rest of the month. A long-wave trough was anchored in the Pacific and the resulting southwesterly flow at upper levels promoted lee troughing along the north coast of Alaska and into the Mackenzie Valley. The 0000 GMT 500-mb charts of July 1 and 5 are reproduced in Figures 2.6 and 2.7.

Occasional shortwaves in the upper flow generated surface waves on the Arctic front located in the quasi-stationary lee trough. The disturbances moved along the trough towards Hudson Bay. The 0000 GMT surface map of July 4, Figure 2.8, shows a situation typical for the period.

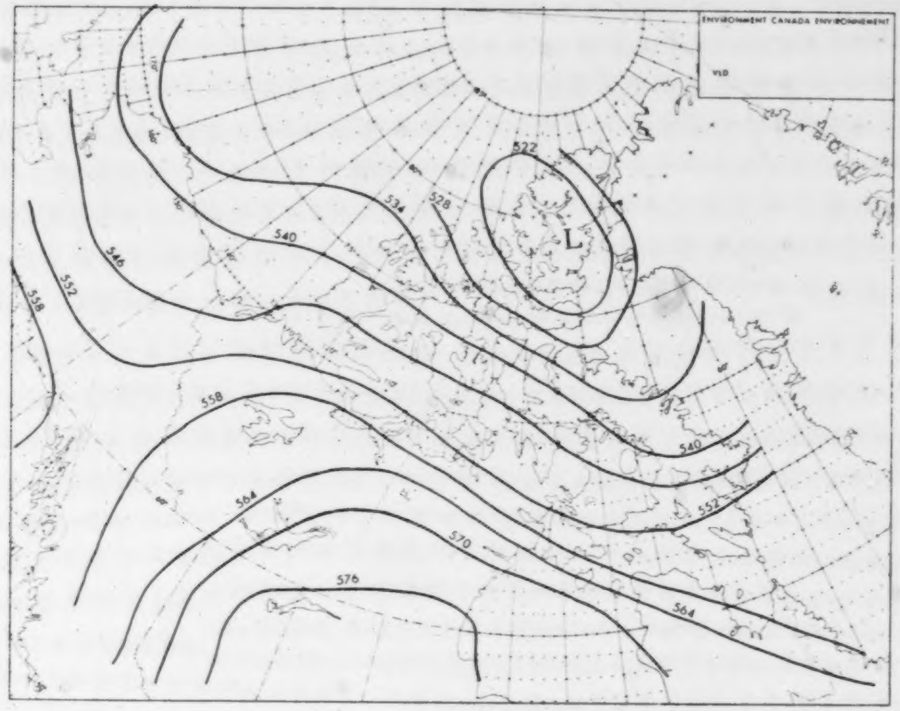
ENVIRONMENT CANADA ENVIRONNEMENT
522
528
534
540
546
552
558
L
558
564
570
576
540
552
564

Figure 2.6: 500-mb Contours, 0000 GMT July 1, 1976

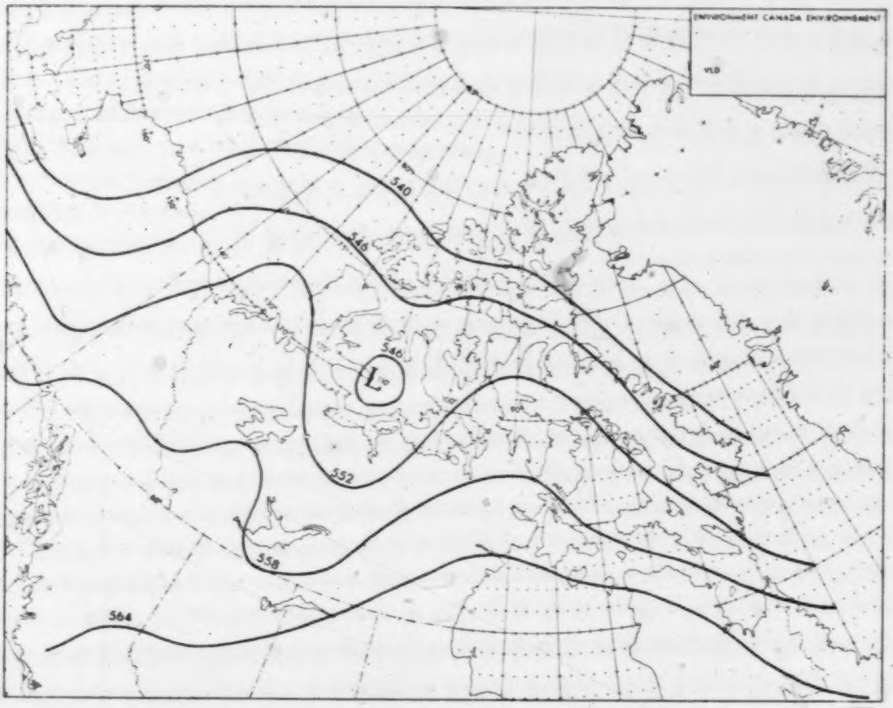
ENVIRONMENT CANADA ENVIRONNEMENT
540
546
546
L
552
558
564

Figure 2.7: 500-mb Contours, 0000 GMT July 5, 1976

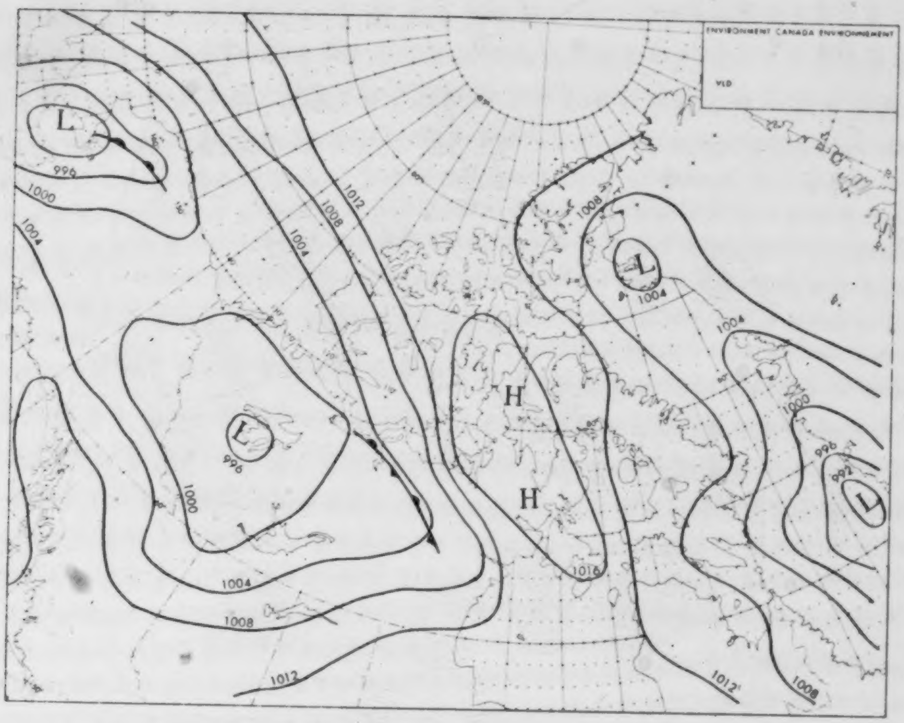
ENVIRONMENT CANADA ENVIRONNEMENT
VLD
L
996
1000
1004
1012
1008
1004
L
996
1000
1004
1008
1012
H
H
1016
1008
L
1004
1004
1000
996
992
L
1012
1008

Figure 2.8: Surface Map, 0000 GMT July 4, 1976

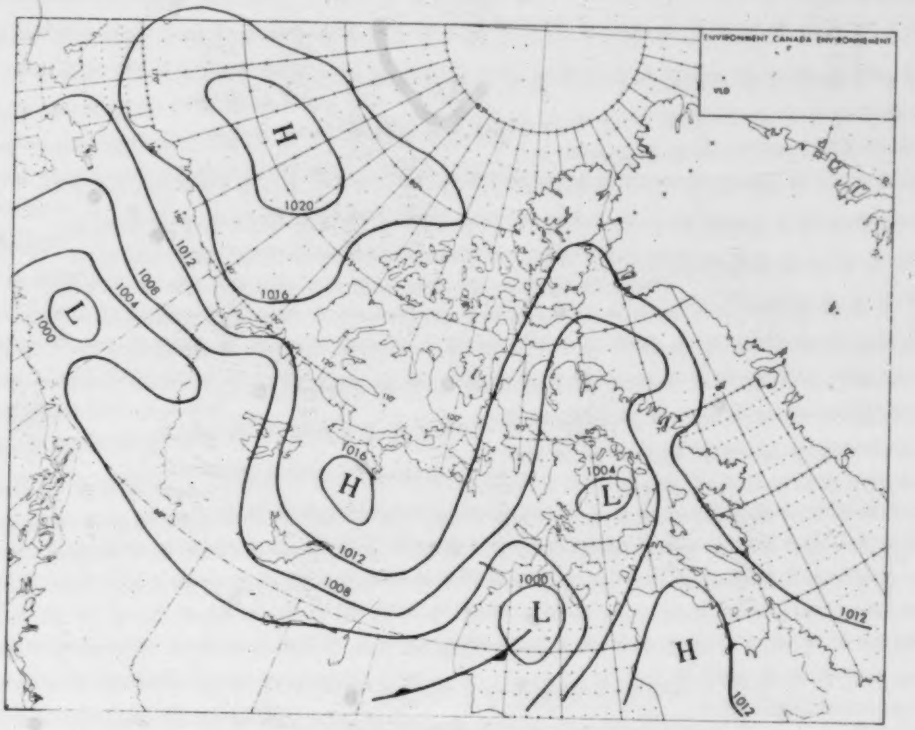
ENVIRONMENT CANADA ENVIRONNEMENT
VLD
H
1020
1016
1012
1008
1004
1000
L
1016
H
1012
1008
1004
L
1000
L
H
1012
1012

Figure 2.9: Surface Map, 0000 GMT July 9, 1976

The Arctic Basin was under the influence of an upper ridge for the next few days. The flow was light and zonal at 500-mb, and at the surface an anticyclone covered much of the Beaufort Sea and the islands to the east, as indicated in Figure 2.9 - a copy of the 0000 GMT surface map of July 9.

The Arctic Coast was in an easterly to southeasterly surface wind regime during this period. The dominance of the anticyclone was broken briefly as a disturbance, given impetus by an upper closed low entering Alaska from the west, moved along the Arctic Coast. This system is shown on the 0000 GMT surface map of July 15, Figure 2.10.

Subsequently, another high pressure centre moved over the Beaufort Sea and remained almost to the end of the month, only shifting slightly eastward during the period. The 0000 GMT surface map of July 23, Figure 2.11, shows this anticyclonic pressure pattern.

The presence of an upper ridge (see Figure 2.12, the 0000 GMT 500-mb chart of July 20) over the surface ridge brought clear skies and warm weather to the western Canadian Arctic.

The 0000 GMT 500-mb chart of July 27, 1976, in Figure 2.13, shows a closed low over the Mackenzie Basin. This low was cut off from a trough extending westward from a major upper low near Baffin Island. The upper low filled quickly as a strong, southwesterly flow developed at 500-mb over Alaska. This flow pattern is depicted in Figure 2.14, the 0000 GMT 500-mb chart of July 30.

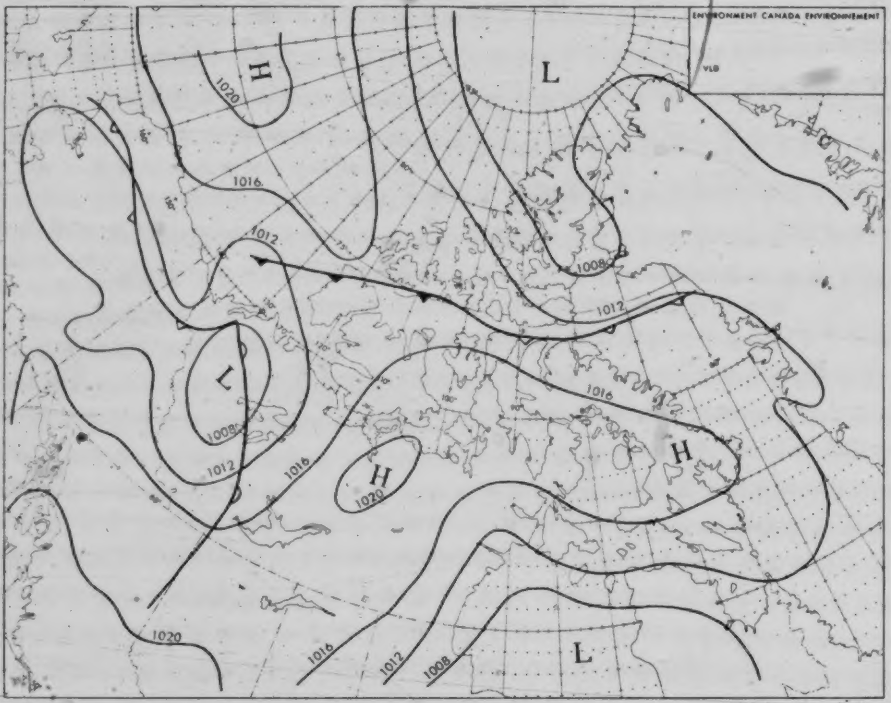
ENVIRONMENT CANADA ENVIRONNEMENT
VLD
H
L
L
H
H
L
1020
1016
1012
1008
1008
1012
1016
1016
1012
1020
1020
1016
1012
1008

Figure 2.10: Surface Map, 0000 GMT July 15, 1976

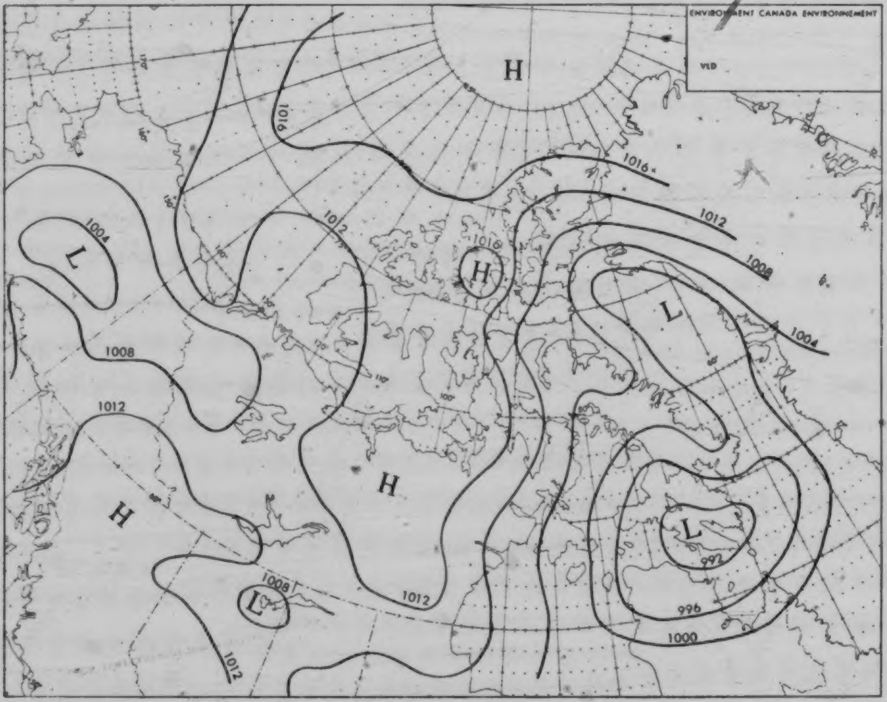
ENVIRONMENT CANADA ENVIRONNEMENT
VLD
H
L
H
L
H
H
L
L
1016
1016
1012
1012
1016
1008
1004
1004
1008
1012
1008
1012
1012
992
996
1000

Figure 2.11: Surface Map, 0000 GMT July 23, 1976

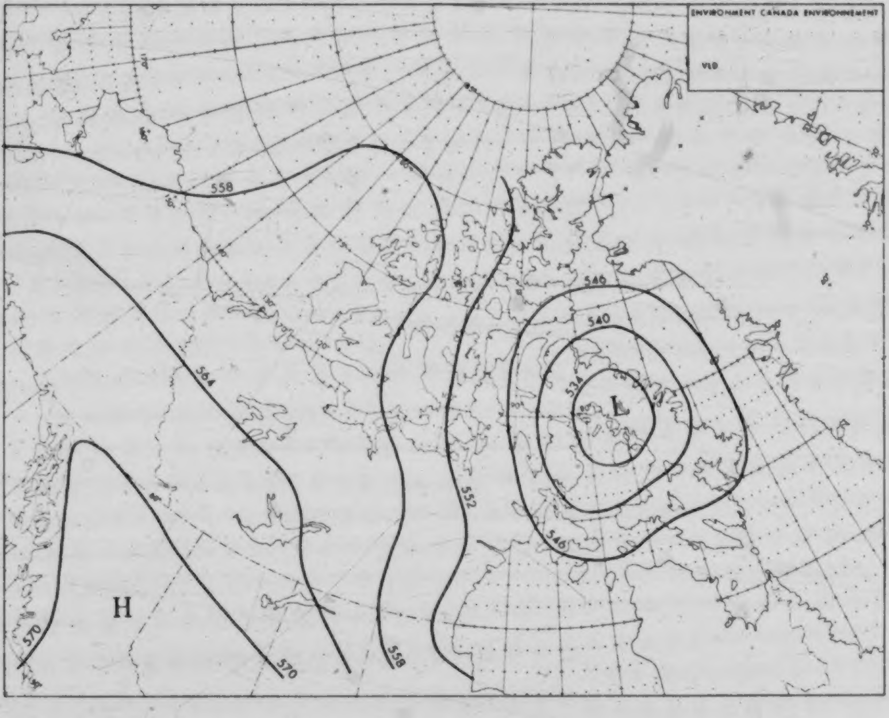
ENVIRONMENT CANADA ENVIRONNEMENT
VLD
558
564
570
H
570
558
552
546
540
534
L
546

Figure 2.12: 500-mb Contours, 0000 GMT July 20, 1976

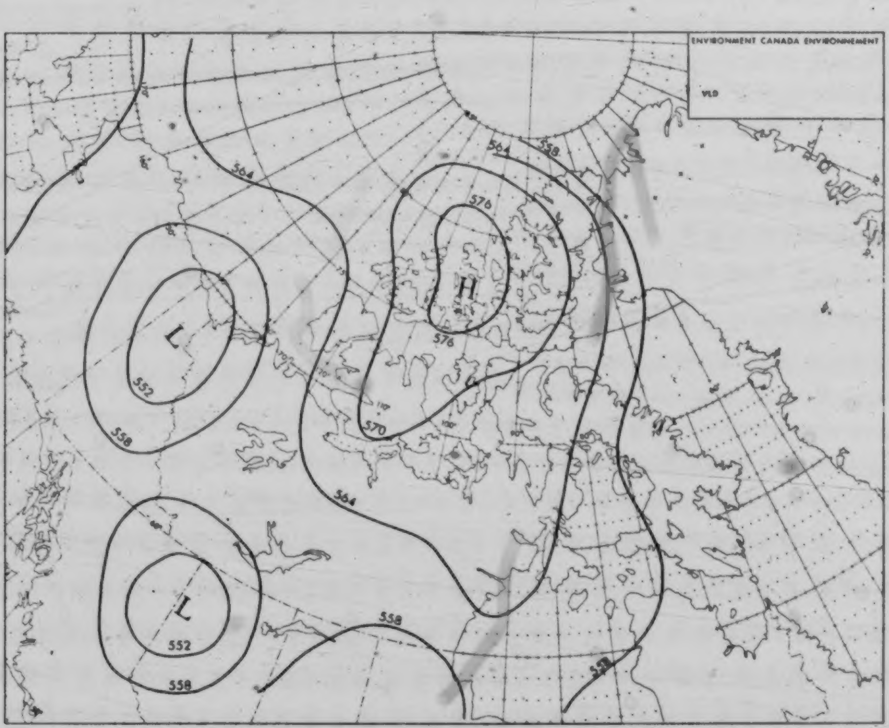
ENVIRONMENT CANADA ENVIRONNEMENT
VLD
564
564
558
576
H
576
570
L
552
558
564
L
552
558
558
558

Figure 2.13: 500-mb Contours, 0000 GMT July 27, 1976

On July 30, a surface depression generated in Alaska moved into the Beaufort Sea near the mouth of the Mackenzie River. Some interesting developments - to be considered in a later context - took place as this system moved out over the open water.

The long-wave ridge remained dominant over western Canada for the first half of August. The upper flow over the western Canadian Arctic tended to be strong and zonal during the first week of the month. The 0000 and 1200 GMT 500-mb charts of August 1 and 5, respectively, (Figures 2.15 and 2.16) clearly demonstrate the persistent nature of this flow regime.

Two similar disturbances moved through the Arctic Basin during this week. The 0000 GMT surface map of August 4, Figure 2.17, shows a north-south trough line sweeping across the Beaufort Sea, with a frontal wave passing to the north of Banks Island. These systems moved quickly, with the second trough being out of the area by August 8.

The 0000 GMT surface map of August 9, Figure 2.18, shows the ridge that built in behind the last trough.

The 1200 GMT 500-mb chart of August 12, Figure 2.19, indicates that the zonal flow had become weaker as an upper closed low from the Gulf of Alaska attempted to break through the long-wave ridge.

On August 11 and 12 a surface frontal system moved along the southern shore of the Beaufort Sea and across Banks Island.

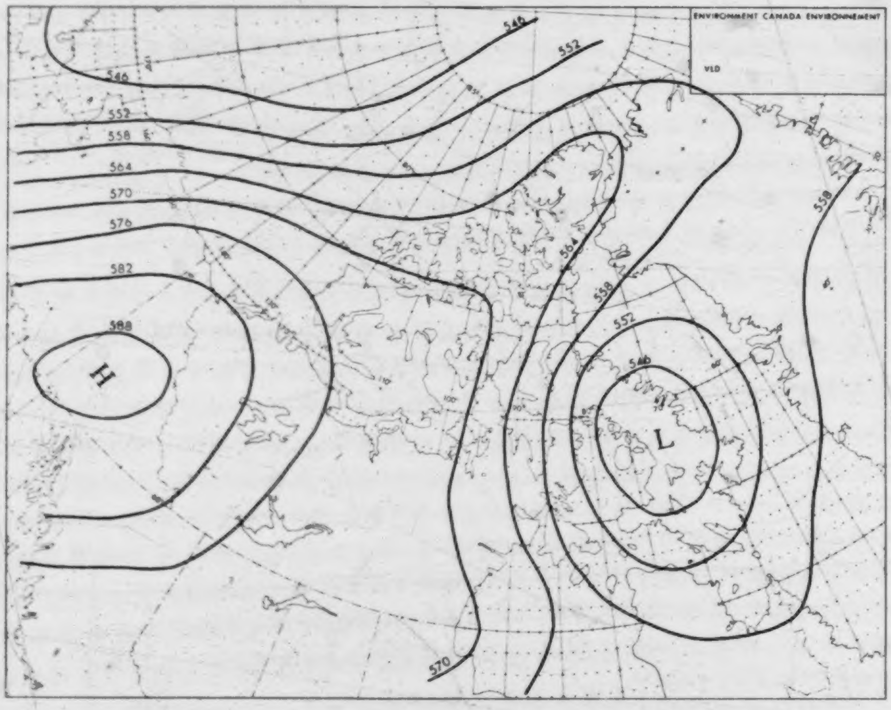
ENVIRONMENT CANADA ENVIRONNEMENT
VLD
546
552
558
564
570
576
582
588
H
L
546
552
558
564
570
558

Figure 2.14: 500-mb Contours, 0000 GMT July 30, 1976

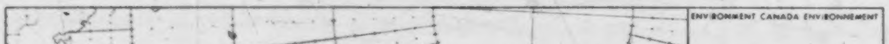
ENVIRONMENT CANADA ENVIRONNEMENT
VLD
L
534
540
546
552
558
564
570
576
582
H
H
582
570
540
L
546
552

Figure 2.15: 500-mb Contours, 0000 GMT August 1, 1976

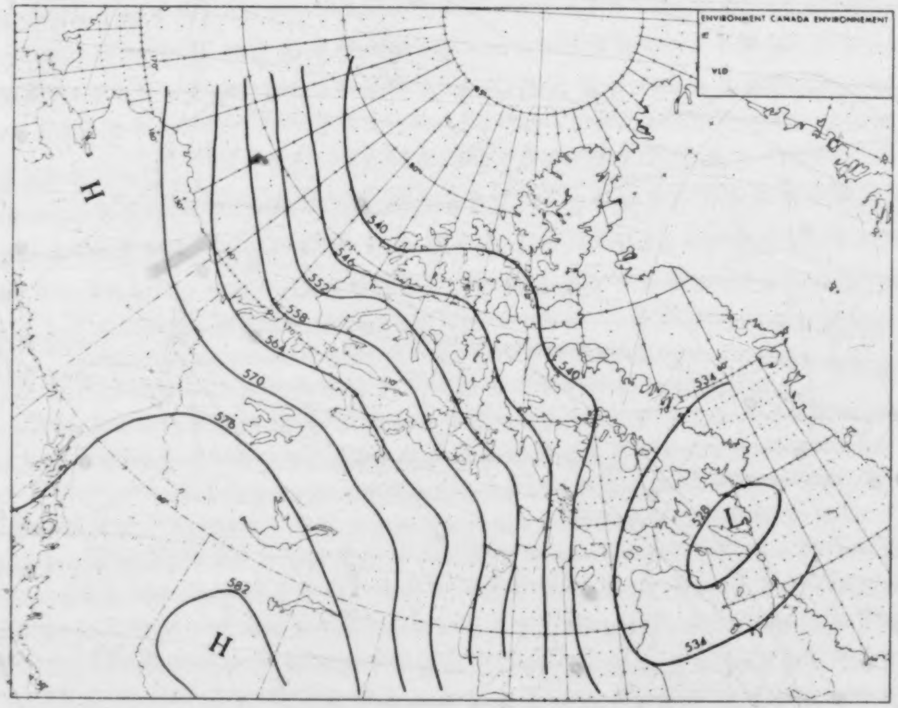
ENVIRONMENT CANADA ENVIRONNEMENT
VLD
H
540
546
552
558
564
570
576
582
H
540
534
528
L
534

Figure 2.16: 500-mb Contours, 1200 GMT August 5, 1976

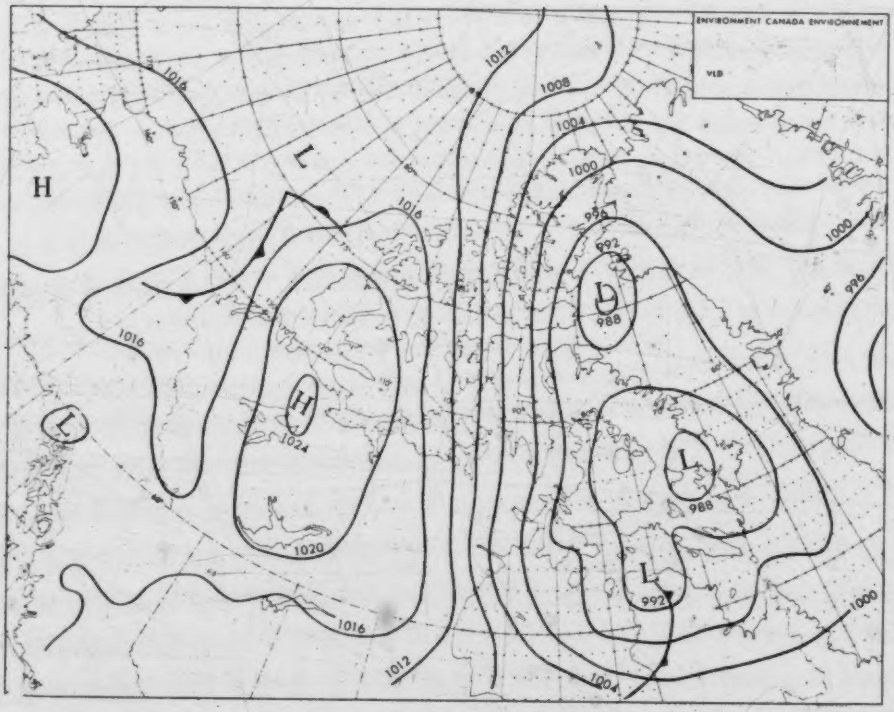
ENVIRONMENT CANADA ENVIRONNEMENT
VLD
1012
1008
1004
1000
996
992
L
988
1016
H
L
1016
1016
H
1024
L
1020
1016
1012
L
988
L
992
1000
1000
996
1004

Figure 2.17: Surface Map, 0000 GMT August 4, 1976

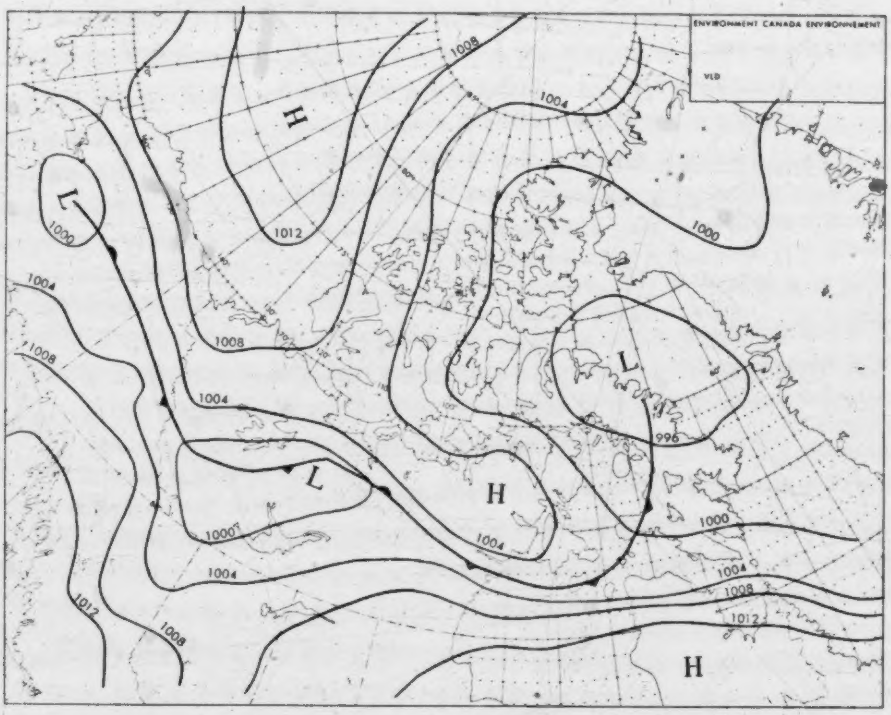
ENVIRONMENT CANADA ENVIRONNEMENT
VLD
1008
1004
H
L
1000
1012
1004
1008
1000
L
996
1004
L
H
1000
1004
1004
1008
1012
1012
1008
H

Figure 2.18: Surface Map, 0000 GMT August 9, 1976

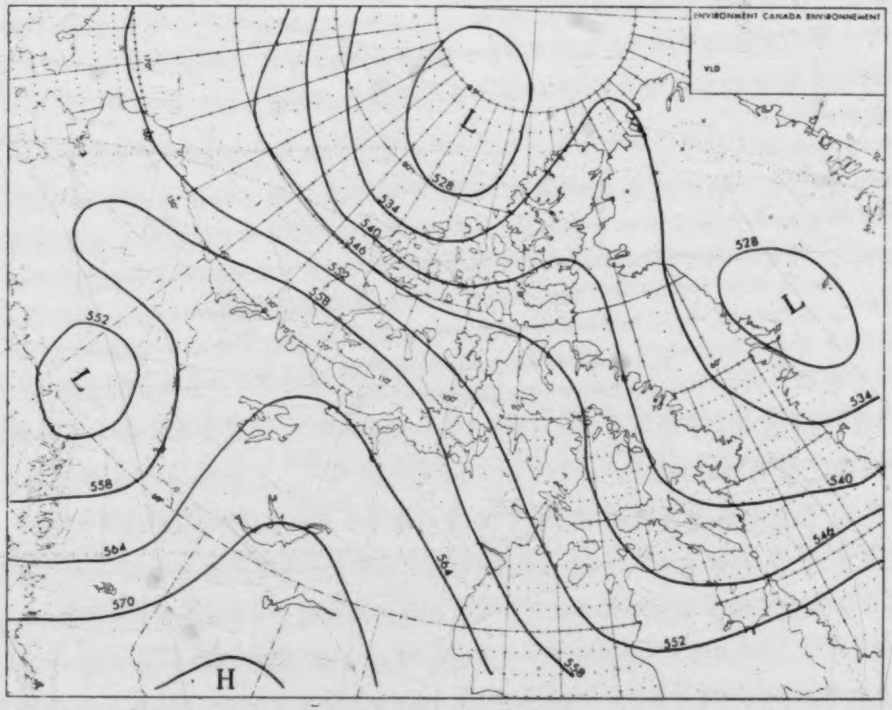
ENVIRONMENT CANADA ENVIRONNEMENT
VLD
L
528
534
540
546
552
558
528
L
552
L
534
558
564
570
564
540
546
552
558
H

Figure 2.19: 500-mb Contours, 1200 GMT August 12, 1976

After August 16, the upper flow underwent a major realignment. The 1200 GMT 500-mb chart of August 16, Figure 2.20, shows the upper trough invading western Alaska. By 0000 GMT August 19 (see Figure 2.21) the trough had progressed further eastward, and by 0000 GMT August 23 had taken a position over the central Canadian Arctic.

A strong, northwesterly flow existed over the Beaufort Sea at this time. A major surface low had developed near the North Pole and had assumed a position such that troughs rotating around the low would pass over the Beaufort Sea. (See Figure 2.22.)

While the realignment of the upper flow was taking place, two small, synoptic-scale disturbances formed in northern Alaska and moved to the Beaufort Sea, in the vicinity of the Mackenzie Delta. Both systems, the first on August 16 and the second on August 18, underwent significant development over a relatively short time period, before filling and tracking northeastward along the west coast of Banks Island.

Troughs rotating around the surface low near the Pole passed over the Beaufort Sea on August 22 and 25. The 0000 GMT surface map of August 22, Figure 2.23, shows one of these troughs (containing a frontal wave) approaching Banks Island.

On August 25 an upper ridge began to build over the western Canadian Arctic. The 0000 GMT 500-mb chart of August 28, Figure 2.24, shows the ridge position that was maintained until the end of the month.

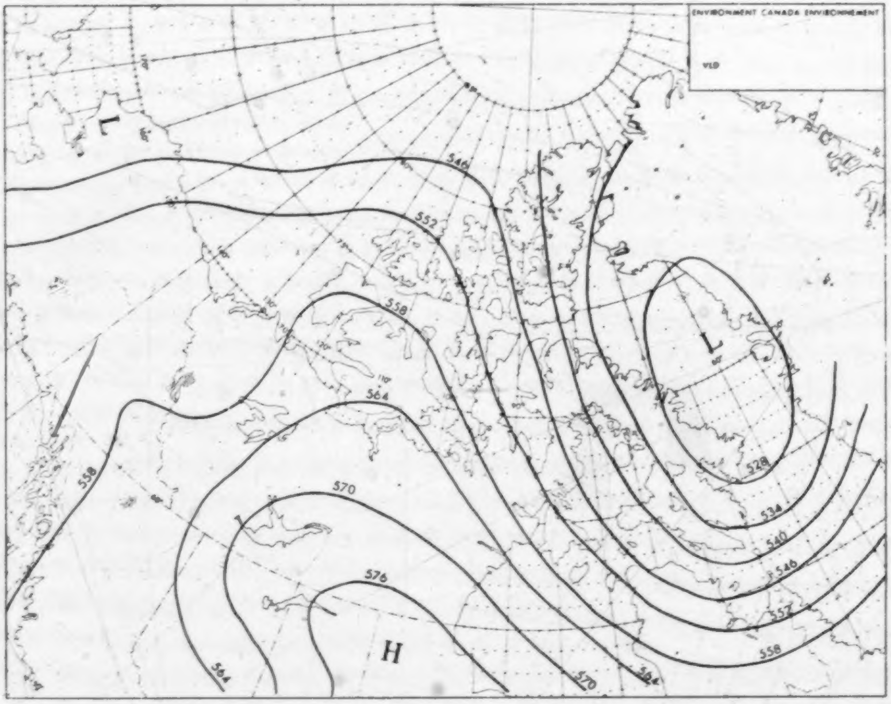
ENVIRONMENT CANADA ENVIRONNEMENT
L
546
552
558
564
570
576
H
L
528
534
540
546
552
558
564
570

Figure 2.20: 500-mb Contours, 1200 GMT August 16, 1976

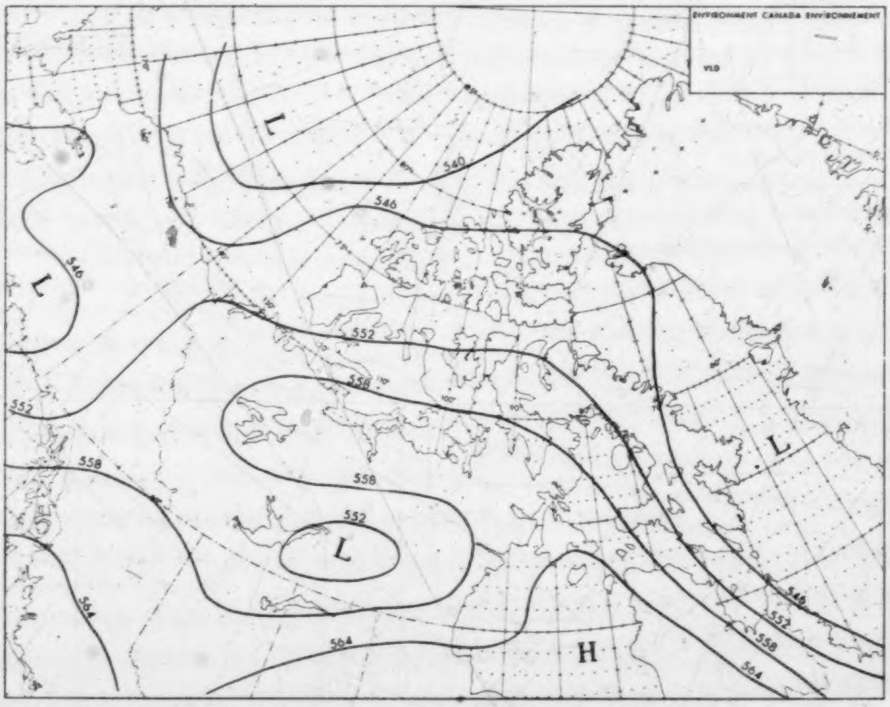
ENVIRONMENT CANADA ENVIRONNEMENT
L
540
546
L
546
552
552
558
558
552
L
558
564
564
H
L
546
552
558
564

Figure 2.21: 500-mb Contours, 0000 GMT August 19, 1976

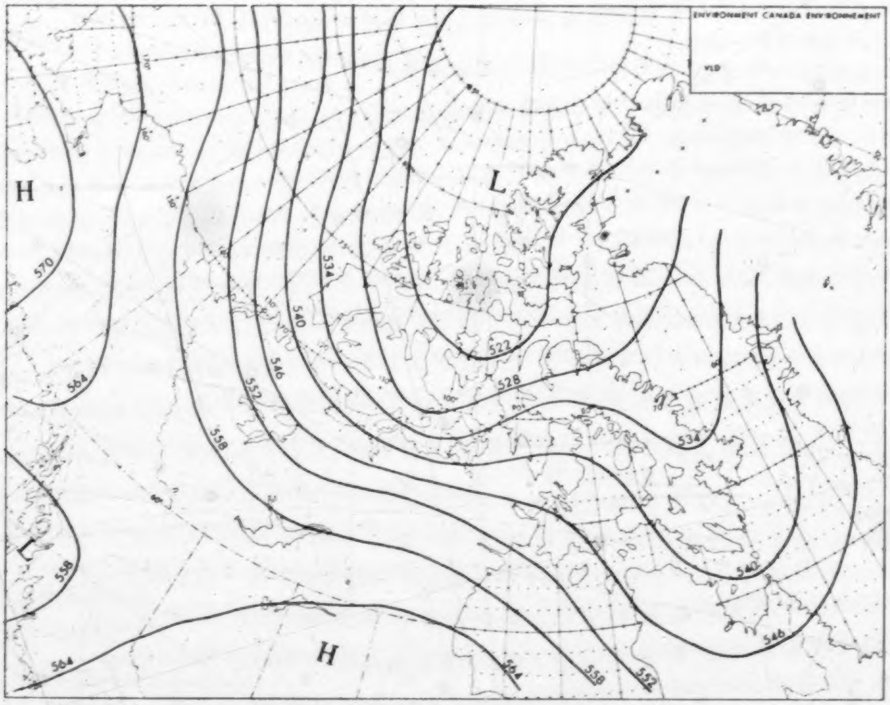
ENVIRONMENT CANADA ENVIRONNEMENT
VLD
H
L
570
564
534
540
546
552
558
522
528
534
L
558
564
H
564
558
552
540
546

Figure 2.22: 500-mb Contours, 0000 GMT August 23, 1976

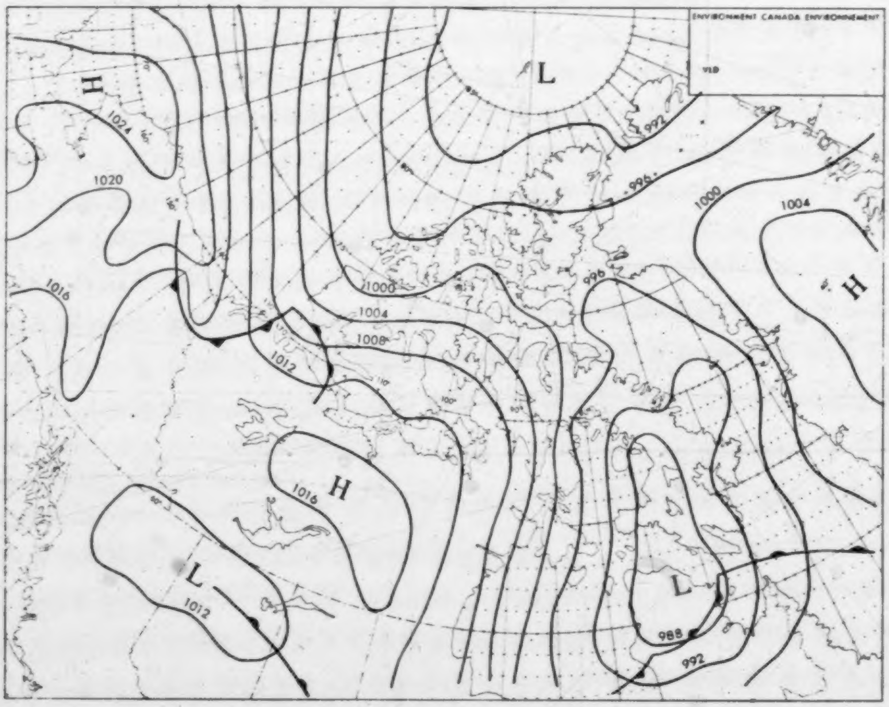
ENVIRONMENT CANADA ENVIRONNEMENT
VLD
L
H
1024
1020
992
996
1000
1004
H
1016
1000
1004
1008
1012
996
H
1016
L
1012
L
988
992

Figure 2.23: Surface Map, 0000 GMT August 22, 1976

The 0000 GMT surface map of August 26, Figure 2.25, shows an anticyclone centred over Banks Island with a deepening trough over Alaska and the Yukon. By 0000 GMT August 28, (Figure 2.26), the amplitude of the trough had increased substantially and a strong, southeasterly flow prevailed over the Beaufort Sea. By 0000 GMT on August 29, (Figure 2.27), the trough, extending from a major low near Siberia, had become quasi-stationary in a line through the Mackenzie Delta and southeastward into northern Alberta. The winds were generally light in the trough, which was traversed by a number of small, frontal waves embedded in the flow. This situation continued to the end of the month.

Feuerherdt (1977) studied wind records from two drilling sites located near the Mackenzie Delta, in the Beaufort Sea, obtained while the Beaufort Advance Base was in operation, from July to October, 1976. Local wind reporting began on July 20. The records for August indicate that the winds had an easterly component 60 percent of the time. This suggests high pressure over the Beaufort Sea to the north, and low pressure over the mainland to the south for most of that period. The easterly circulation kept the coastal waters relatively ice-free during the drilling season.

Strong winds can cause problems for off-shore drilling. In cataloging disturbances which caused winds in excess of 20 knots for at least six hours duration, eight such incidents were recorded in July and twelve in August, a windy month with marked cyclonic activity.

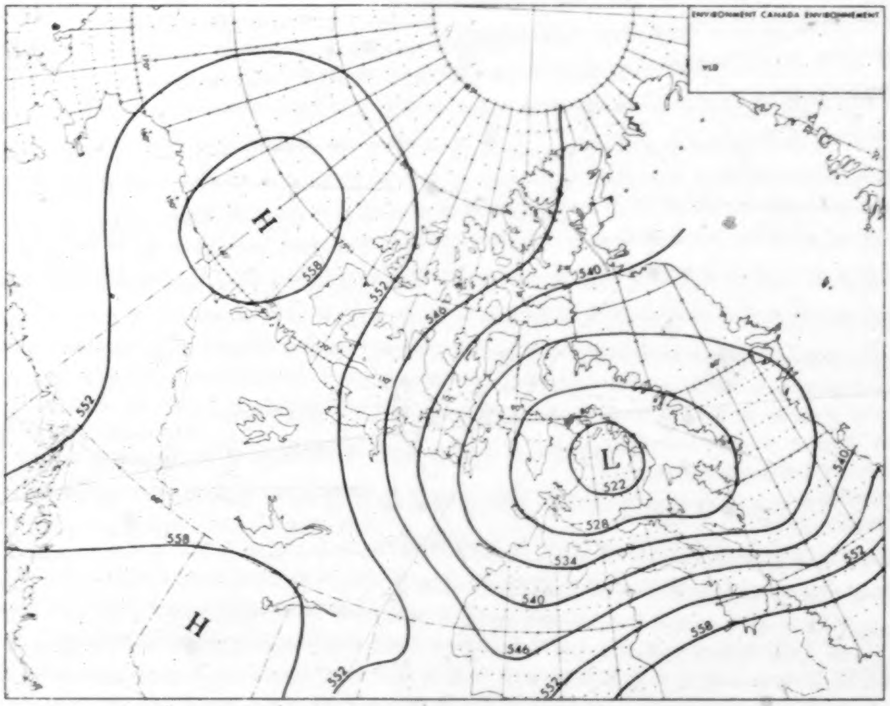
ENVIRONMENT CANADA ENVIRONNEMENT
H
558
552
546
540
L
522
528
534
540
546
552
558
H
558
552
552
540
552

Figure 2.24: 500-mb Contours, 0000 GMT August 28, 1976

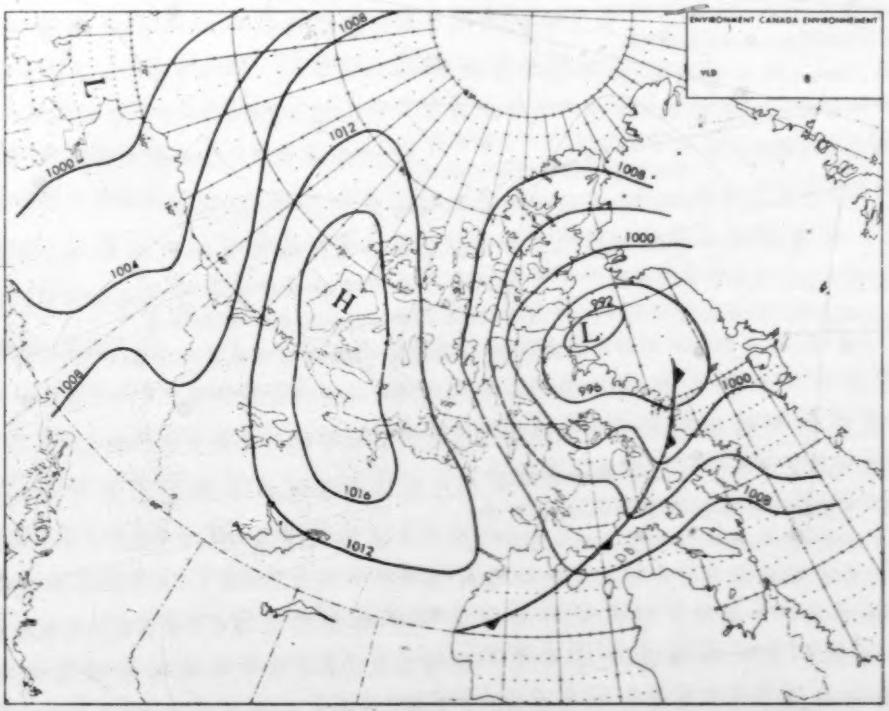
ENVIRONMENT CANADA ENVIRONNEMENT
L
1008
1000
1004
1008
1012
H
1016
1012
1008
1000
992
L
996
1000
1008

Figure 2.25: Surface Map, 0000 GMT August 26, 1976

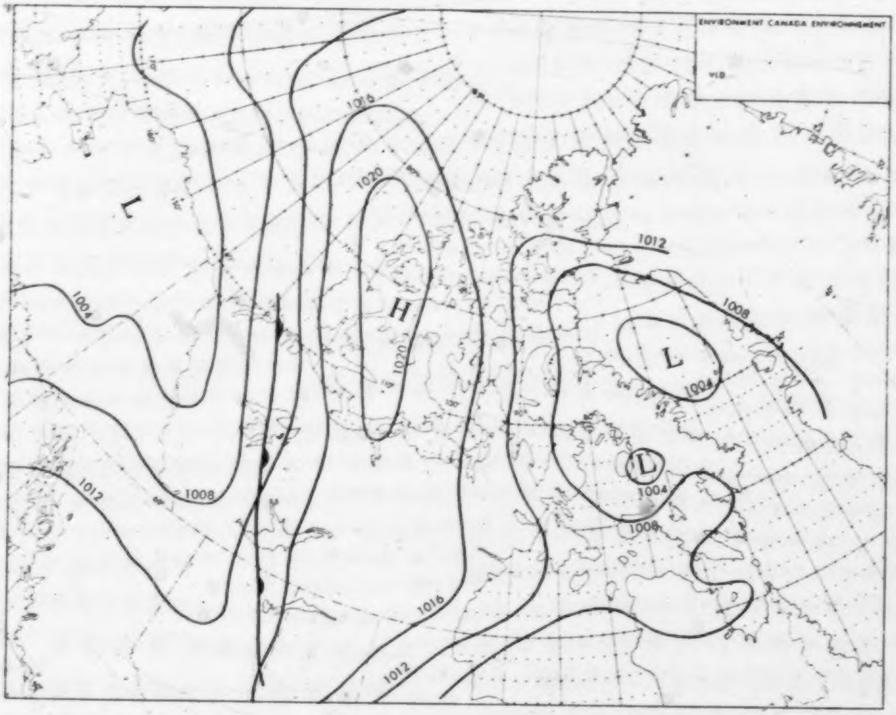
ENVIRONMENT CANADA ENVIRONNEMENT
VLD
L
H
L
L
1004
1008
1012
1016
1020
1020
1016
1012
1012
1008
1004
1004
1008

Figure 2.26: Surface Map, 0000 GMT August 28, 1976

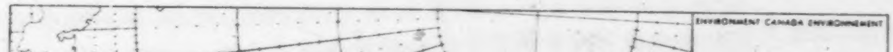
ENVIRONMENT CANADA ENVIRONNEMENT
VLD
1012
1016
1020
1008
1012
L
L
L
H
H
L
L
1008
1016
1020
1020
1012
1012
1008
1004
996
1000

Figure 2.27: Surface Map, 0000 GMT August 29, 1976

Since wind is a critical forecast parameter for safe offshore operations, it is important to identify as early as possible those disturbances which are likely to undergo rapid intensification in the drilling area. In the 1976 drilling season three small, synoptic-scale depressions were observed to intensify suddenly over the waters of the Beaufort Sea. These disturbances which occurred on July 30, August 16 and August 18, are described in detail in Chapter 5.

CHAPTER 3

THE ARCTIC INVERSION

3.1 Introduction

An inversion is defined as a layer of air through which the temperature increases with height. This is the reverse of the normal lapse rate. The most important characteristic of an inversion layer is that it is very stable and exerts a damping or stabilizing effect on meteorological processes below the inversion.

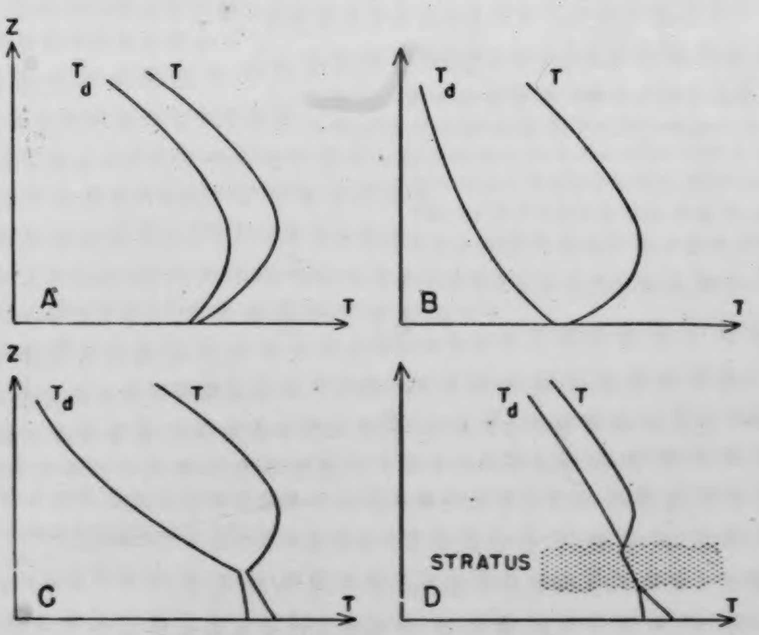

Figure 3.1: Temperature inversions (After Petterssen, 1956).

Petterssen (1956) has described four principal mechanisms for the formation of temperature inversions. In Figure 3.1, Diagram A shows an inversion caused by cooling from the surface below, resulting in smaller dewpoint depressions nearer to the surface. The base of the inversion is usually at the ground, but may be modified by mixing and heating at the surface, and so may be above ground. This type will form in most areas under conditions of clear skies, little or no insolation and light winds.

The inversion in Diagram B is formed by the subsidence or sinking of a layer of air. The base of the subsidence inversion can be on the ground, but frequently develops in the free atmosphere, at almost any level above the ground. The main feature is the decreased relative humidity of the air in the inversion layer. Diagram C shows a subsidence inversion which has been modified by surface heating or by turbulent mixing caused by strong winds.

The inversion in Diagram D has been formed by surface cooling followed by mixing. If sufficient moisture is present a layer of stratiform cloud often forms below the base of the inversion.

Ignoring frontal inversions, subsidence and radiative cooling produce most inversions. Inversions can be modified by processes such as mechanical turbulence, differential advection, moisture distribution, wind shear and orographic effects.

There are two classes of semi-permanent inversions on the Earth. The trade-wind inversion is found at low latitudes and is associated with the subsidence in the subtropical highs. The polar inversion is radiational in nature and a characteristic feature of the Arctic and Antarctic regions.

3.2 Climatology of the Arctic Inversion

Since the characteristic Arctic inversion is formed when the surface of the Earth radiates more energy than it receives, winter is the most favourable time of the year for its occurrence. The development of the Arctic inversion in winter is analogous to a nocturnal inversion at lower latitudes, only on a larger scale in time and height. The formation process is described by Wexler (1936).

The situation in summer differs from winter in that solar insolation reaching the Arctic has increased, causing an increase in the radiation absorbed by the Earth's surface, especially over snow-free land. However, large areas of the Arctic Ocean remain ice-covered throughout the summer and cool the air above. Strong inversions develop over the ice and water regions, and also along coasts that are susceptible to onshore flows. Cold air from the ice fields moves inland and wedges under air that has been heated over the ground, producing particularly strong inversions at some coastal stations.

Several authors have examined the climatology of the Arctic inversion, including Belmont (1956), Vowinckel (1965) and Thompson (1972). Belmont considered the inversions measured on the Arctic ice island T-3. He used two years of statistics to establish criteria for the intensity of inversions, frequency of occurrence, and a classification system. This study showed the very complicated nature of Arctic inversions.

Vowinckel (1965) investigated inversions over the Arctic Ocean. Using radiosonde data from coastal stations in the Arctic, he classified the ascents as having no inversion, a surface inversion or an upper inversion. The inversions were characterized by ΔT, the difference between the temperature minimum below the inversion and the highest temperature reached in the inversion, the height of the maximum temperature reading, and the depth of the inversion or isothermal layer. By compiling the frequency distribution of inversion types over a part of the Arctic Ocean, Figure 3.2, Vowinckel found that inversions of some description were present no less than 59 percent of the time during any month of the year. The lowest frequency of 59 percent was observed in June, and the highest, close to 100 percent, in March and April. The number of upper inversions increases in the summer, since they are caused by mechanisms other than radiation loss.

Figure 3.3 from Vowinckel shows the area distribution of the frequency of surface-based inversions in winter. The highest frequencies are found north of Siberia. A similar map is not available for the summer months; however, Vowinckel (Figure 3.4) provides a map showing the vertical temperature gradient between the surface and the 850-mb level in summer. Positive numbers indicate a higher temperature at 850 mb. The only area with positive numbers is the Alaskan sector of the Beaufort Sea. This suggests that inversions would most likely be found in this area on most days of the year.

Bilello (1966) and Munn et al. (1970) summarized the frequencies of ground-based inversions at some Canadian Arctic radiosonde stations. The study by Munn and his co-workers included all of Canada. Figure 3.5, adapted from Munn et al., gives the summer frequencies for 2300 and 1100 GMT radiosonde ascents. Maximum

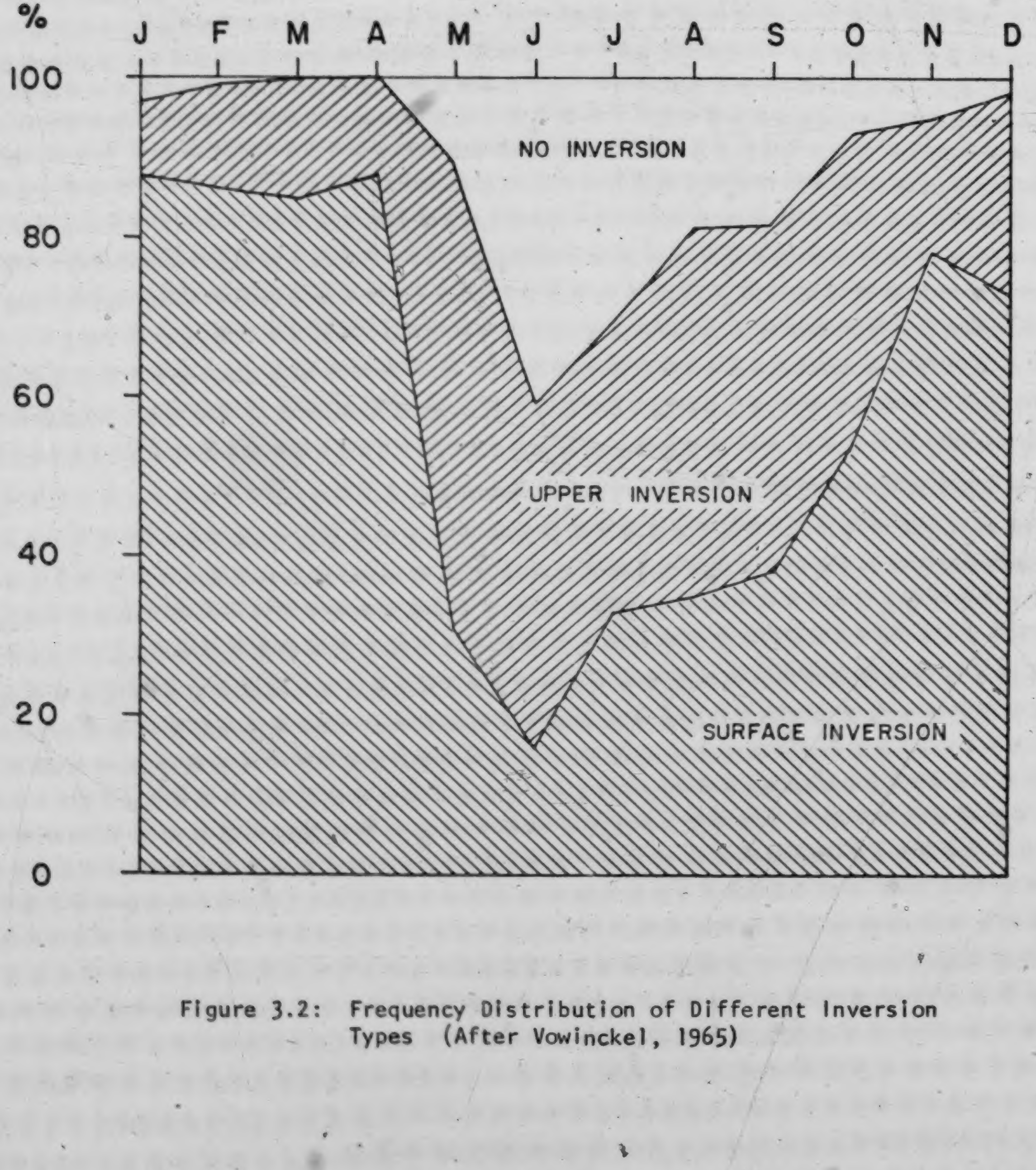

Figure 3.2: Frequency Distribution of Different Inversion Types (After Vowinckel, 1965)

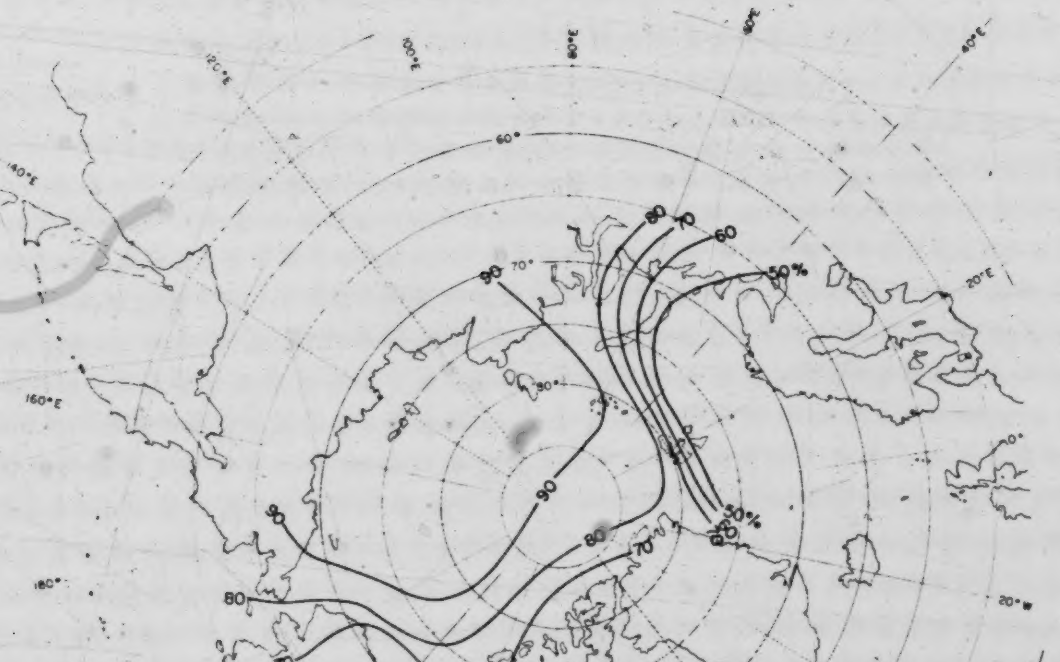
120°E
100°E
80°E
60°E
40°E
20°E
0°
20°W
40°W
60°W
80°W
100°W
120°W
140°W
160°W
180°
160°E
140°E
60°
70°
80°
90°
90
90
80
70
60
50%
50%
60
70
80
80
80
70
60
50
60
50
FREQUENCY (%) OF SURFACE
INVERSION
WINTER
FIG. 7

Figure 3.3: Area Distribution of the Frequency of Surface-based Inversions in Winter (After Vowinckel, 1965)

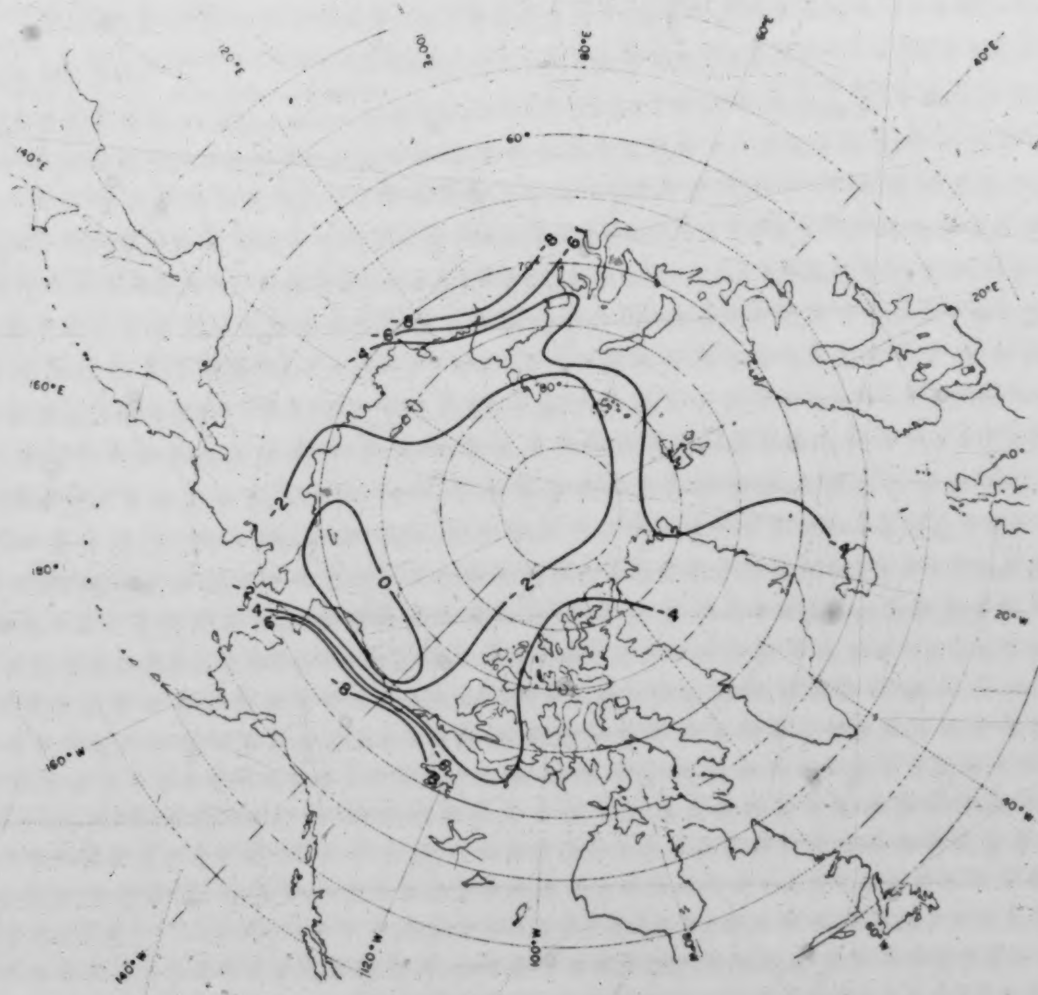
120°E
100°E
80°E
60°E
40°E
140°E
60°
20°E
160°E
70°
80°
0°
180°
20°W
160°W
40°W
140°W
120°W
100°W
80°W
60°W
-8
-6
-4
-6
-8
-2
0
-2
-4
-4
-2
-4
-6
-8
-6
-8

Figure 3.4: Vertical Temperature Difference Between the Surface and the 850-mb Level in Summer ($^{\circ}C$) (After Vowinckel, 1965)

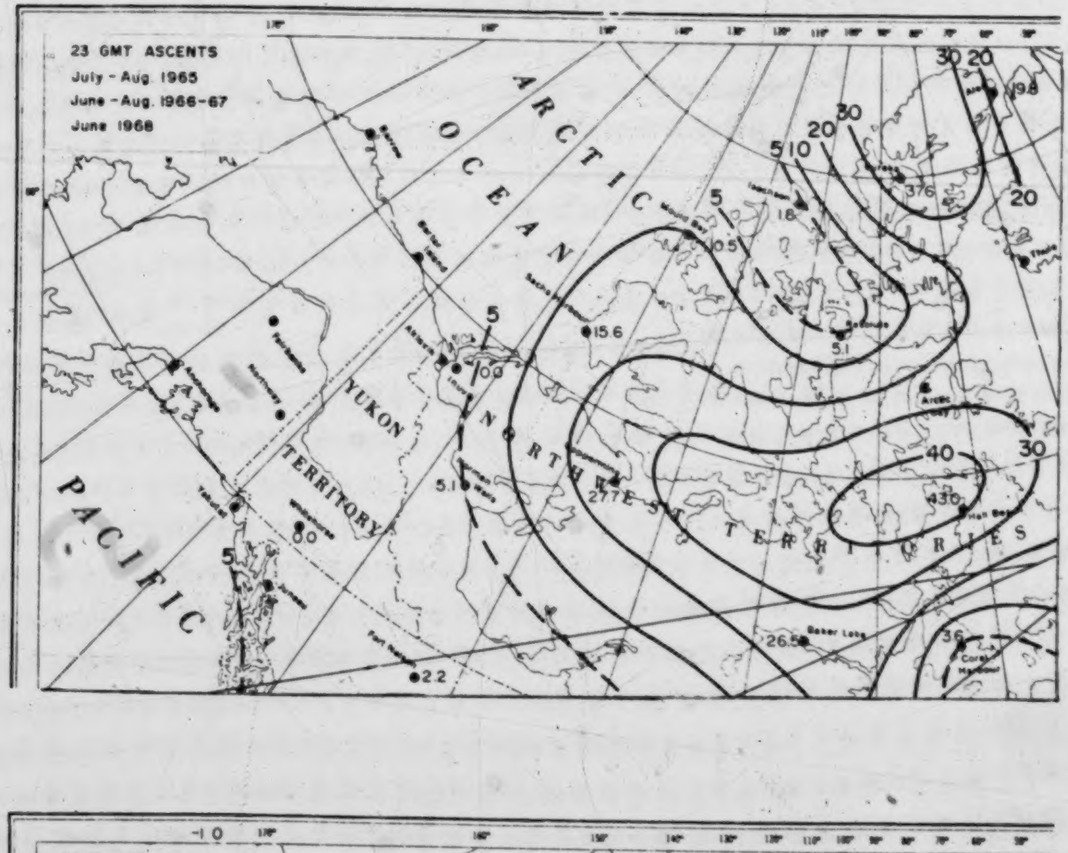
23 GMT ASCENTS
July - Aug. 1965
June - Aug. 1966-67
June 1968
ARCTIC OCEAN
YUKON TERRITORY
NORTH WEST TERRITORIES
PACIFIC
30
20
19.8
5
10
20
30
37.6
20
1.8
10.5
5
15.6
5.1
5
0.0
5.1
27.7
40
30
43.0
0.0
5
26.5
36
2.2
11 GMT ASCENTS
July - Aug. 1965
June - Aug. 1966-67
June 1968
40
42.3
30
36.1
40
20
10
9.8
20
10
19.3
40
30
50
60
43.8
26.7
60.8
60
68.6
44.4
65.6
50.1
45.9
25.3

Figure 3.5: Percentage Frequencies of Ground-based Inversions in Summer (After Munn et al., 1970)

frequencies for 2300 GMT soundings occur near the northwestern corner of Baffin Island and decrease towards the Beaufort Sea. For the 1100 GMT ascents, a minimum frequency is found near Isachsen, and values increase towards the south and west, the result of overnight cooling. Only the eastern edge of the Beaufort Sea is included in the area of calculated frequencies. The percentage frequencies at Sachs Harbour are given as 15.6 percent at 2300 GMT and 43.8 percent at 1100 GMT. The corresponding values for Inuvik are zero and 60.8 percent. The percentiles obtained by Munn et al., Bilello, and Vowinckel seem to be in reasonably good agreement.

Figure 3.6 (Vowinckel, 1965) gives the intensity of surface-based inversions at different times of the year. The diagram shows that in summer a temperature rise of 10°C from the surface to the warmest point in the inversion occurs less than 5 percent of the time. Radiational cooling plays a smaller role in summer. Inversions are known to be much more pronounced in the winter months. The more intense inversions are supported by subsidence and warm air advection aloft.

In summary, the Arctic inversion in summer is much less intense than in winter. Nevertheless, the frequency of occurrence of summer inversions is still relatively high. The inversions are strengthened by subsidence and, especially near coastlines, by the advection of warm air aloft over cold air at the surface - air that has been cooled by an ocean of ice and water, a mixture which remains near 0°C throughout the summer.

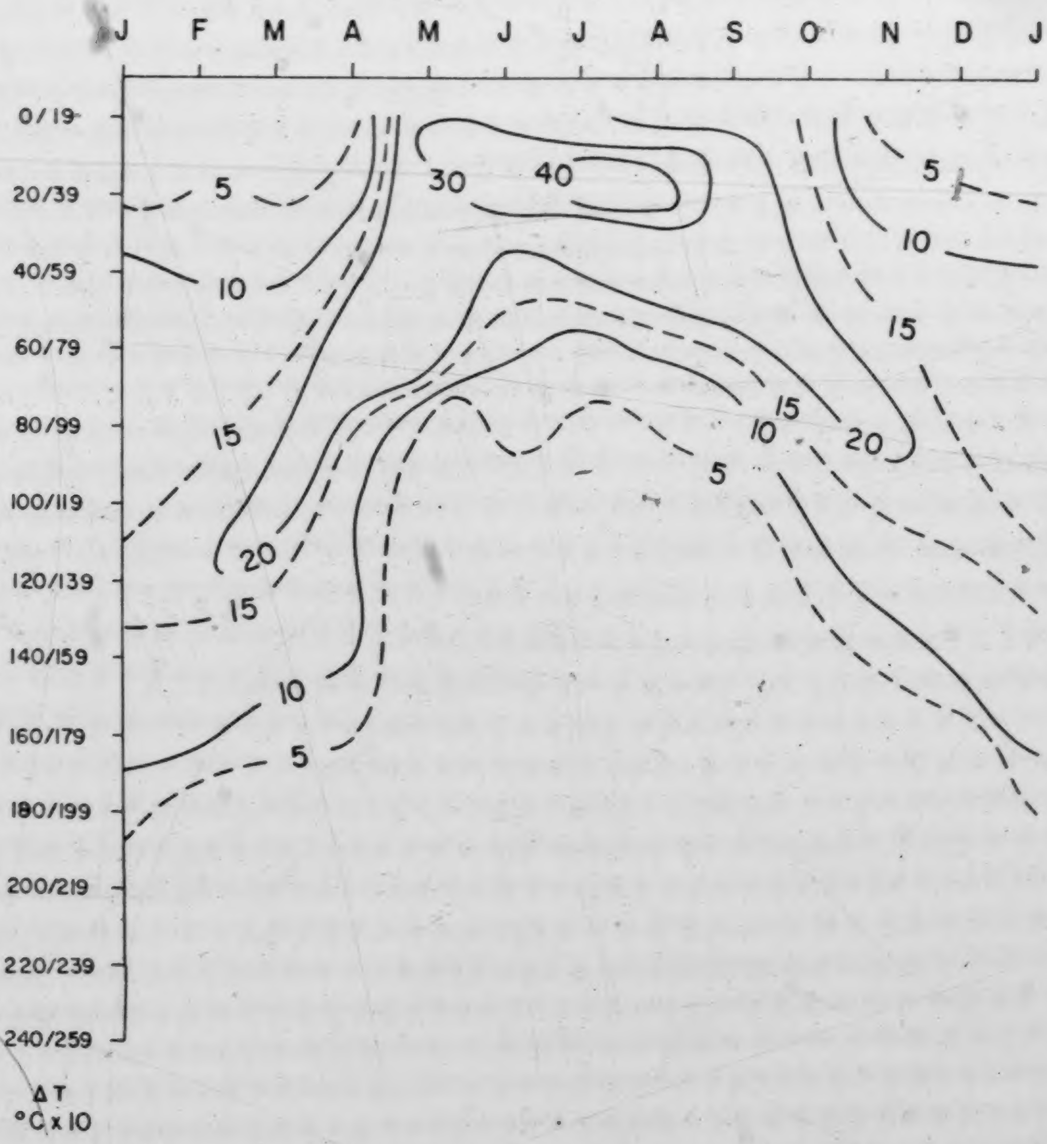

Figure 3.6: Intensities of Surface-based Inversions throughout the Year, Expressed in Terms of Percent Frequencies of Different ΔT Intervals (From Vowinckel, 1965)

D

The Beaufort Sea is a favoured area for inversions in the warm months. Coastal stations that border on the Arctic Ocean are more likely to show inversions than inland stations. When sufficient moisture is available, low stratiform cloud or haze will often be present at the base of an inversion.

3.3 Inversions Observed in Summer 1976

Five upper-air reporting stations were selected for the study of inversions. Sachs Harbour, Barter Island and Point Barrow are coastal stations that border the Arctic Ocean, while Inuvik and Norman Wells are more representative of inland points. Upper-air temperatures were extracted from the radiosonde reports issued twice daily at 0000 and 1200 GMT. (In practice, the ascents usually commence at 2315 and 1115 GMT.) The early collection of significant-level data was received at the Arctic Weather Centre, Edmonton, Alberta. Since the data could not be checked against official records, some errors introduced in transmitting and transcribing the reports may have gone undetected.

The months of July, August and September, 1976, were chosen as representative of summer in the Arctic. A total of 865 ascents from the five stations were cataloged for these months. Temperatures and dew points were recorded for the 700-mb level and below.

Norman Wells (65° 17'N, 126° 48'W) located in the Mackenz River Valley, is relatively remote from any large body of water. Inversions observed at Norman Wells should be characteristic of most inland areas.

Inuvik (68° 18'N, 133° 29'W) is situated in the Mackenzie Delta. This observation site is quite close to the Beaufort Sea; it is influenced by onshore winds, but not to the same extent as the coastal stations immediately adjacent to the ocean. Inuvik is subject to inversion conditions similar to those found at inland stations.

Sachs Harbour (71° 59'N, 125° 17'W) located on the west coast of Banks Island, is exposed to cold air off the Beaufort Sea whenever the wind has a westerly component. When winds are from other directions, the air may be modified by heating as it passes over the island.

Barter Island (70° 08'N, 143° 38'W) and Point Barrow (71° 18'N, 156° 47'W) are both on the north coast of Alaska. The daily weather at the two stations is highly influenced by their close proximity to the Beaufort Sea. Some very strong inversions develop when air heated over the land is undercut by cold air off the Beaufort Sea.

The observed inversions were divided into three main categories. The first two groups include the strongest inversions as determined by temperature difference. The third group contains the weaker inversions, further classified into three sub-categories. It was desired to identify those inversions which involved the largest temperature increase from the base of the inversion to the warmest layer above. These inversions should be the easiest to find on IR satellite imagery. The strongest inversions are usually confined to levels below 850-mb, since they are largely the result of various boundary layer processes, such as radiational cooling and low-level cold-air advection modified by turbulent mixing. The classification system was set up with the nature and extent of these processes in mind.

Class 1. The difference between the surface temperature and the highest temperature in any layer up to, and including, the 850-mb level is greater than or equal to 10°C.

Class 2. The difference between the surface temperature and the highest temperature in any layer up to, and including, the 850-mb level is greater than or equal to 5°C, but less than 10°C.

Class 3. The difference between the surface temperature and the highest temperature in any layer up to, and including the 850-mb level is less than 5°C but either:

A. The base of the inversion is not on the surface, and the temperature difference between the base and the highest temperature in the layer is greater than or equal to 5°C; or

B. near-isothermal conditions exist between the surface and 850-mb (i.e., the difference in temperature between the levels is less than or equal to 4°C); or

C. neither of the above conditions exist, but at some level a temperature in the layer is higher than that at the surface.

Class 4. The ascent is free of inversions in the sense that none of the above conditions applies.

Each ascent was examined and classified in accordance with the above criteria. The results for each of the five stations are presented in tabular form in Appendix A. For the three months a total of 920 radiosonde reports were possible from the five stations. However, 55 of the data sets were missing, leaving 865 ascents to be classified. Point Barrow accounted for 29 of the missing reports; of these, 18 reports were missing in July (out of a possible 62) which makes the statistics for this month less reliable. A total of only 14 reports were missing from the three Canadian stations and these were quite evenly distributed, three each from Sachs Harbour and Inuvik, and eight from Norman Wells.

In compiling the totals for each inversion classification, some interesting aspects come to light. The incidence of inversions at the coastal stations was far greater than at the stations farther inland. The frequency tables below give evidence of this. The table for each month shows the frequency of occurrence of each inversion class at 0000 and at 1200 GMT.

Individual frequencies are calculated for each time period in order to identify the nocturnal inversions better. The tables show that very few inversions were present at Norman Wells or Inuvik in the late afternoon near the time of the 0000 GMT ascent. At the coastal stations temperature inversions showed up frequently in both the 0000 and 1200 GMT ascents. In fact, for Barter Island every reported ascent in July fitted readily into one of the three inversion classifications.

Table 3.1

July 1976

		Class 1	Class 2	Class 3			Class 4
				A	B	C	
Norman Wells	00Z	0	0	0	0	.07	.93
	12Z	.03	.36	0	.32	.13	.16
Inuvik	00Z	0	0	0	.10	0	.90
	12Z	0	.10	.10	.23	.42	.16
Sachs Harbour	00Z	0	.13	0	.26	.06	.55
	12Z	.03	.13	.03	.55	.10	.16
Barter Island	00Z	.25	.39	.07	.21	.07	0
	12Z	.40	.37	0	.23	0	0
Point Barrow	00Z	.09	.35	.13	.22	.09	.13
	12Z	.29	.24	.10	.33	.05	0

Table 3.2

August 1976

		Class 1	Class 2	Class 3			Class 4
				A	B	C	
Norman Wells	00Z	0	0	0	0	0	1.00
	12Z	0	.17	0	.41	.10	.31
Inuvik	00Z	0	0	0	.03	0	.97
	12Z	0	.14	.07	.45	.14	.21
Sachs Harbour	00Z	0	.03	0	.63	0	.33
	12Z	.03	.17	.07	.63	0	.10
Barter Island	00Z	.24	.24	.07	.28	.10	.07
	12Z	.33	.23	.03	.30	.07	.03
Point Barrow	00Z	.10	.23	.10	.40	.03	.13
	12Z	.22	.22	0	.56	0	0

Table 3.3

September 1976

		Class 1	Class 2	Class 3			Class 4
				A	B	C	
Normal Wells	00Z	0	0	0	.07	.03	.90
	12Z	.12	.23	0	.38	.04	.23
Inuvik	00Z	0	.03	.07	.17	.07	.67
	12Z	0	.24	.03	.41	.17	.14
Sachs Harbour	00Z	0	.07	.07	.40	0	.47
	12Z	0	.10	.07	.59	.07	.17
Barter Island	00Z	0	.38	0	.42	.04	.15
	12Z	.07	.31	.14	.38	.03	.07
Point Barrow	00Z	0	.07	.22	.25	.04	.41
	12Z	0	.19	.07	.44	.11	.19

Norman Wells and Inuvik had much higher frequencies of occurrence at 1200 GMT than at 0000 GMT. This emphasizes the inland nature of the two stations, characterized by afternoon instability produced by daytime heating, and morning inversions caused by nocturnal cooling. Sachs Harbour had a greater frequency of inversions than Norman Wells or Inuvik but a lower frequency than the two Alaskan coastal stations. Near-isothermal conditions (Class 3B) occurred more often at Sachs Harbour than at other stations. The highest frequency of strong inversions (Class 1) was reported at Barter Island.

The combined frequencies of occurrence of all Class 1, 2 and 3 inversions encountered in both the 0000 and 1200 GMT ascents are listed below in Table 3.4.

Table 3.4

Frequency of Occurrence of All Classes of Inversions

	July	August	September
Norman Wells	.46	.35	.44
Inuvik	.47	.41	.60
Sachs Harbour	.65	.79	.68
Barter Island	1.00	.95	.89
Point Barrow	.94	.94	.70

The Norman Wells frequencies vary only by some 10 percent from the three-month summer mean, suggesting that most temperature inversions at interior sites are due to nocturnal cooling.

The Inuvik frequencies closely resemble the figures for Norman Wells except for September, when the number of inversions increased substantially. Referring back to Table 3.3, it is seen that, in September, the higher frequency at Inuvik largely reflects an increase in the number of afternoon (0000 GMT) inversions. This can be attributed to decreasing solar radiation, i.e., less heating at the Earth's surface in late summer.

The Sachs Harbour figures are fairly consistent, peaking slightly in August. Barter Island and Point Barrow, with very high frequencies in July and August, show a definite decrease in September. This decrease is probably the result of more frequent air-mass destabilization along the Alaskan coast, caused by advection of unstable maritime Arctic air at all levels.

Obviously, a great deal more information could be extracted from the radiosonde data. However, it is not the purpose of this study to investigate the structure of inversions in detail. It was only desired to demonstrate the extent and persistence of the Arctic inversion in summer, and to provide a brief climatological summary of its main characteristics.

CHAPTER 4

THE USE OF SATELLITE IMAGERY FOR OBSERVING THE TEMPERATURE STRUCTURE NEAR THE EARTH'S SURFACE

4.1 Introduction

When satellite data are used for estimating temperature, it is, of course, the IR image that contains the required information. IR radiation is emitted at many levels of the Earth - atmosphere system - from the ground, by water, ice, cloud and by concentrations of dense water vapour in the air that are not normally visible as cloud. The IR data can be used to estimate the equivalent blackbody temperature of the source of the long-wave radiation. The visible range image can also be useful in a qualitative way for identifying the origin of radiation.

Two basic approaches are used for displaying the thermal characteristics of the atmosphere near the surface of the Earth by the use of satellite imagery. One method involves converting the digitized IR data into a series of shades of gray and displaying the results as a photographic image. This procedure offers the advantage of putting the data into an easily recognizable, compact form, practical for covering a large geographical area. It has the disadvantage of not being readily adaptable to quantitative applications. When several shades of gray are used, it often becomes difficult to differentiate visually between neighbouring levels.

The second method entails a more objective usage of the IR digital values. Each data point resolved by the SR and digitizing process can be examined and operated on in turn. In this manner a quantitative analysis of the satellite imagery is performed. Representative temperatures and temperature gradients may be inferred by converting the digitized IR data into equivalent blackbody temperatures using the known response curve of the SR. The resulting temperatures may then be displayed in their original scan line positions, and the ensuing thermal field subjected to a conventional isotherm analysis.

A combination of the two display methods is sometimes helpful in providing an overview of, as well as deeper insight into the thermal conditions near the surface of the Earth.

4.2 Temperature Structure in Gray-Scale Display

Early-morning imagery of the Western Arctic is not available because of the cyclic variation of the satellite orbit throughout the day. However, by local noon the satellite has progressed far enough westward to be able to "see" the Western Arctic for the first time. Thereafter, several successive orbital passes provide a series of partially overlapping images of the Canadian and Alaskan sectors of the Arctic Basin throughout the afternoon and evening. The study of the Arctic inversion in summer by the use of satellite imagery is thus largely confined to the very time of the day when inversions are likely to be least intense.

The classification detailed in Chapter 3 was used to select days with intense inversions at the coastal stations. It was thought to be advantageous to consider the most intense 0000 GMT inversions first, since the satellite data should then contain the most obvious examples of anomalies in the thermal structure.

The inversions of July 22 were examined first. As noted in the classification tables of Appendix A, Class 1 inversions were present in the early morning (1200 GMT) at Barter Island and in the evening (0000 GMT, July 23) at Barter Island and Point Barrow. In addition, the evening ascent at Sachs Harbour showed a Class 2 inversion. It is evident that a warm airmass was present over all three stations. Surface temperatures at Inuvik and Norman Wells were about 25°C. The tephigrams for the stations at 0000 GMT, July 23, (reproduced in Figure 4.1) give a good indication of the intensity of the inversions. The highest temperatures encountered in the ascents at the coastal stations averaged 14°C. Surface temperatures on the Alaskan coast at Barter Island and Point Barrow were less than 4°C.

The 0000 GMT surface analysis for July 23, Figure 2.11, shows a slack pressure gradient over much of the Beaufort Sea. From the orientation of the isobars easterly winds might be expected along the Alaskan coast. Winds should tend to be more southeasterly over Banks Island. The surface observations taken at 2300 and 0000 GMT showed very little cloud cover at any of the stations. The surface

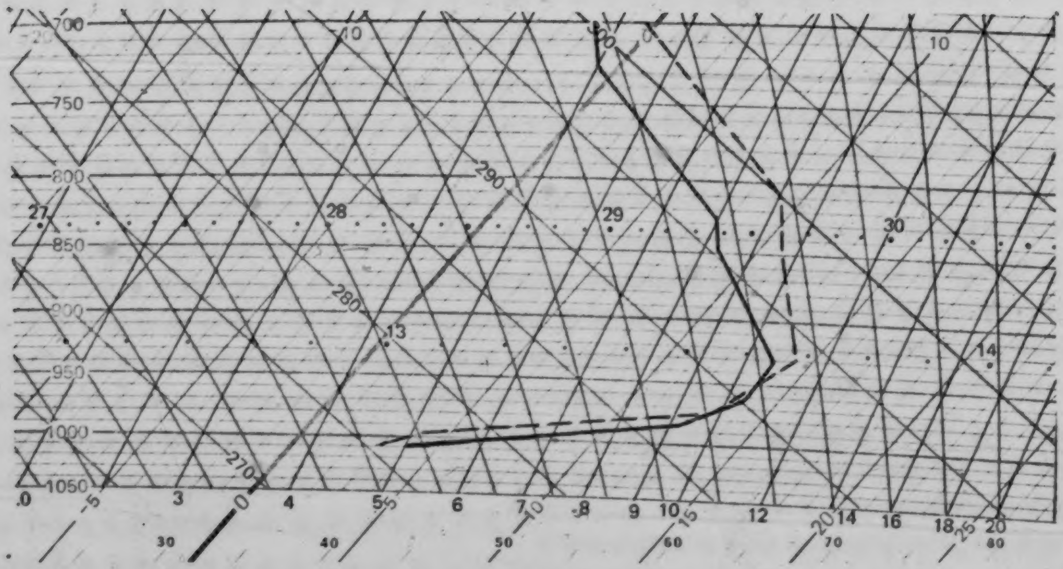

A. (i) Point Barrow —— (ii) Barter Island ----

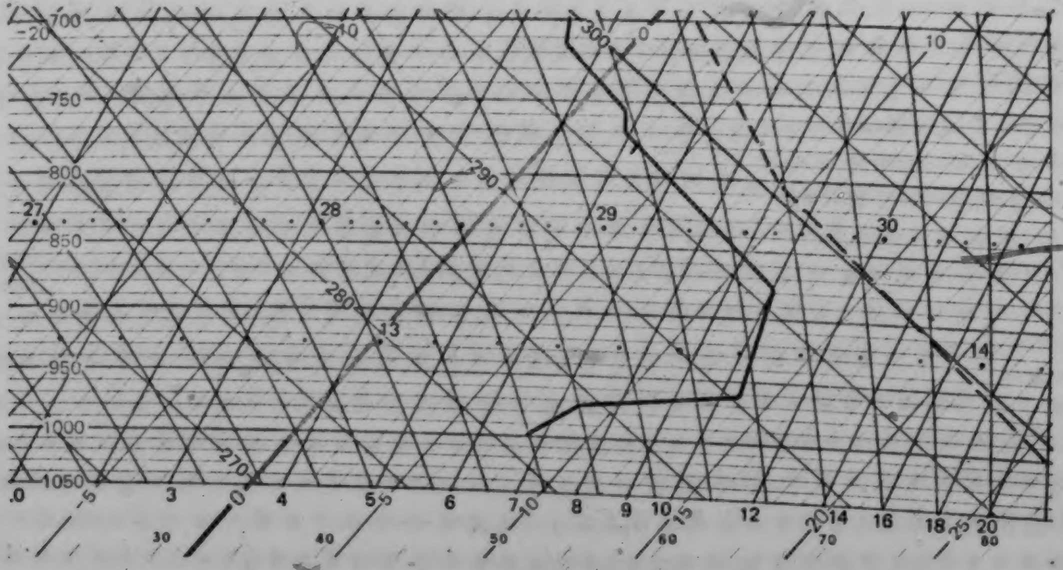

B. (i) Sachs Harbour —— (ii) Norman Wells ----

Figure 4.1: Tephigrams for 0000 GMT July 23, 1976

winds at Barter Island and Point Barrow had onshore components. At Sachs Harbour the wind was straight southerly, i.e., almost directly onshore.

The visible and IR satellite images displayed in Figures 4.2 and 4.3 are from Orbit 7704 of NOAA 4, 2256 to 2312 GMT on July 22, 1976, very close to the time of the radiosonde ascents. The images are generally centred on the Arctic Islands and the Beaufort Sea. Shades of gray are used to display the data. The short, double bars mark the intersections of meridians and parallels, at intervals of 20 degrees of longitude and 5 degrees of latitude. The single, solid marks indicate the 120°W meridian.

The late-afternoon surface observations indicate that very little cloud was present over the regions contiguous to the Beaufort Sea. These observations are supported by the satellite images, which show cellular patches of convective cloud over the mainland. There are also a few small patches of convective cloud over Banks Island, and a larger patch over Victoria Island. North of the Beaufort Sea toward the Pole, larger amounts of low and high cloud are present.

The Arctic Ocean is mostly ice-covered, but there is some open water along the coast of Alaska and Canada. Off the mouth of the Mackenzie River there is a relatively large area of open water which extends northward along the west coast of Banks Island. The open water has lower albedo than the ice and shows up as a darker area on the visible image. On the IR image there is some evidence of darker shades of gray in the areas of open water, indicative of higher temperatures. However, since the open water registers at almost the

SATELLITE IMAGE
GRIDDED ELC ENHANCED
SCALE=1:20M SRVIS
22JUL 7704 -135D 2256-2312Z
DORA IEPP UOFA YXD NOAA ITOS

Figure 4.2: Visible Range Image July 22, 1976, Orbit 7704 2256-2312 GMT. An example of strong inversion conditions.

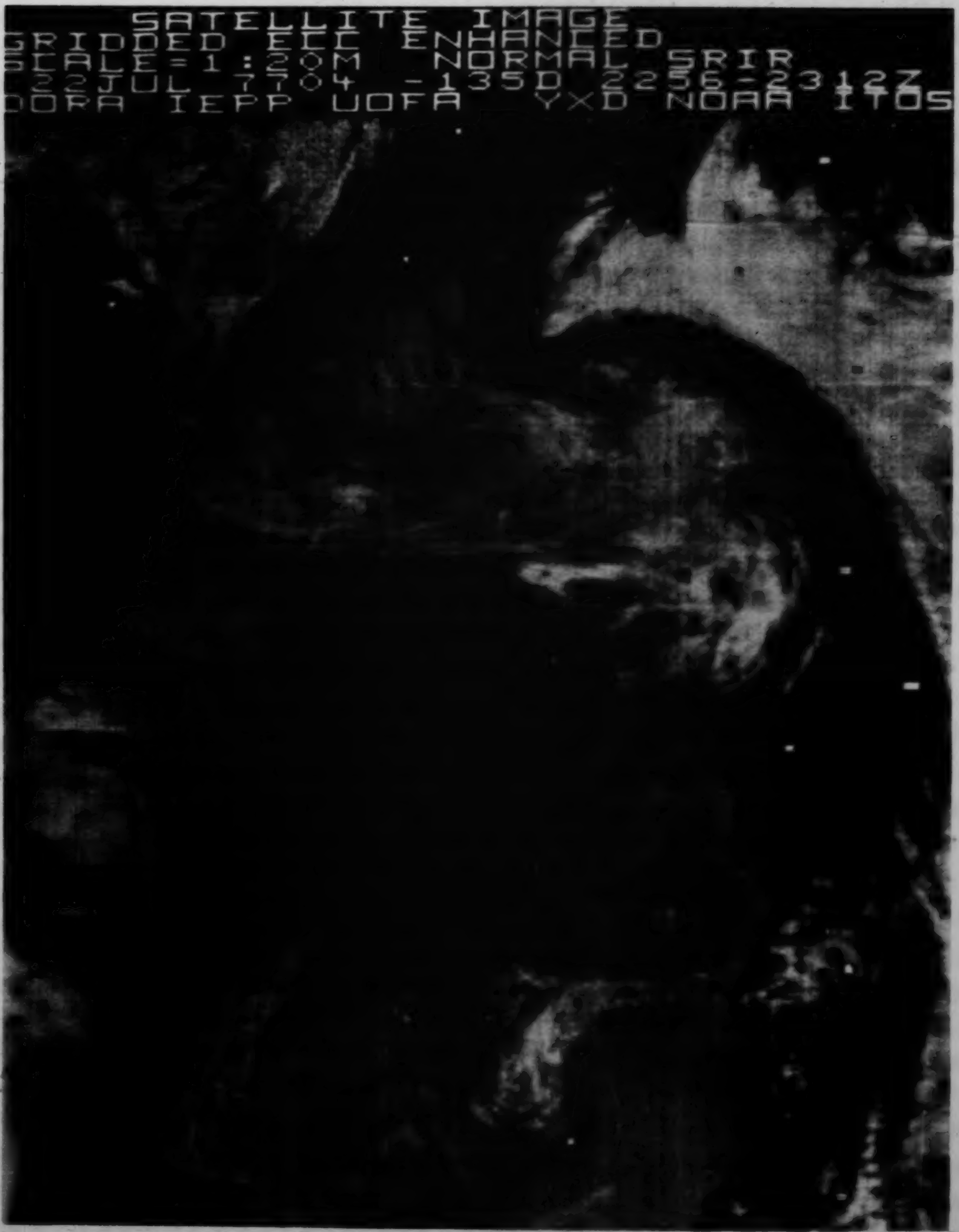
SATELLITE IMAGE
GRIDDED ECC ENHANCED
SCALE=1:20M NORMAL SRIR
22JUL 7704 -135D 2256-2312Z
DORA IEPP UOFA YXD NOAA ITOS

Figure 4.3: IR Image July 22, 1976, Orbit 7704 2256-2312 GMT. An example of strong inversion conditions.

same intensity level on the gray scale as the ice-covered water, there is likely very little difference in temperature between the two. Moreover, many open areas consist of ice and water and thus remain at near-freezing temperature.

There is evidence of stratus or fog in the cloud north of the Beaufort Sea. The visible image indicates the presence of low cloud; in the IR image the low cloud is nearly the same shade of gray as the ice, i.e., at much the same temperature.

In some instances the cloud is a darker shade of gray than the ice beneath it. This means that the cloud is warmer than the ice, and reveals the presence of an inversion layer.

In the relatively cloud-free areas along the north coast of Alaska, there seems to be no indication of an inversion, although it is known from the radiosonde data that an inversion exists. There is no discernible warm air in the IR image above the ice or the ice-water mixture which borders the land mass. The water regions closest to the heated land should have the warmest air at upper levels, but there is no significant difference in the IR gray shades over these ice-choked waters.

While not much can be said about the presence of inversions in the absence of low cloud, the imagery provides good evidence of a contrary kind by singling out those regions where inversions do not exist. On the IR image the Arctic islands appear almost as dark as the warmest areas on the mainland. This suggests similar surface temperatures. If this is true, then inversion conditions do not exist over a large part of the island land masses in summer. In fact, the air over the islands would likely be unstable. Inversions would also be weaker and modified over open, shallow water which has been heated by the sun.

August 14, 27 and 28 were also days with extreme inversion conditions. These three examples provided, on the whole, no significantly different information from the July 22 data; nevertheless, they do deserve some comment.

The tephigrams for August 15, 0000 GMT are displayed in Figure 4.4. Surface temperatures at the inland stations approached 20°C, while the temperatures on the coast were less than 5°C. The inversion at Sachs Harbour was rather weak, but Barter Island and Point Barrow had good Class 1 type inversions. The 0000 GMT surface observations on August 15 showed Sachs Harbour below an overcast of stratocumulus, and Barter Island and Point Barrow with stratus cloud. The stratus had likely formed in the inversion layer.

The visible and IR satellite images in Figures 4.5 and 4.6, respectively, are from Orbit 7992 of NOAA-4, 2256 to 2313 GMT on August 14, 1976. The cloud over the southern part of Banks Island appears to be at low levels, since the IR image indicates little difference in temperature between the cloud and the ice on the Beaufort Sea. High cloud obscures the western Alaskan coast. The coastal areas bordering the Beaufort Sea are quite distinct in the cloud-free areas. Again, there is little direct evidence of the presence of inversion conditions in regions devoid of stratus cloud. The darker gray shades in the IR image over the land masses show again the areas of high surface temperature, where inversions would break down.

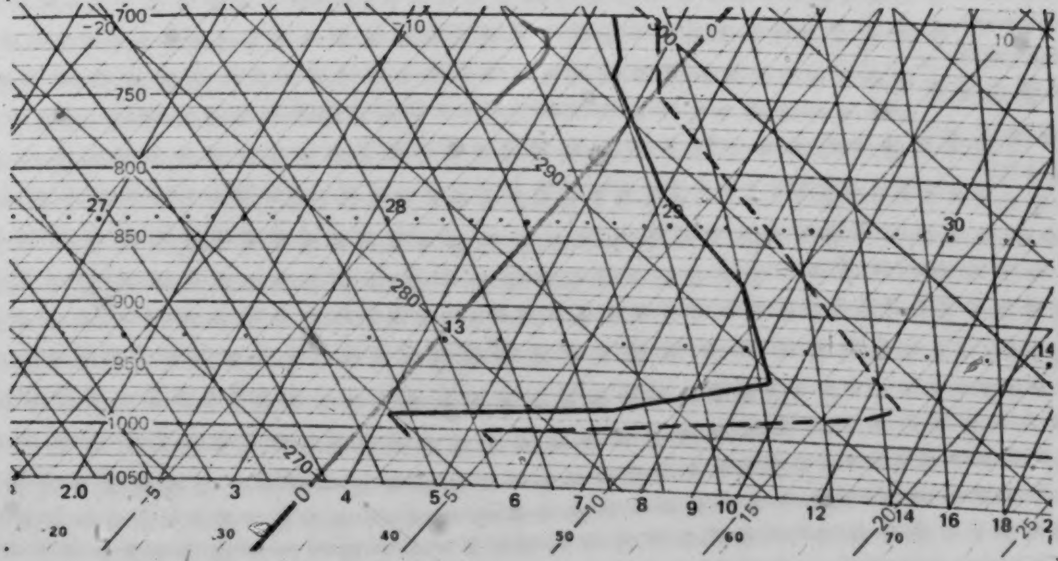

A. (i) Point Barrow —— (ii) Barter Island ----

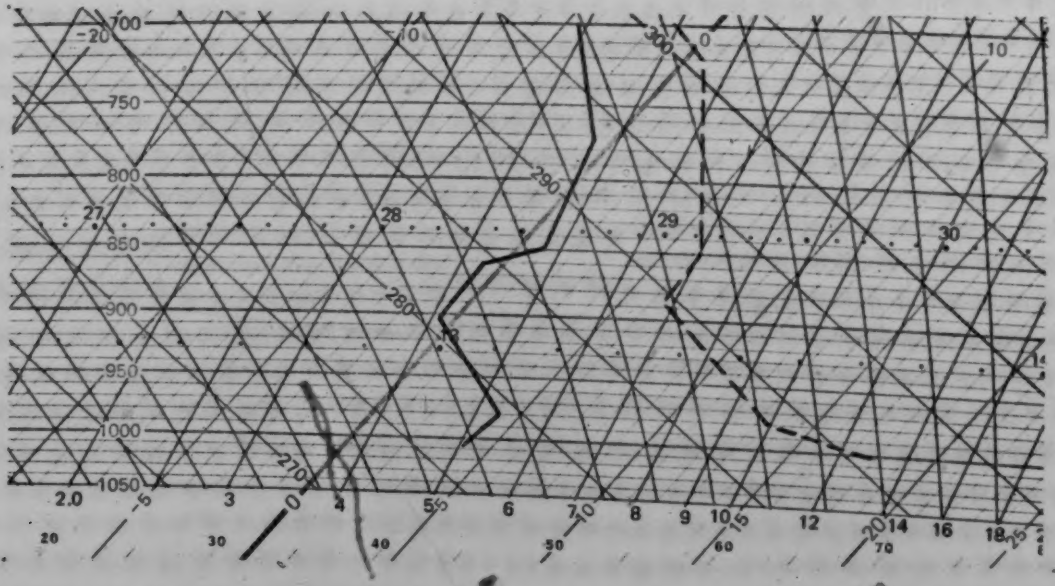

B. (i) Sachs Harbour —— (ii) Norman Wells ----

Figure 4.4: Tephigrams for 0000 GMT August 15, 1976

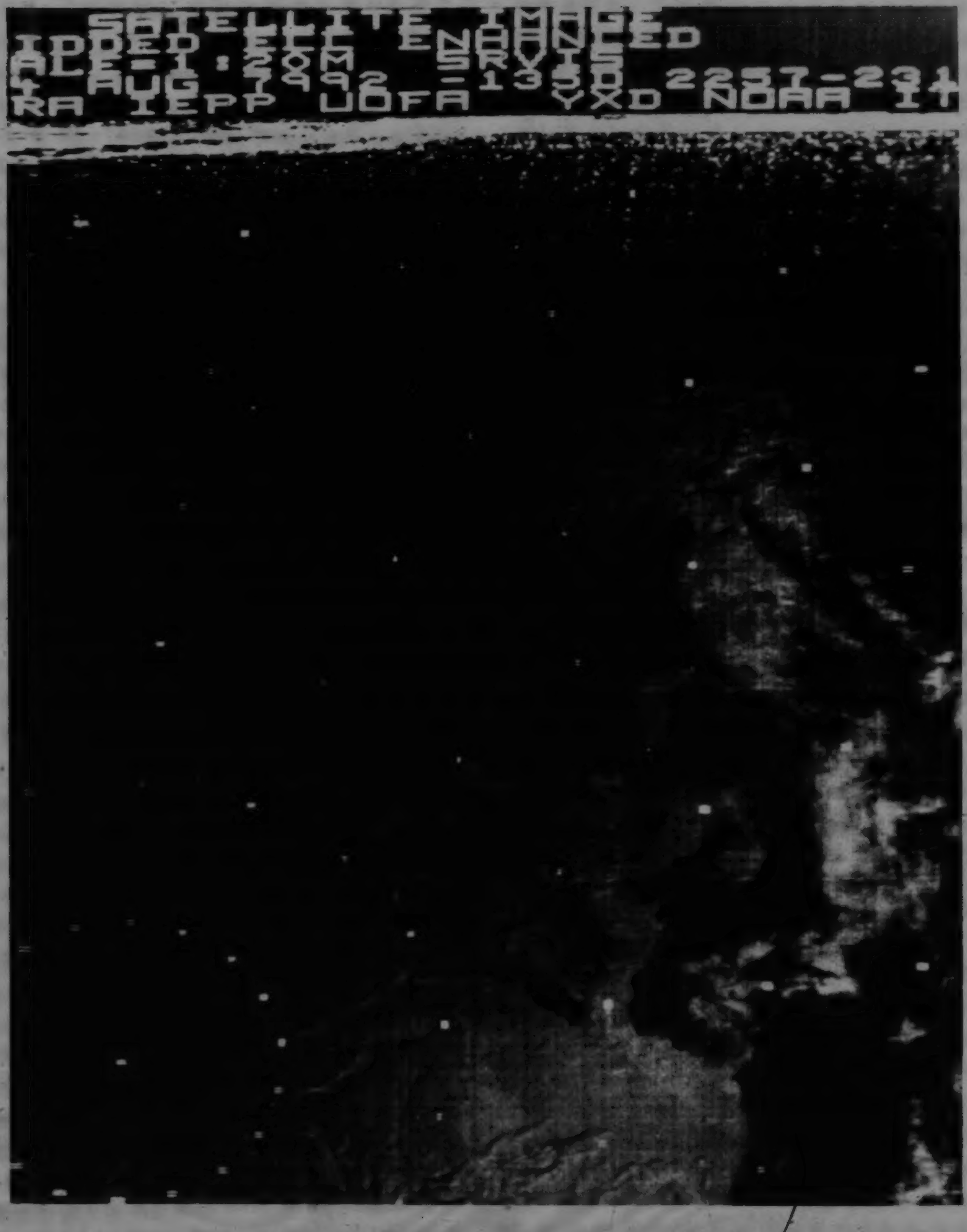
SATELLITE IMAGE
ENHANCED
AUG 7992
2257-231
NOAA

Figure 4.5: Visible Range Image August 14, 1976, Orbit 7992 2257-2313 GMT. An example of strong inversion conditions.

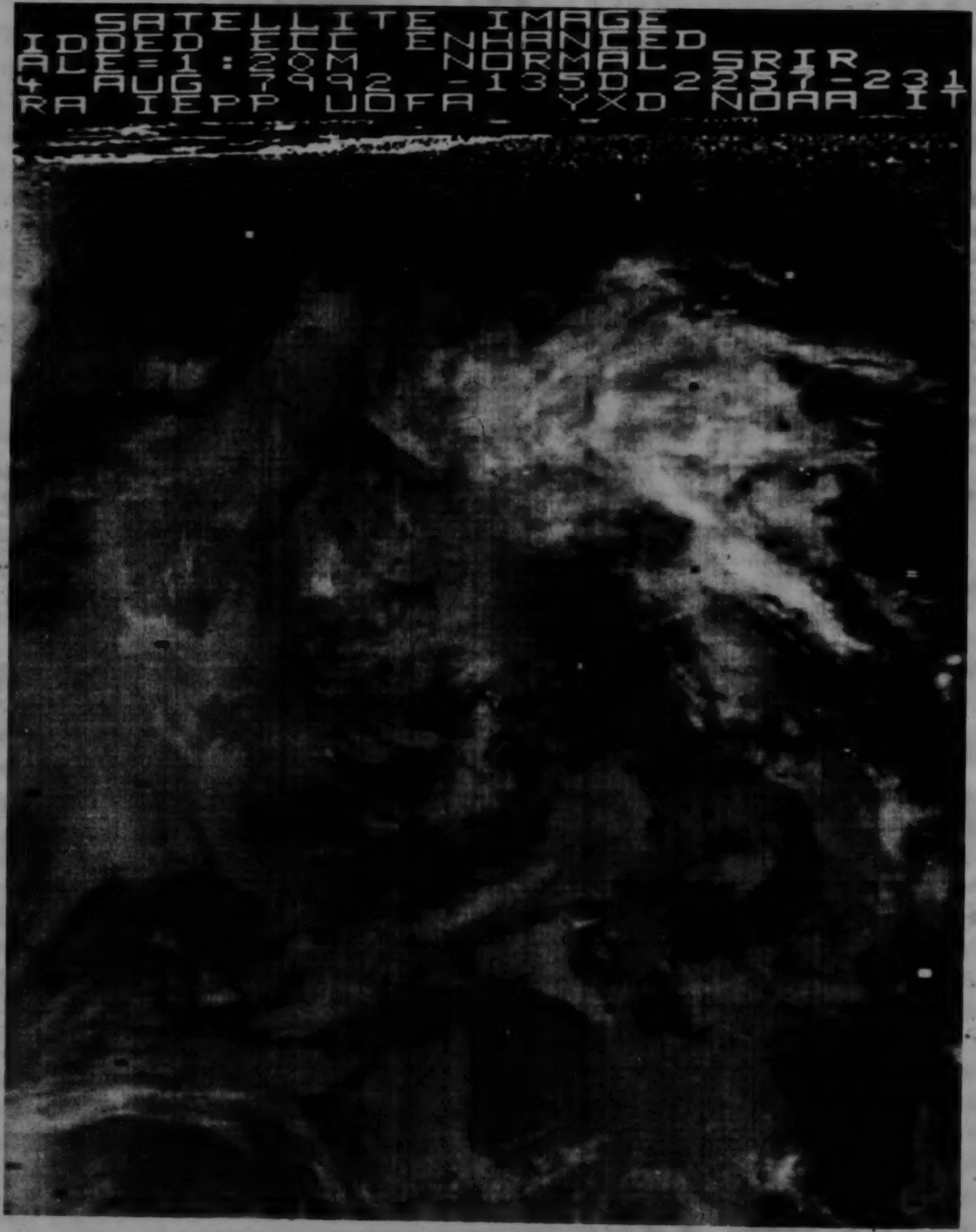
SATELLITE IMAGE
IDDED ECC ENHANCED
ALE=1:20M NORMAL SRIR
4 AUG 7992 -135D 2257-231
RA IEPP UDFA YXD NOAA IT

Figure 4.6: IR Image August 14, 1976, Orbit 7992 2257-2313 GMT.
An example of strong inversion conditions.

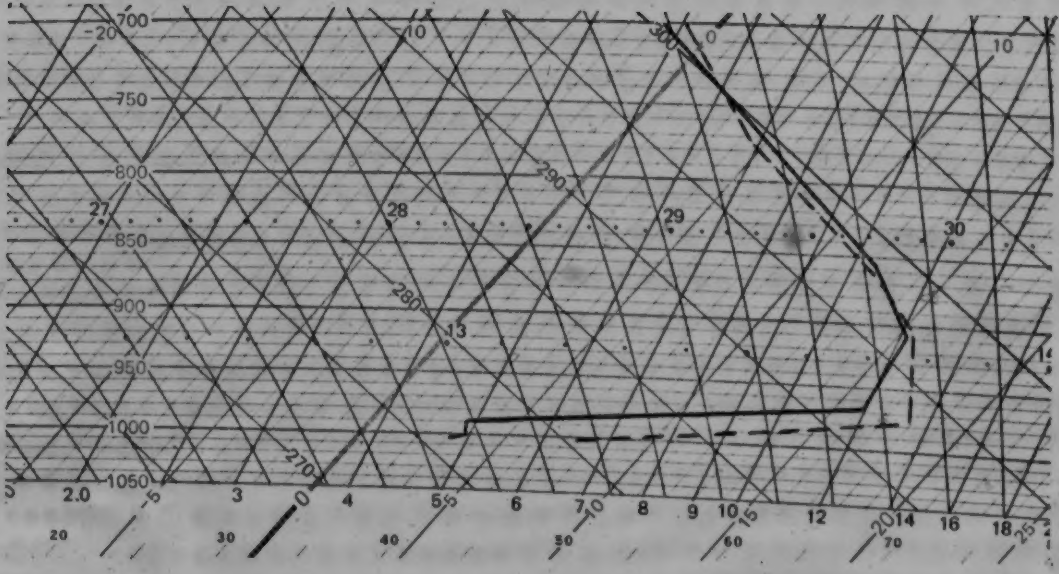

A. (i) Point Barrow —— (ii) Barter Island ----

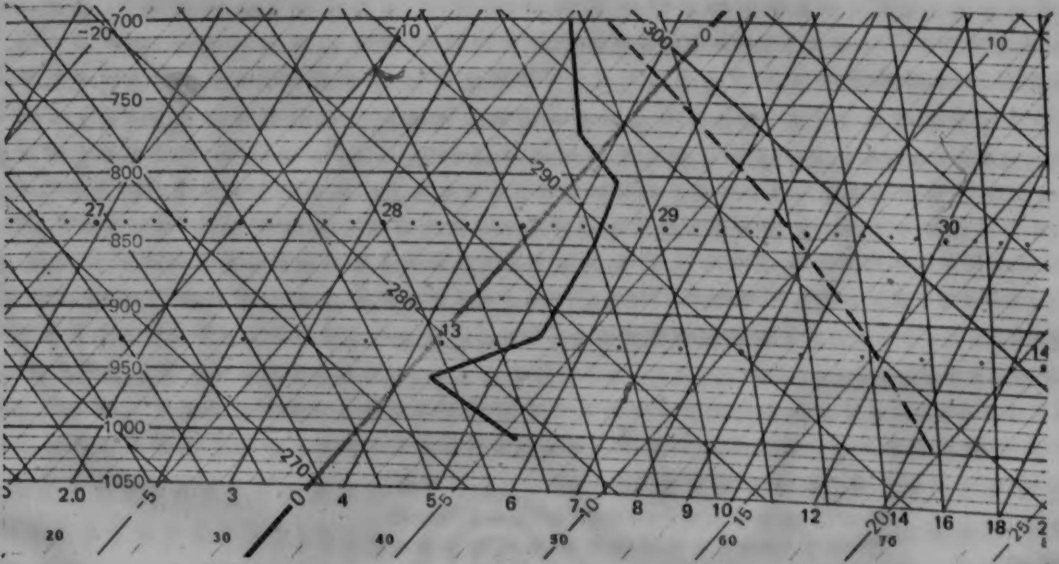

B. (i) Sachs Harbour —— (ii) Norman Wells ----

Figure 4.7: Tephigrams for 0000 GMT August 28, 1976

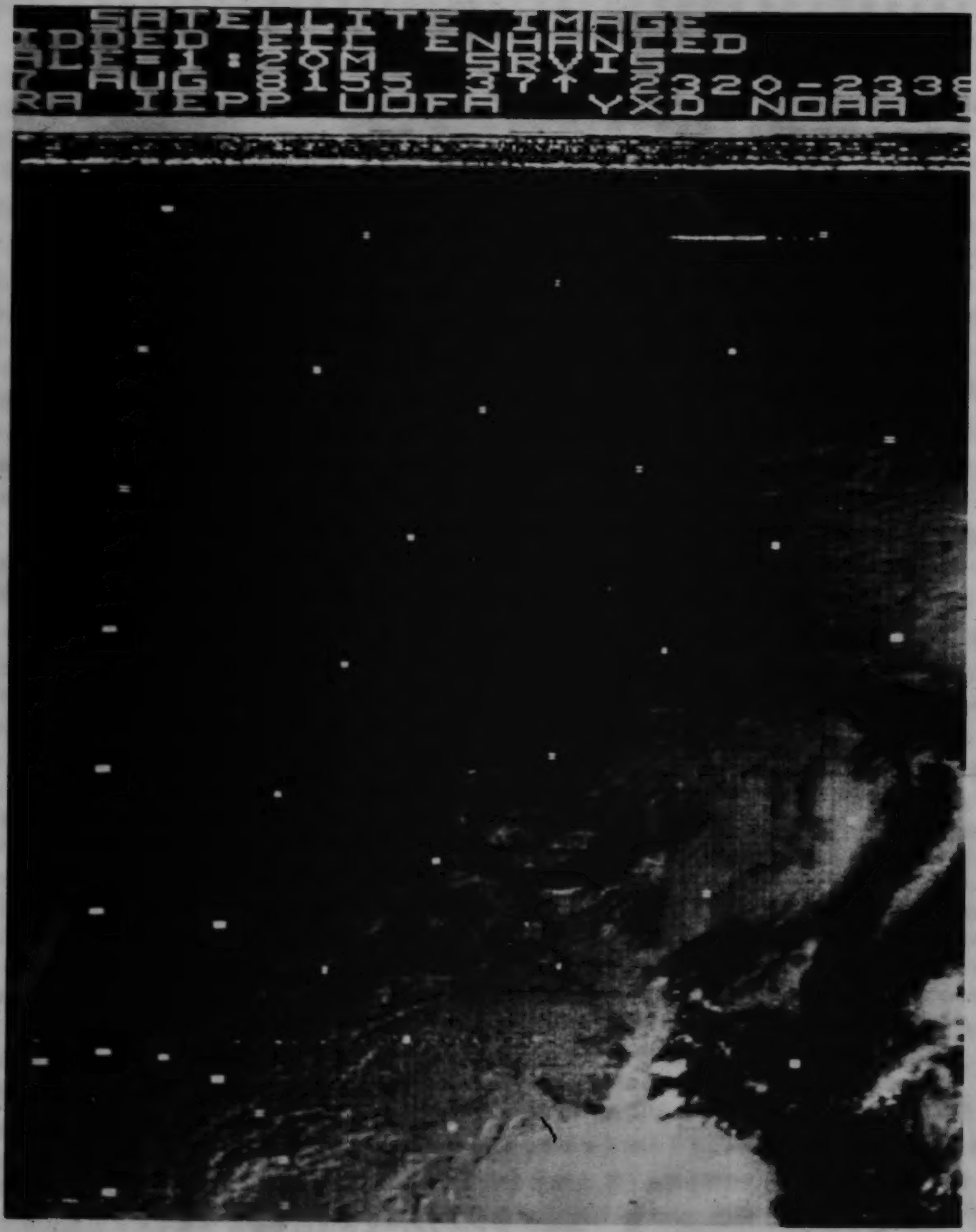
SATELLITE IMAGE
IDDED ELC ENHANCED
ALE=1:20M SRVIS
7 AUG 8155 37↑ 2320-2338
RA IEPP UDFA YXD NOAA

Figure 4.8: Visible Range Image August 27, 1976, Orbit 8155 2320-2338 GMT. An example of strong inversion conditions.

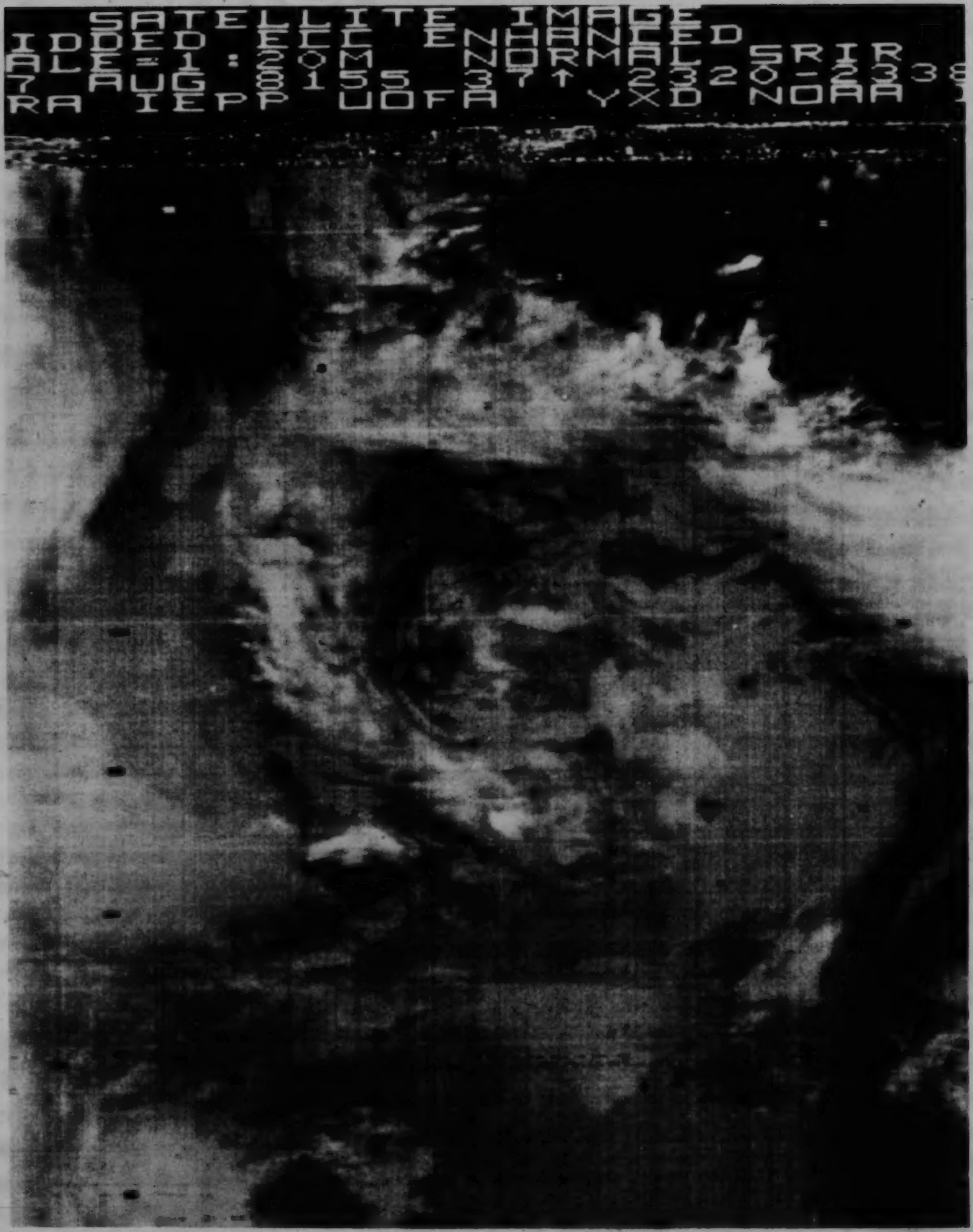
SATELLITE IMAGE
IDDED ECC ENHANCED
ALE=1:20M NORMAL SRIR
7 AUG 8155 37↑ 2320-2338
RA IEPP UOFA YXD NOAA

Figure 4.9: IR Image August 27, 1976, Orbit 8155 2320-2338 GMT. An example of strong inversion conditions.

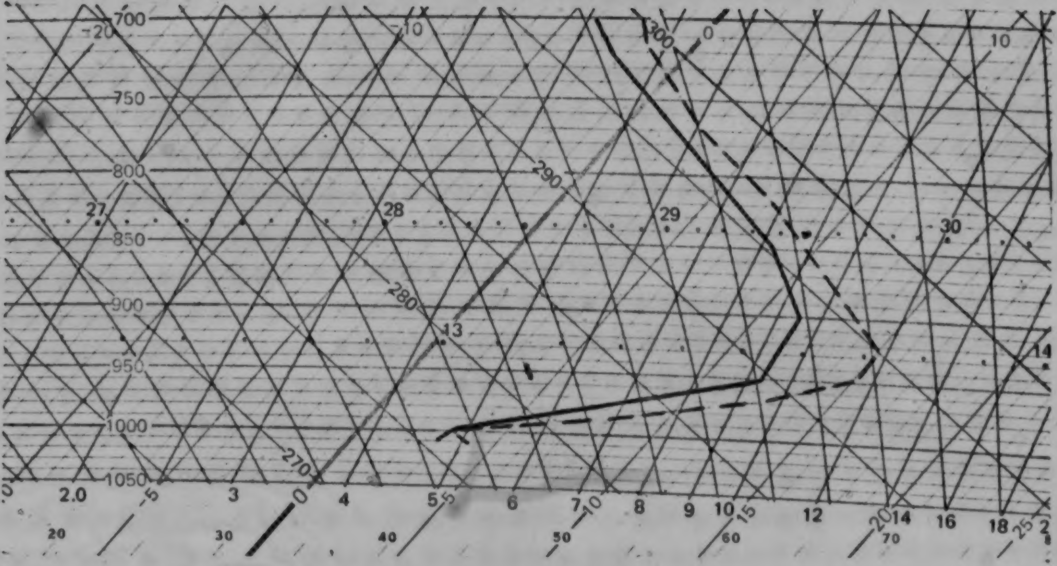

A. (i) Point Barrow —— (ii) Barter Island ----

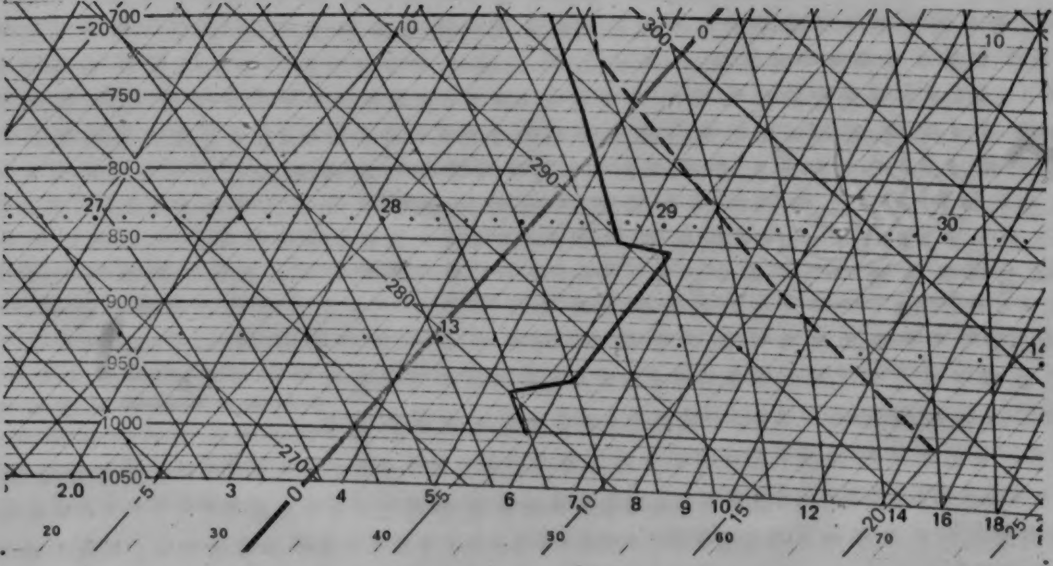

B. (i) Sachs Harbour —— (ii) Norman Wells ----

Figure 4.10: Tephigrams for 0000 GMT August 29, 1976

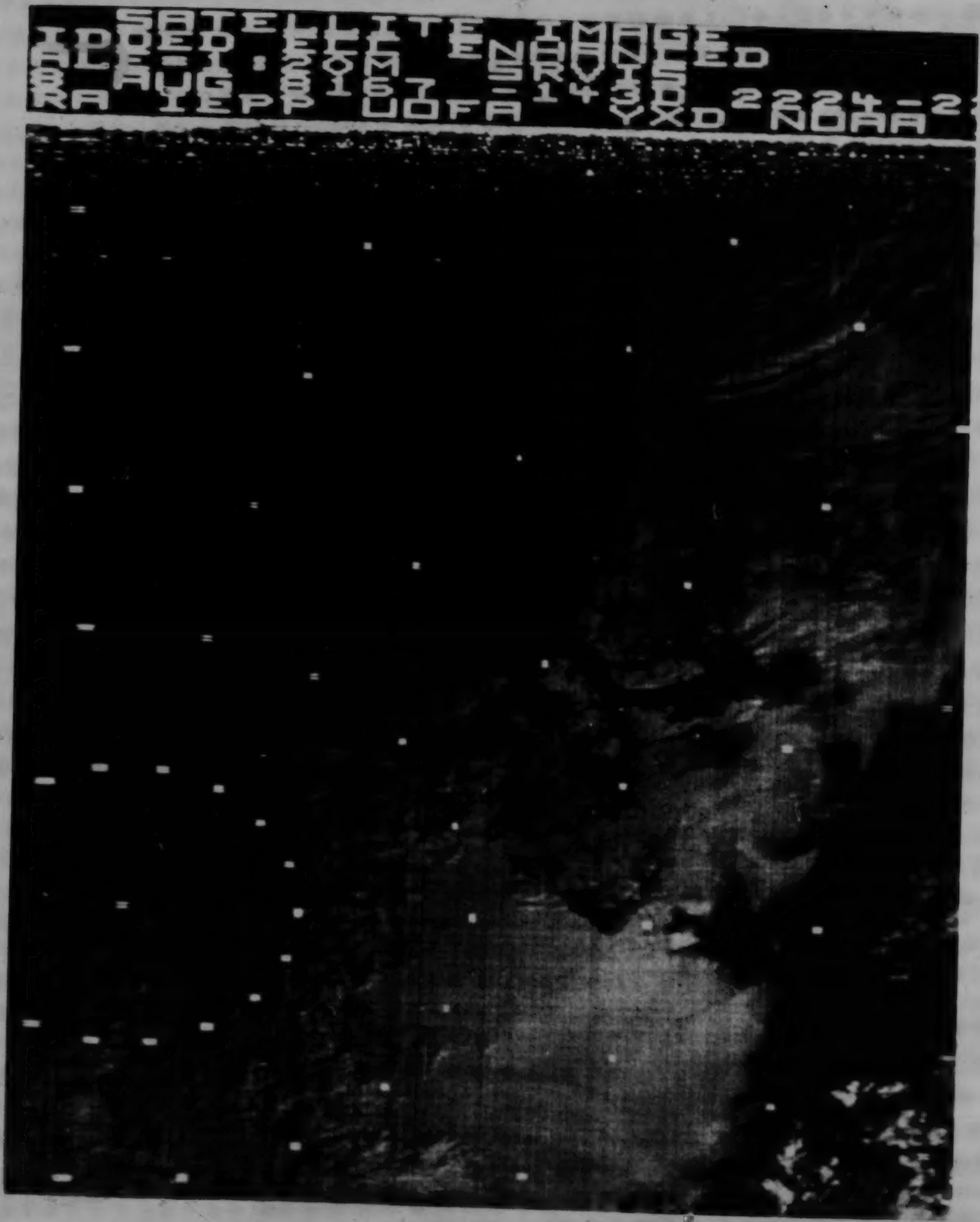
SATELLITE IMAGE
ENHANCED
NOAA

Figure 4.11: Visible Range Image August 28, 1976, Orbit 8167 2224-2240 GMT. An example of strong inversion conditions.

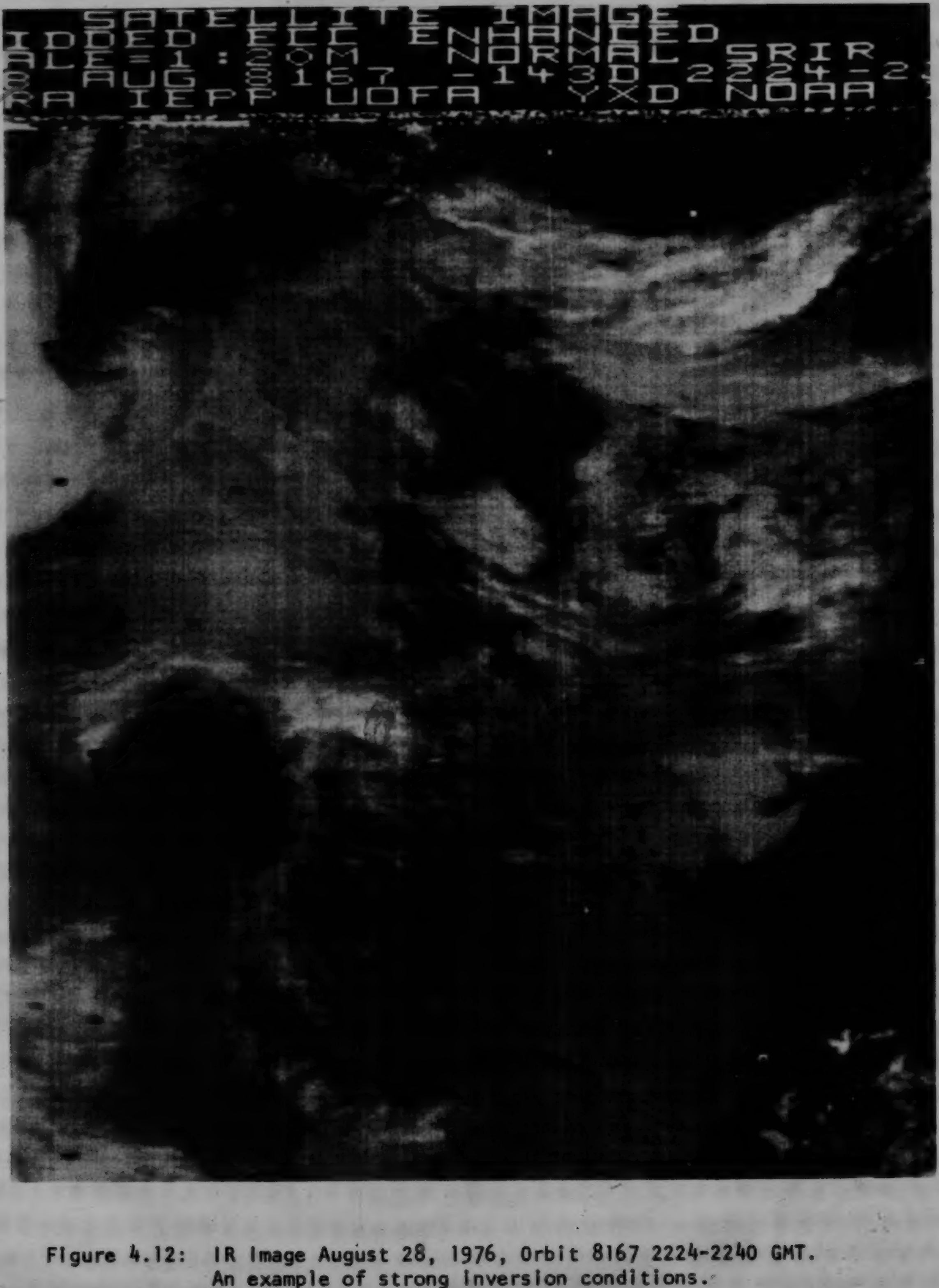
SATELLITE IMAGE
IDDED ECC ENHANCED
ALE=1:20M NORMAL SRIR
8 AUG 8167 -143D 2224-2
RA IEPP UOFA YXD NOAA

Figure 4.12: IR Image August 28, 1976, Orbit 8167 2224-2240 GMT. An example of strong inversion conditions.

Similar observations were made from the data for August 27 and 28. Figure 4.7 contains the tephigrams for 0000 GMT, August 28. The visible and IR satellite images in Figures 4.8 and 4.9 are taken from Orbit 8155, 2320 to 2338 GMT, August 27, 1976.

Strong inversions are indicated on the tephigrams of the Alaskan stations, but Sachs Harbour had closer to isothermal conditions. The visible satellite image shows very little cloud over Banks Island. This is supported by the surface observations at Sachs Harbour. In the IR image Banks Island appears as a rather indistinct patch of gray. This suggests that the surface temperatures over the entire island were quite low, as compared to the warm mainland to the south. It may be presumed that the isothermal lapse rate and temperature structure observed at Sachs Harbour is representative of the entire island.

The situation was very similar on August 28. The tephigrams for 0000 GMT August 29, 1976, are shown in Figure 4.10. The visible and IR satellite images in Figures 4.11 and 4.12, respectively, are from Orbit 8167, 2224 to 2240 GMT, August 28, 1976.

The tephigrams indicate little change in the low-level temperature structure from the previous day. Again, very little cloud is observed over Banks Island. However, the IR satellite image indicates only slightly higher temperatures over Banks Island than for the Beaufort Sea. It can be surmised that there was not very much surface heating on the island.

It was apparent, from the above examples, that, in the absence of suitable low cloud, the IR radiation emitted by the Earth's surface overwhelms the IR radiation emitted by cloud-free air at upper levels. There was no perceivable effect in the IR image that could be attributed to the IR radiation originating in the warmer air of an inversion layer. However, the IR images clearly show the higher surface temperatures over the areas of open water and ice-free land masses, and do reveal the noteworthy fact that the interior regions of the Arctic Islands frequently attain surface temperatures comparable to those found over the mainland.

4.3 Quantitative Analysis of the IR Imagery

The gray-scale method of displaying the surface temperature structure deduced from an IR image is not very satisfactory from a quantitative point of view. The human eye has a limited ability to resolve the different levels of gray. Once the number of levels on the gray scale is more than six or seven it becomes difficult to differentiate between neighbouring values. It is hence desirable to display the IR image in such a manner that the radiation level of each data point be identified by, and assigned a definite numerical value.

The numerical values of the digitized IR data can be used to obtain a quantitative measure of the observed temperature fields. This alternative to the gray-shade display enables detailed investigation of selected sets of data, and allows the stored information to be manipulated and displayed in many different ways. Much of the information is "lost" in a gray-scale representation since interpretation ultimately depends upon the ability to discriminate visually between the levels of gray. This task becomes quite difficult when it is desired to make maximum use of the resolving power of the scanning radiometer.

In the IR region of the spectrum the NOAA-4 scanning radiometer (SR) has a resolution of four nautical miles along the satellite subpoint track. At a digitizing frequency of 2400 Hz, one numerical piece of information - called a daton - is generated for every interval of approximately two nautical miles traversed near the satellite subpoint. There are thus more digital values generated than is warranted by the resolution of the SR. It is necessary to keep this in mind when analyzing the digital data.

The digitized satellite data are commonly stored on magnetic tape. In a single satellite pass of approximately 20 minutes duration, the IR and visible scans generate about 1.75 million datons. Considering the IR data alone, each scan of the SR will produce about 900 datons. With close to 1000 scans in each satellite pass, it becomes impractical to output the numbers from an entire pass on a line printer and attempt to analyze the information directly. It is necessary to reduce the data to a more manageable form, or else concentrate on only a small portion of the satellite image. In either case, a great deal of computation is required for processing an image in this manner.

The data are stored in sequence, as arranged in the original scan lines. In order to select a desired portion of the image, and subsequently identify the image location in the output display, the data must undergo some kind of gridding process. The computer program

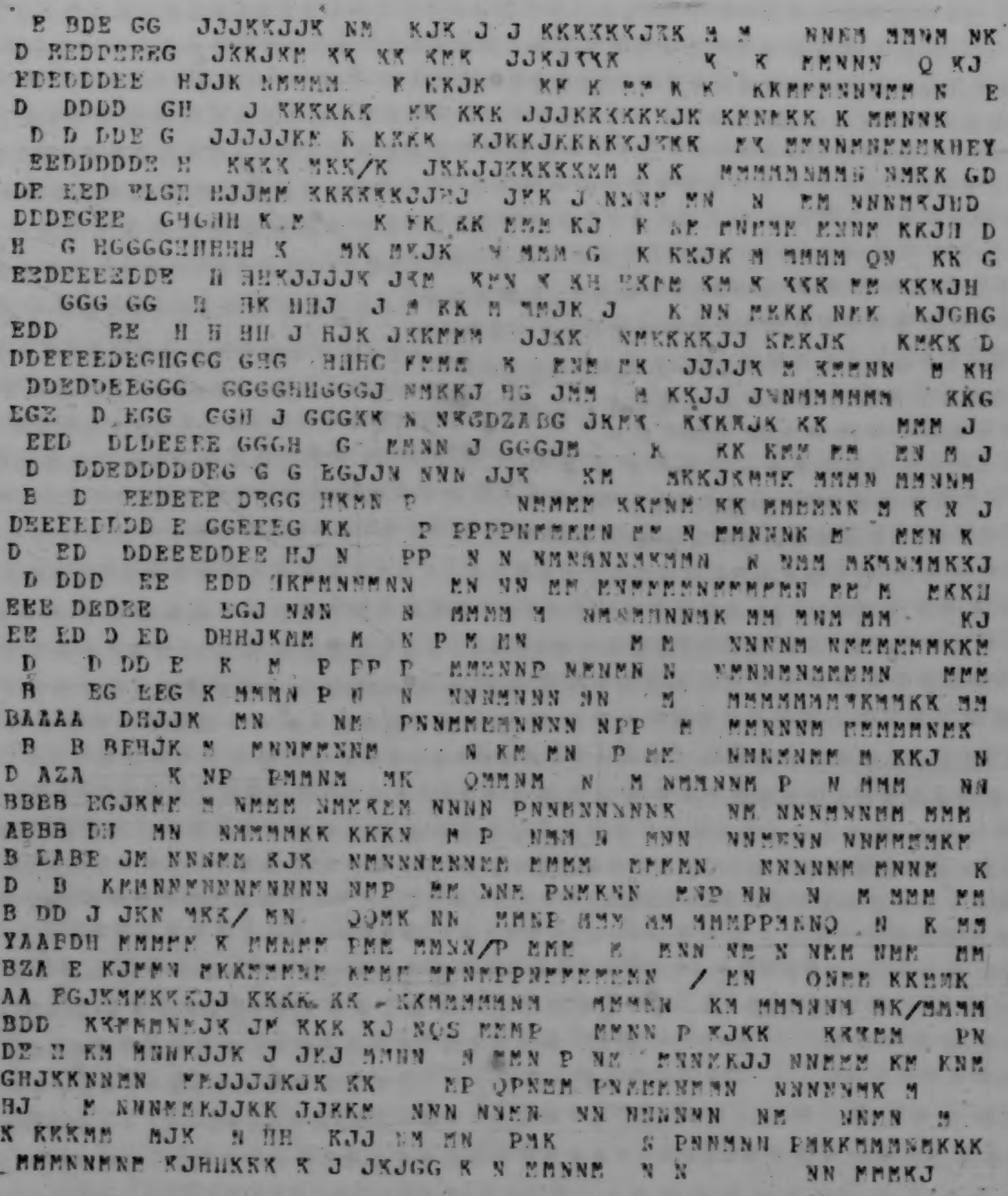

```
 E BDE GG  JJJKKJJK NM  KJK J J KKKKKJKK M M   NNEM MMNM NK
D EEDDEEEG  JKKJKM KK KK KMK  JJKJKKK     K K  MMNNN  Q KJ
EDEDDDEE  HJJK MMMMM  K KKJK   KM K MM K K  KKMMMNNMMM K  E
D  DDDD  GH   J KKKKKK  KK KKK JJJKKKKKKJK KMNMKK K MMNNK
 D D DDE G  JJJJJKM K KKKK  KJKKJKKKKKJKKK  MK MMNNMMMMMKHEY
 EEDDDDDE H  KKKK MKK/K  JKKJJKKKKKMM K K  MMMMMNMMM NMKK GD
DE EED MLGE HJJMM KKKKKKJJMJ  JMK J NNNM MN  N  MM NNNMKJHD
DDDEGEE  GHGHH K M    K KK KK MMM KJ  K KM MNMMM MNNM KKJH D
H  G HGGGGHHHHH K   MK MKJK  N MMM G  K KKJK M MMMM QN  KK G
EEDEEEEDDE  H HHKJJJJK JKM  KMN K KH MKMM KM K KKK MM KKKJH
   GGG GG  H  HK HHJ  J M KK M MMJK J   K NN MKKK NKK  KJGHG
EDD   EE  H H HH J HJK JKKMMM  JJKK  NMKKKKJJ KMKJK   KMKK D
DDEEEEDEGHGGG GHG  HHHG MMMM  K  MNM MK  JJJJK M KMMNN  M KH
 DDEDDEEGGG  GGGGHHGGGJ NMKKJ HG JMM  M KKJJ JNNMMMMMM   KKG
EGE  D EGG  GGH J GGGKK N NKGDZABG JKMK  KKKKJK KK    MMM J
 EED  DDDEEEE GGGH  G  MMNN J GGGJM    K   KK KMM MM  MN M J
 D  DDEDDDDDEG G G EGJJN NNN JJK   KM   MKKJKMMK MMMN MMNNM
 E  D  EEDEEE DEGG HKMN P      NMMMM KKMNM KK MMMMNK M K N J
DEEEEDDDD E GGEEEG KK    P PPPPNMMMMN MM N MMNNNK M   MMN K
D  ED  DDEEEDDEE HJ N    PP  N N NMNMNNMMMMN  N NMM MKMNMMKKJ
 D DDD  EE  EDD HKMMNNMMNN  MN NN MM MNMMMMNMMMMMN MM M  MKKH
EEE DEDEE    EGJ NNN    N  MMMM M  NMMMNNNMK MM MNM MM    KJ
EE ED D ED  DHHJKMM  M  N P M MN       M M   NNNNM NMMMMMMKKM
 D    D DD E  K  M  P PP P  MMMNNP NMNMN N  MMNNNMMMMMN   MMM
 B    EG EEG K MMMN P M  N  NNNMNNN NN   M   MMMMMMMMKMMKK MM
BAAAA  DHJJK  MN    NM  PNNMMMMNNNN NPP  M  MMNNNM MMMMMNMK
 B  B BEHJK M  MNNMMNNM    N KM MN  P MK   NNNNNMM M KKJ  N
D AZA      K NP  PMMNM  MK   QMMNM  N  M NMMNNM P  N MMM   NN
BBBB EGJKMM M NMMM NMMKMM NNNN PNNMNNNNNK   NM NNNMNNMM MMM
ABBB DH  MN  NMMMMKK KKKN  M P  NMM N  MNN  NNMMNN NNMMMMKM
B EABE JM NNNMM KJK  NMNNNMMNMM MMMM  MMMMN   NNNNNM MNNM  K
D  B  KMMNNMNNNMNNNN NMP  MM NNM PNMKNN  MNP NN  N  M MMM MM
B DD J JKN MKK/ MN   QOMK NN  MMMP MMM MM MMMPPMNNQ  N  K MM
YAABDH MMMMM K MMMMM PMM MMNN/P MMM  M  MNN NM N NMM NMM  MM
BZA E KJMMN MKKMMMMM KMMM MMNMPPNMMMMMMN  / MN   ONMM KKMMK
AA EGJKMMKKKJJ KKKK KK  KKMMMMMNM    MMMMN  KM MMNNNM MK/MMMM
BDD  KKMMMNNJK JM KKK KJ NQS MMMP   MMNN P KJKK   KKMMM   PN
DE H KM MHNKJJK J JKJ MMHN  N MMN P NM  MNNKKJJ NNMMM KM KNM
GHJKKNNMN  MMJJJJKJK KK    MP QPNMM PNMMMNMMN  NNNNNMK M
HJ   M NNNMMKJJKK JJKKM  NNN NNMN  NN NNNNNN  NM   NMMN  M
K KKKMM  MJK  N HH  KJJ MM MN   PMK     N PNNMNH PMKKMMMNMKKK
 MMMMNMMM KJHHKKK K J JKJGG K N MMNNM  N N        NN MMMKJ
```

Figure 4.13: Sample of Computer Output from SRGRID-2.

which was used for gridding and displaying the data is described in Appendix B. An example of the output of the program is shown in Figure 4.13, with superimposed latitude and longitude lines, and the IR data converted to letters of the alphabet, each of which represents a specified range of numerical values. The digitizing process generates numbers between 0 and 255. In the case of IR imagery, the low numbers represent the highest temperatures, and the high numbers the lowest temperatures. Input parameters for the computer program determine the range of values equivalent to, and denoted by an alphabetic character. The choice of particular parameters depends upon the range and scope of the atmospheric system under investigation.

It must be kept in mind that the IR data are representative of the temperatures of the radiating surfaces. The numerical values are characteristic of digitized, equivalent blackbody temperatures. The conversion from the digital value to the actual temperature of the radiation source is carried out by using the response curve of the SR on board the satellite. Before launching, the instrument is calibrated against a blackbody, yielding a response curve of radiation versus blackbody temperature. An example of such a calibration curve, that for the SR carried by NOAA-4, is shown in Figure 4.14.

The response of the instrument depends on its internal operating temperature, a quantity which varies according to sun angle and distance. This is a seasonal type of variation that can be predicted and measured. Errors that cannot be removed so easily are caused by noise in the transmitting and receiving systems of the spacecraft and on the ground. Moreover, the radiation measured by

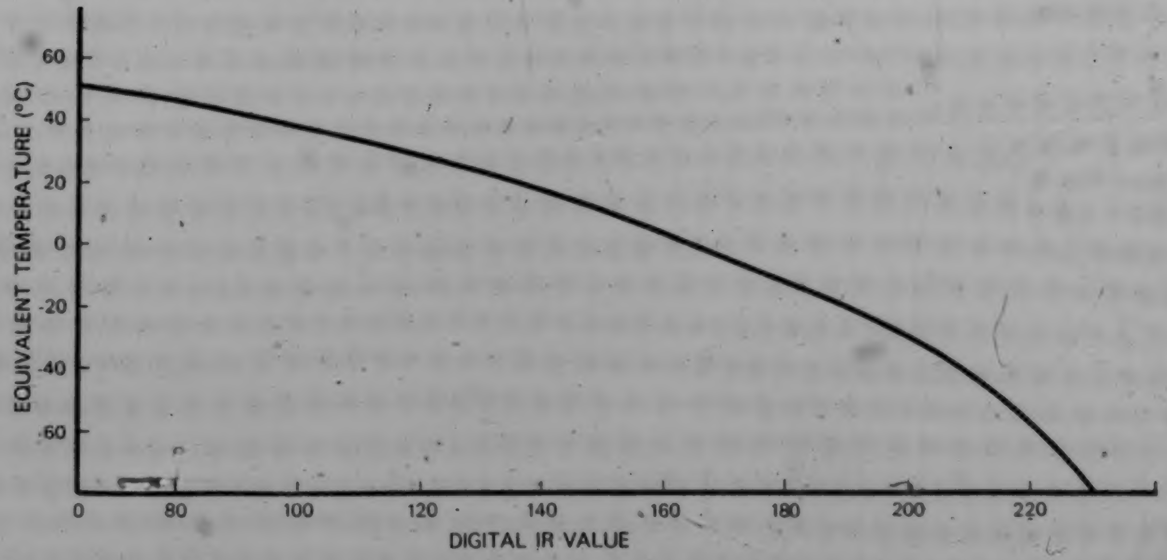

Figure 4.14: Temperature Calibration Curve for IR Signal

the SR on the spacecraft is not the same as that originally emitted by a source on the ground. The radiation is subject to absorption by atmospheric gases such as water vapour and carbon dioxide. An object on the surface would have a higher temperature than indicated by the SR measurement of the IR radiation. This effect, as mentioned earlier, is called "limb-darkening" and can be corrected to a certain extent.

The signal strength of the satellite transmission received by a ground-based antenna will vary, depending on the position of the spacecraft in relation to the antenna. Without automatic gain control (AGC) the signal strength and, correspondingly, the digitized data, will increase from the time the signal is first received near the horizon. Under typical conditions, the signal strength will be nearly 10 percent higher by the end of the pass.

The satellite receiver at the University of Alberta did not have AGC at the time the 1976 summer data were recorded. Full AGC was not implemented until April 1977. Up to that time, the gain was set manually at the start of a pass, so that the maximum reading would fall in the range from 245 to 250. The signal strength was allowed to increase as the pass continued. If only a small area of the SR image is considered, the effect on the digital values is relatively small. Moreover, the greatest variation in signal strength is encountered with those orbital passes which are directed most nearly north to south (or south to north). The late-afternoon orbits which are more nearly east to west in direction - as "seen" from Edmonton - are less subject to variation. Since these orbits are close to the 0000 GMT radiosonde ascents, they were generally found to be the most useful.

Part of the satellite transmission may be used for calibrating the SR while the spacecraft is in flight. In this way, changes in the response of the instrument can be detected and appropriate corrections applied when converting the IR digital readings into temperatures. However, rather extensive computer processing is required in order to perform this operation adequately. It was impractical to include such corrective measures in the computational procedures used in this investigation.

Recognizing that most sources of error were difficult to eliminate, it was decided to forego precise determination of absolute temperature, and concentrate on relative temperature relationships instead. The response curve (Figure 4.14) is nearly linear over a large range of temperature and only deviates markedly from linearity at temperatures lower than -20°C. Since this study is concerned with temperatures near the surface of the Earth in summer, the temperatures of primary interest are higher than -20°C. In the Arctic regions in summer, the mixture of melting ice and open water would be expected to be near 0°C. This can be used as a reference calibration temperature in an IR image.

Afternoon temperatures over inland areas in summer often are in the 20 to 25°C range. In general, then, temperatures near the Earth's surface will fall into a range from a few degrees below freezing to about 25°C. Referring again to the response curve in Figure 4.14, it is seen that this temperature range lies in the nearly-linear portion of the curve. It is, therefore, possible to assign an approximate temperature to a digital IR level, and to estimate the temperature difference between this reference level and other digital IR values nearby. It is obvious that this procedure cannot yield a very accurate determination of actual temperatures. However, quite precise relative temperature differences can be deduced from the IR data, and if a good reference temperature can be found, the estimated temperatures will closely resemble the "true" temperatures measured by more conventional means. In the present case, the near-freezing temperature of the ice-water mixture of the Arctic Ocean provides a fairly reliable reference temperature which can be used with confidence in the calibration of digital IR data in summer.

Since temperatures can be assigned to digital IR measurements, it is possible to analyze a display of the quantitative IR data, for a selected area, in terms of isotherms. This type of analysis leads to a detailed representation of the temperature gradients in the Arctic.

4.4 Temperature Structure from the Quantitative Analysis of IR Imagery

The IR data for July 22 were re-examined by subjecting them to the quantitative method of analysis described in the previous section. The temperature calibration curve in Figure 4.14 was used to select a range of digital IR values representing temperatures from -10°C to +25°C. The output from the SRGRID-2 computer program, described in Appendix B, consisted of letters of the alphabet with a superimposed grid of lines of latitude and longitude. Each letter of the alphabet represented a specific interval comprised of two IR digital values. This corresponded to a temperature interval of between 1 and 2°C. Areal coverage of the analysis was restricted to the coastal regions and islands contiguous to the Beaufort Sea.

An isotherm analysis was carried out manually on the computer output of the July 22 IR data, a small part of which is reproduced in Figure 4.15. The radiation emitted by the surface of the Beaufort Sea was used to establish a reference temperature. This large expanse of ice and water produced readings between -3°C and 3°C. The isotherms

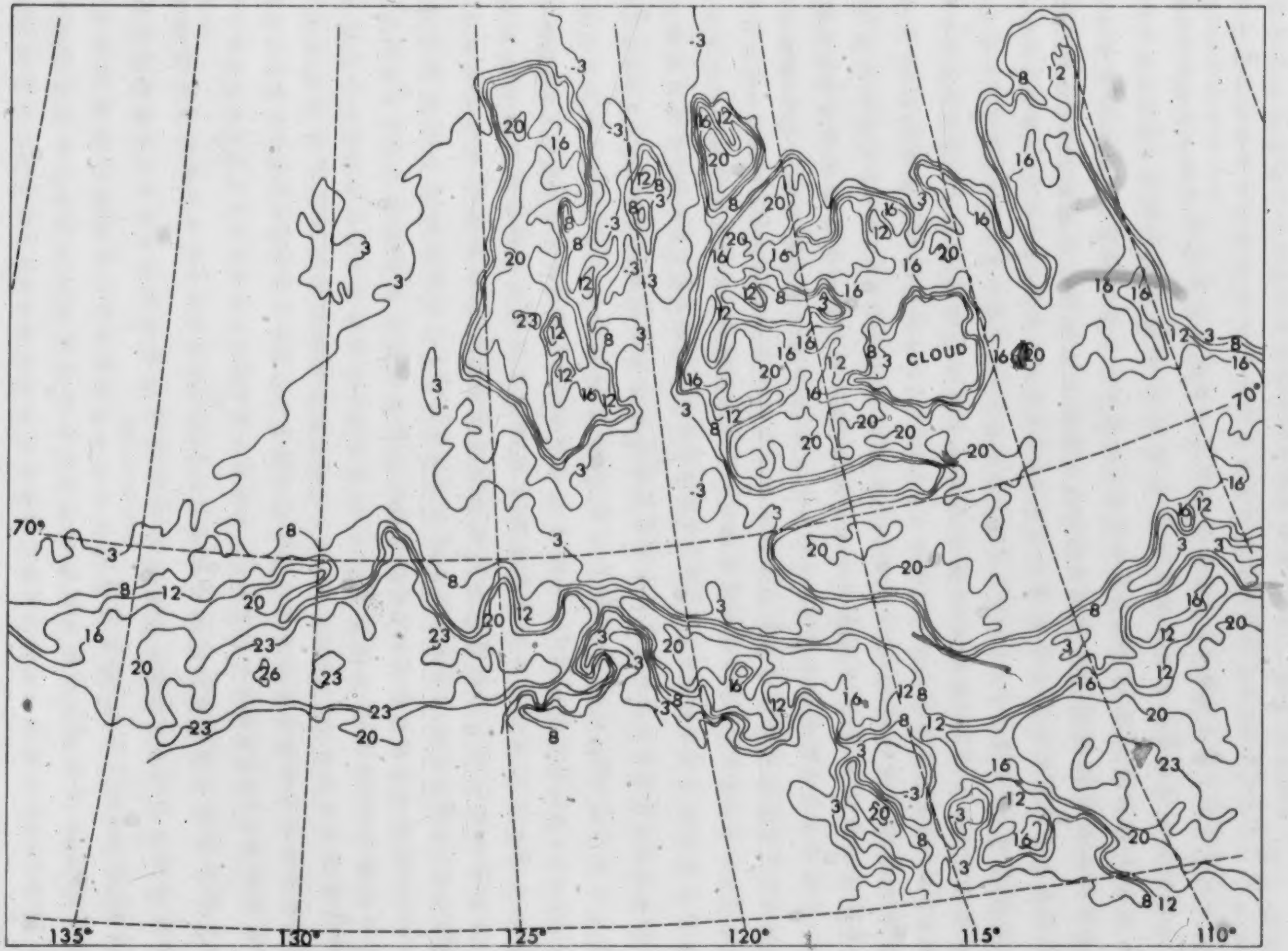
70°
70°
135°
130°
125°
120°
115°
110°
CLOUD

Figure 4.15: SURFACE ISOTHERMS 22 JULY 1976
ORBIT 7704 2256-2304 GMT

are shown for an area which includes Banks and Victoria islands and the mainland coast to the south. The gray-scale imagery of this same area shows very little cloud, implying that the IR radiation is mainly of surface origin.

It is immediately apparent from the quantitative display that surface temperatures in the interior of the large island attain values comparable to those on the mainland. The isotherms outline large areas on Banks and Victoria islands with temperatures above 20°C. The analysis over the mainland suggests maximum temperatures in excess of 26°C. Such temperatures were in fact reported by the weather observers at Inuvik and Norman Wells. The contrast in temperatures between the land masses and the water and ice creates a complex thermal pattern. Very strong temperature gradients exist along the coastlines, sharply delineated by dense ribbons of isotherms.

The isotherms drawn in this analysis are labelled -3, 3, 8, 12, 16, 20, 23, and 26°C. Additional, intermediate isotherms could have been drawn, by simple interpolation, but such procedures, apart from cluttering the diagram, would convey a degree of precision not present in the IR data, because of the limited resolving power of the radiometer. Generally speaking, areas of water interspersed with ice are enclosed by the -3 and +3°C isotherms. The open water west of Banks Island and along the shallows of the mainland coast was warmer, and registered mostly in the 3 to 8°C range. For the most part the areas enclosed by the -3°C isotherm consisted of cloud. Isotherms below -3°C are not shown, although lower temperatures were indicated in some of the data from areas covered by cloud.

An interesting cluster of cloud is found in central Victoria Island. The cloud is delineated by a 3°C isotherm with no interior parts colder than -3°C. A cloud within this temperature range must be relatively low and thin. However, since the temperature of the land surrounding the cloud is generally above 20°C, it must be concluded that this cloud is not indicative of stable inversion conditions, but rather the product of convective processes. The ascending air over the heated island suggests a compensating, quasi-horizontal inflow of air from the frigid waters towards the warm interior of the island, a circulation pattern typical of the sea breeze. Air masses converging toward the island must undergo considerable modification on the way from sea to land. Sea breeze circulations and related phenomena observed in the Arctic are examined further in the next chapter.

A second example of the horizontal temperature distribution in the Arctic on a relatively clear and warm day - June 17, 1977 - is taken from Orbit 3999 of the NOAA-5 satellite. A portion of the June 17 IR image is reproduced in Figure 4.16. Two overlapping sections of the isotherm analysis are shown in Figures 4.17 and 4.18.

Figure 4.17 centres on Banks Island, but also includes part of Victoria Island and the mainland to the south. Two arms of Great Bear Lake are shown in the lower right-hand corner of the figure. The isotherms in this analysis are labelled -7, -3, 0, 3, 7, 10, 13, 16, and 19°. The water west of Banks Island and along the south shore of the Beaufort Sea appears to be a few degrees above freezing. As might be expected, the water on June 17, 1977, was not as warm as the water on July 22, 1976.

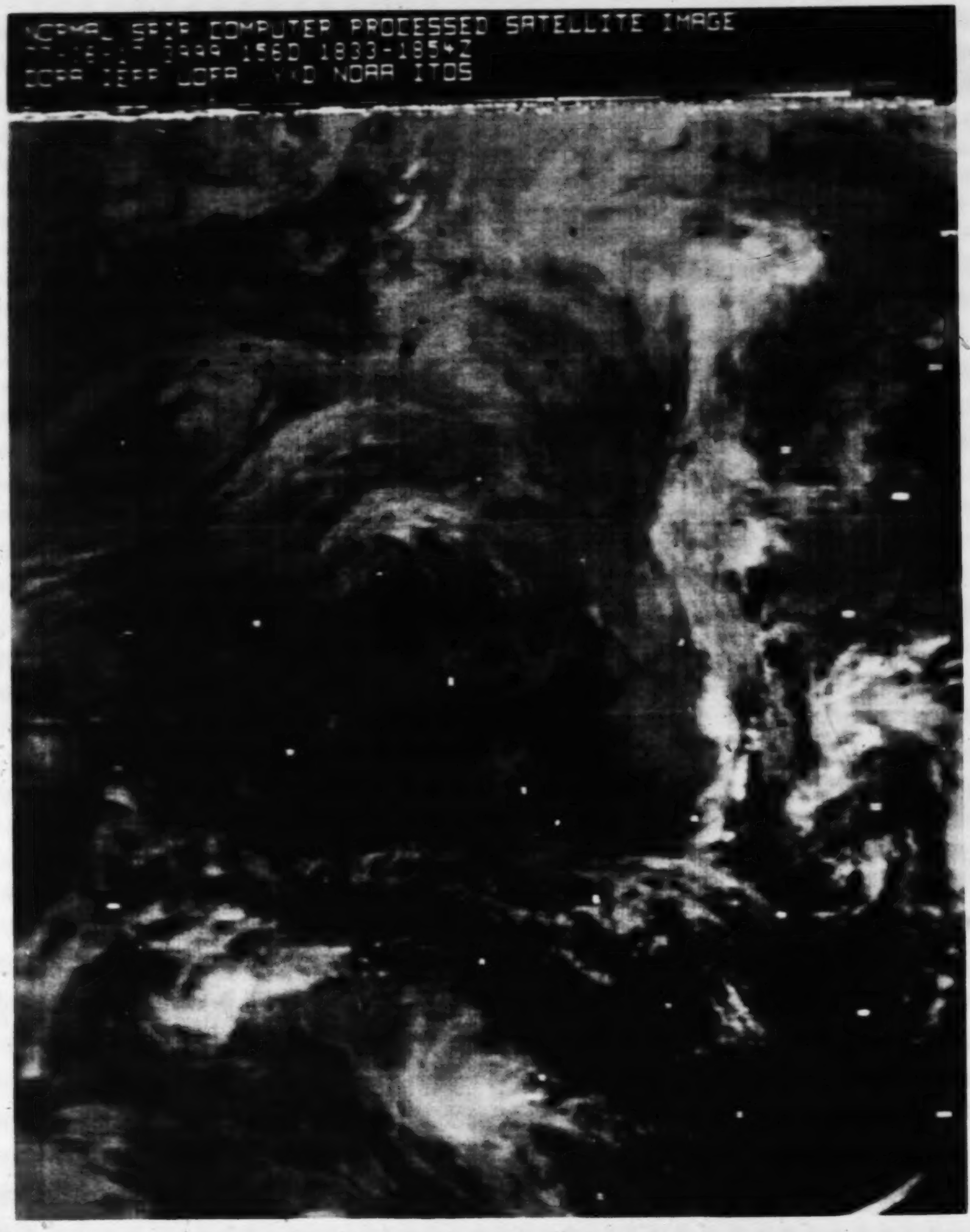
COMPUTER PROCESSED SATELLITE IMAGE
3999 156D 1833-1854Z
NOAA ITOS

Figure 4.16: IR Image June 17, 1977, Orbit 3999 1833-1854 GMT.
A clear day with strong surface heating.

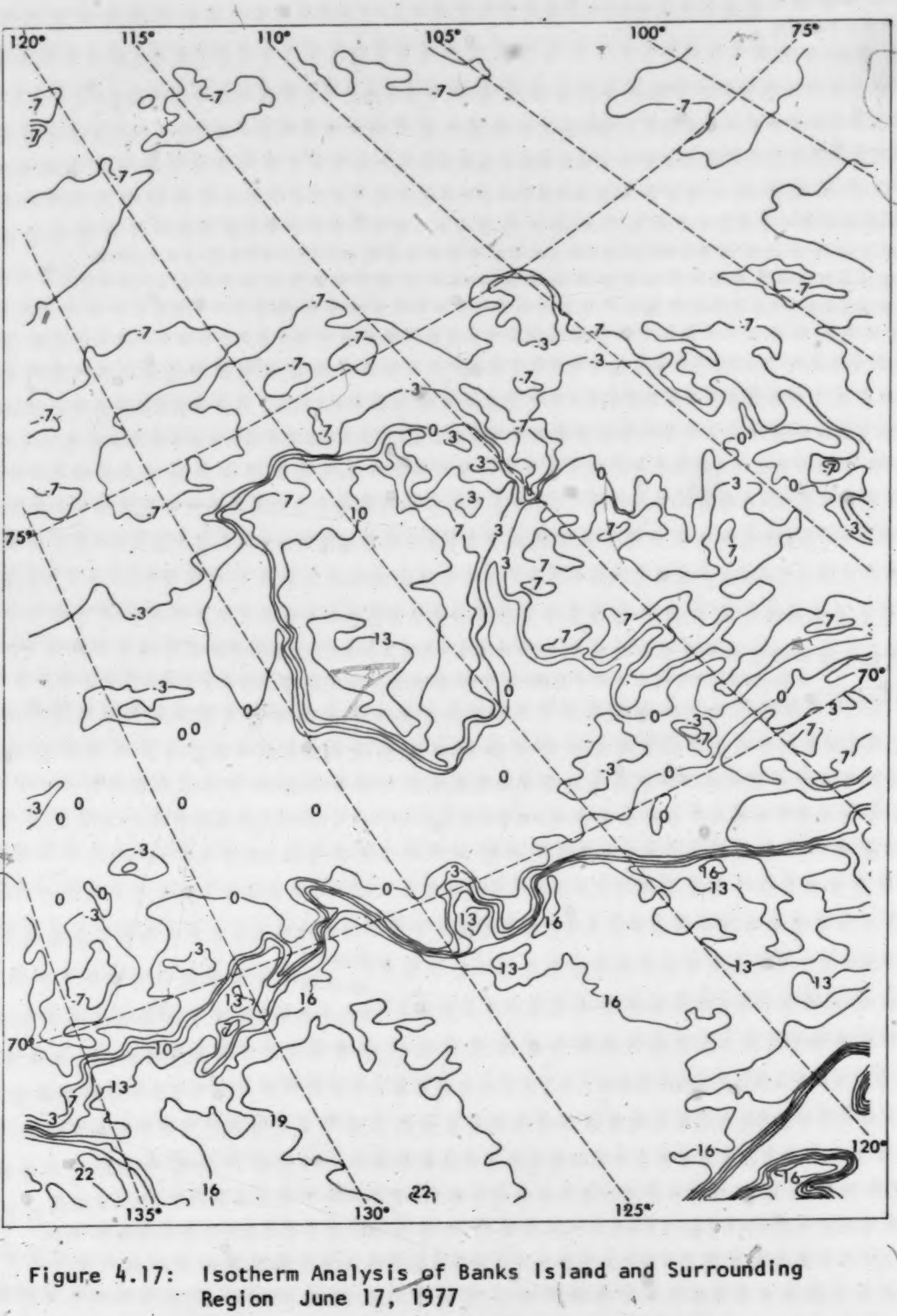
120°
115°
110°
105°
100°
75°
75°
70°
70°
120°
135°
130°
125°
-7
-3
0
3
7
10
13
16
19
22

Figure 4.17: Isotherm Analysis of Banks Island and Surrounding Region June 17, 1977

Figure 4.18, another section of the June 17 analysis, includes Great Bear Lake and Victoria Island. Because of obscuring cloud cover, Victoria Island is not as well defined by the isotherms as Banks Island, in Figure 4.17.

Dense ribbons of isotherms are again present between the land and sea, indicative of strong temperature gradients. The Arctic coast and major geographical features such as Great Bear Lake and Banks Island, are quite clearly outlined by the isotherm pattern.

These two examples demonstrate clearly some important aspects of the complex temperature regime of the Western Arctic in summer. While it is difficult to deduce the vertical temperature structure from the IR imagery, it is relatively easy to determine the horizontal temperature distribution in considerable detail. By the choice of appropriate thermal reference levels such as the near-freezing surface of the Arctic Ocean, realistic estimates can be made of the prevailing temperature regime at the Earth's surface.

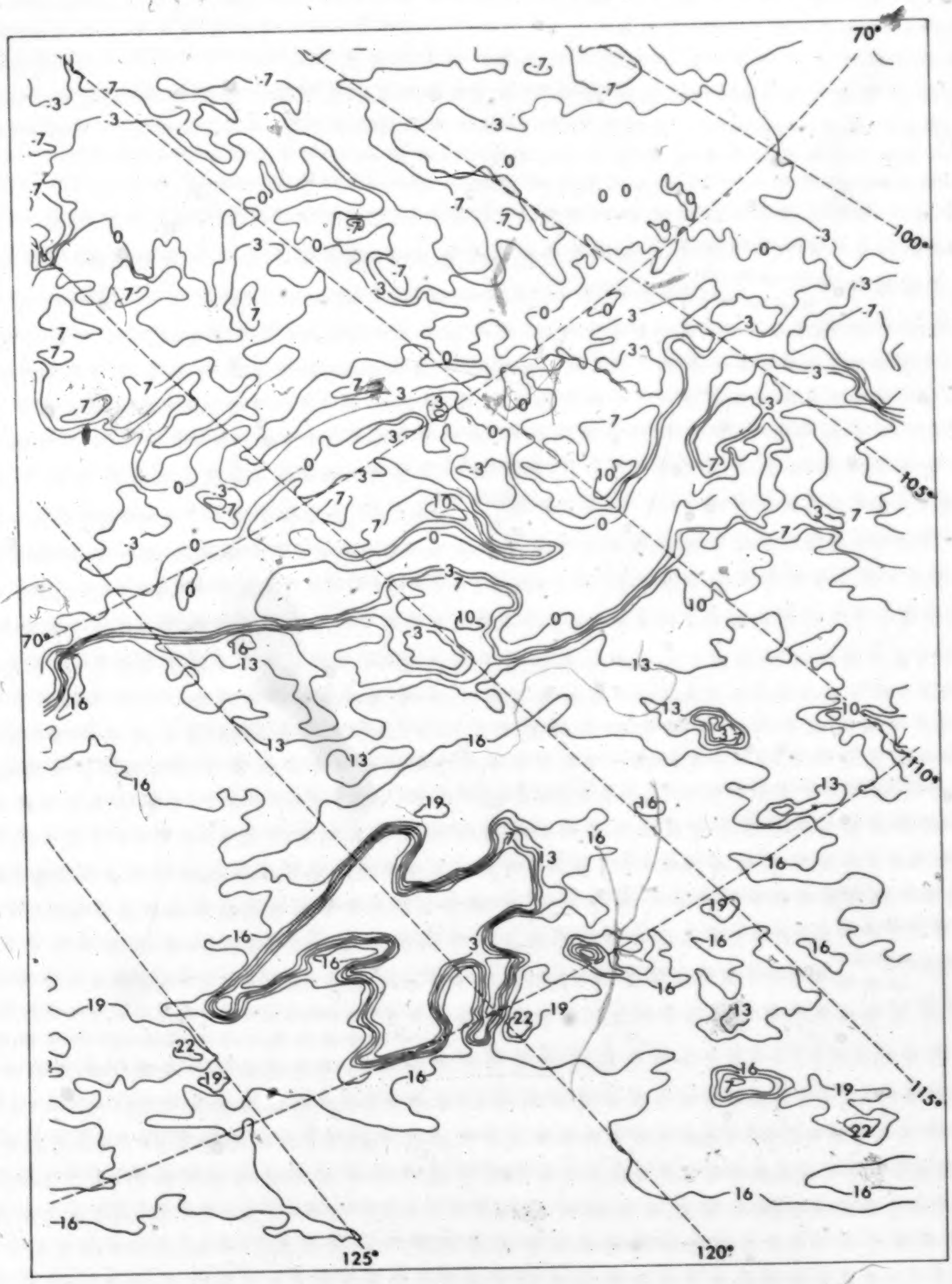
70°
100°
105°
110°
115°
120°
125°
70°
-7
-3
0
3
7
10
13
16
19
22

Figure 4.18: Isotherm Analysis of Great Bear Lake Region and Victoria Island June 17, 1977

CHAPTER 5

SECONDARY AND TERTIARY CIRCULATIONS

5.1 Introduction

The thermal patterns that were derived from the IR satellite imagery represent conditions near the surface of the Earth, when the view was relatively unobstructed by clouds. It was found that the low-level temperature structure was very complex, reflecting the contrasting temperatures over the water, ice and land surfaces in the Arctic during summer. Strong temperature gradients occur along the Arctic coast and the islands of the archipelago.

The thermal structure observed has a pronounced effect on local circulations and also influences small synoptic-scale disturbances. These are referred to as secondary and tertiary circulations in order to distinguish them from the major synoptic-scale systems which are linked to upper troughs and planetary wave patterns. The circulations of prime concern in this study include (1) small synoptic-scale depressions, that are basically low-level disturbances with little or no support in the upper air; and (2) local circulations associated with sea breezes and thermal lows. Three case studies are presented of small, synoptic-scale lows moving along the Arctic coast of Alaska and Canada, and into the Beaufort Sea. In a later section, wind records from coastal stations are examined for sea breeze effects and related circulations over heated islands.

5.2 Three Case Studies Involving Small, Synoptic-Scale Lows

In the earlier description of normal summer circulation patterns in the Arctic, reference was made to the increased latitudinal temperature gradient observed to exist at approximately 70°N along the coasts of Siberia, Alaska and Canada. Direct evidence of this increased gradient was found in the analysis of satellite imagery, along the southern shore of the Beaufort Sea. Large temperature gradients indicate the presence of baroclinic zones, similar in nature to the frontogenetic zones observed in middle latitudes, i.e., quasi-substantial surfaces of discontinuity favourable to the initiation and development of extra-tropical cyclones. In the summer of 1976, there were at least three small, synoptic-scale depressions which exhibited characteristics suggesting this type of development. These disturbances were observed to undergo intensification over a relatively short time period of a few hours, while moving along the Arctic coast and out over the Beaufort Sea. These systems had short life-spans and tended to weaken as they drifted northeastward. The main effect of these lows was to strengthen the winds at the oil-drilling sites near the Mackenzie Delta. Since winds with speeds greater than 20 knots are critical to drilling operations, even relatively minor intensification of such systems can become important.

The Atmospheric Environment Service operated, in the summer months of 1976, a forecast office - the Beaufort Advance Base (BAB) - at Tuktoyaktuk. This office had access to meteorological reports from the drill sites and nearby ships that enabled the forecasters to perform more detailed in situ analyses than were possible at the Arctic Weather Centre in Edmonton. The BAB surface maps were thus particularly useful for tracking small, short-lived disturbances.

(i) Case 1

This example deals with a surface depression which first appeared in Alaska and subsequently moved out over the Beaufort Sea near the Alaska-Yukon border. The system is depicted on the BAB 1900, 1200 and 1800 GMT surface maps of July 30, and the 0000 GMT map of July 31, 1976.

The 0900 GMT surface map of July 30 (Figure 5.1), shows a trough from the west across northern Alaska, with a weak, closed, cyclonic circulation in the northeastern corner of the state. The central pressure of the low was estimated at about 1010 mb. The isobars, drawn every 2 mb, indicate a moderately strong pressure gradient between the low and a weak anticyclone west of Banks Island.

The 0000 GMT 500-mb chart of July 30, (Figure 2.14) was referred to earlier in the circulation summary of Chapter 2. This upper-air chart shows a strong, southwesterly flow over western Alaska which could support a surface trough along the Arctic coast.

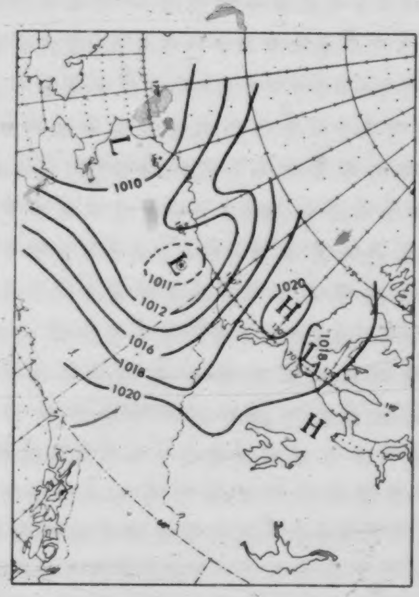
L
1010
1011
L
1012
1016
1018
1020
H
1020
1018
L
H

Figure 5.1: BAB Surface Map
0900 GMT
July 30, 1976

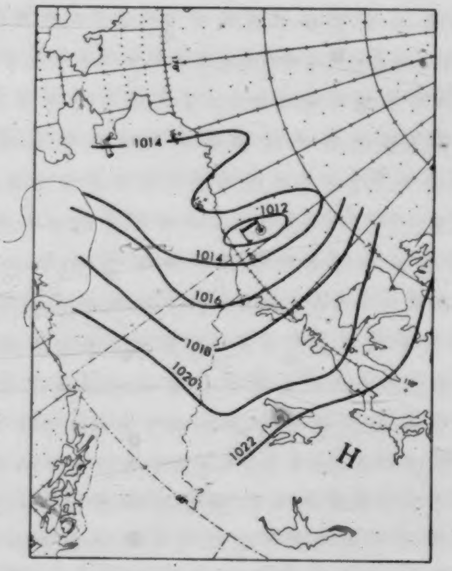
1014
L
1012
L
1014
1016
1018
1020
1022
H

Figure 5.2: BAB Surface Map
1200 GMT
July 30, 1976

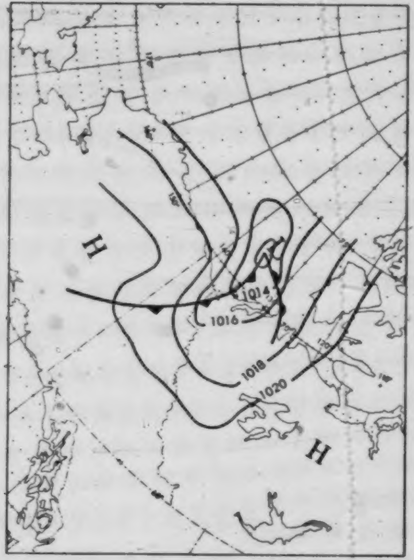
H
L
1014
1016
1018
1020
H

Figure 5.3: BAB Surface Map
1800 GMT
July 30, 1976

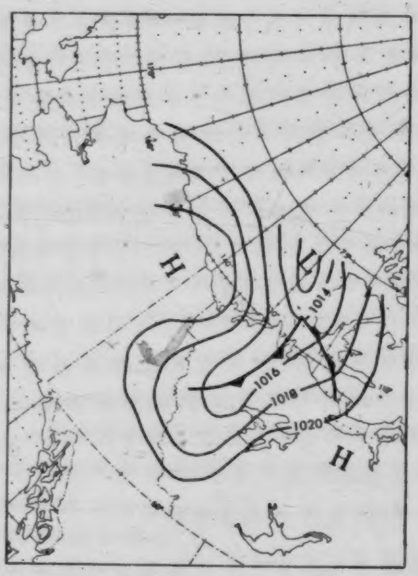
H
L
1014
1016
1018
1020
H

Figure 5.4: BAB Surface Map
0000 GMT
July 31, 1976

However, with a high over the Yukon, the upper flow becomes westerly to the east of 140°W longitude. The zonal flow was maintained in this area over the next 24 hours.

The 1200 GMT surface map of July 30, (Figure 5.2) shows the low centre to have moved over the Beaufort Sea. The central pressure has not changed significantly, but the cyclonic circulation has become better organized over the water. The direction of motion of the low centre is toward the northeast.

By 1800 GMT further development is indicated on the surface map reproduced in Figure 5.3. A frontal wave has been drawn into the centre of the low, and a trough extends southwest over the mainland. It is not clear whether this wave was actually part of the original system. Indeed, six hours later, the 0000 GMT surface map of July 31 (Figure 5.4), shows the wave to be separated from the low. The wave has moved eastward, in the direction of the upper flow, while the low has drifted northeastward along the west coast of Banks Island. Subsequent maps show that the wave and southerly trough continued in an easterly direction, while the low tended to become stationary and fill.

Satellite imagery was available for this area from about 1700 GMT July 30, onward. The visible and IR images from Orbit 7802, 1855-1915 GMT are displayed in Figures 5.5 and 5.6. These are typical for the time in question. Very little cloud is evident in the vicinity of the surface low drawn on the 1800 GMT surface map (Figure 5.3).

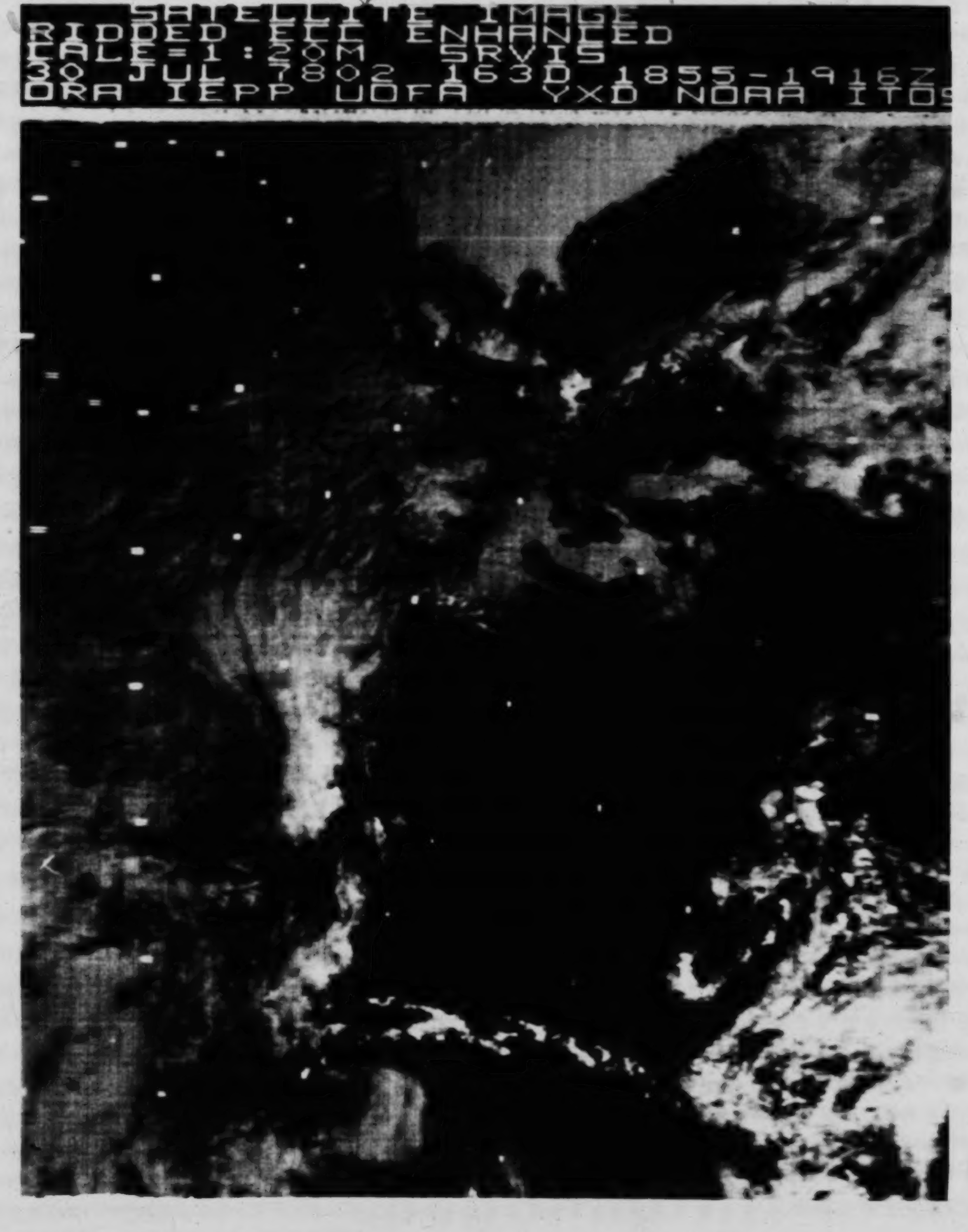
SATELLITE IMAGE
RIDDED ECC ENHANCED
CALE=1:20M SRVIS
30 JUL 7802 1630 1855-1916Z
DRA IEPP UDFA YXD NOAA ITOS

Figure 5.5: Visible Range Image July 30, 1976, Orbit 7802 1855-1916 GMT. Case Study 1.

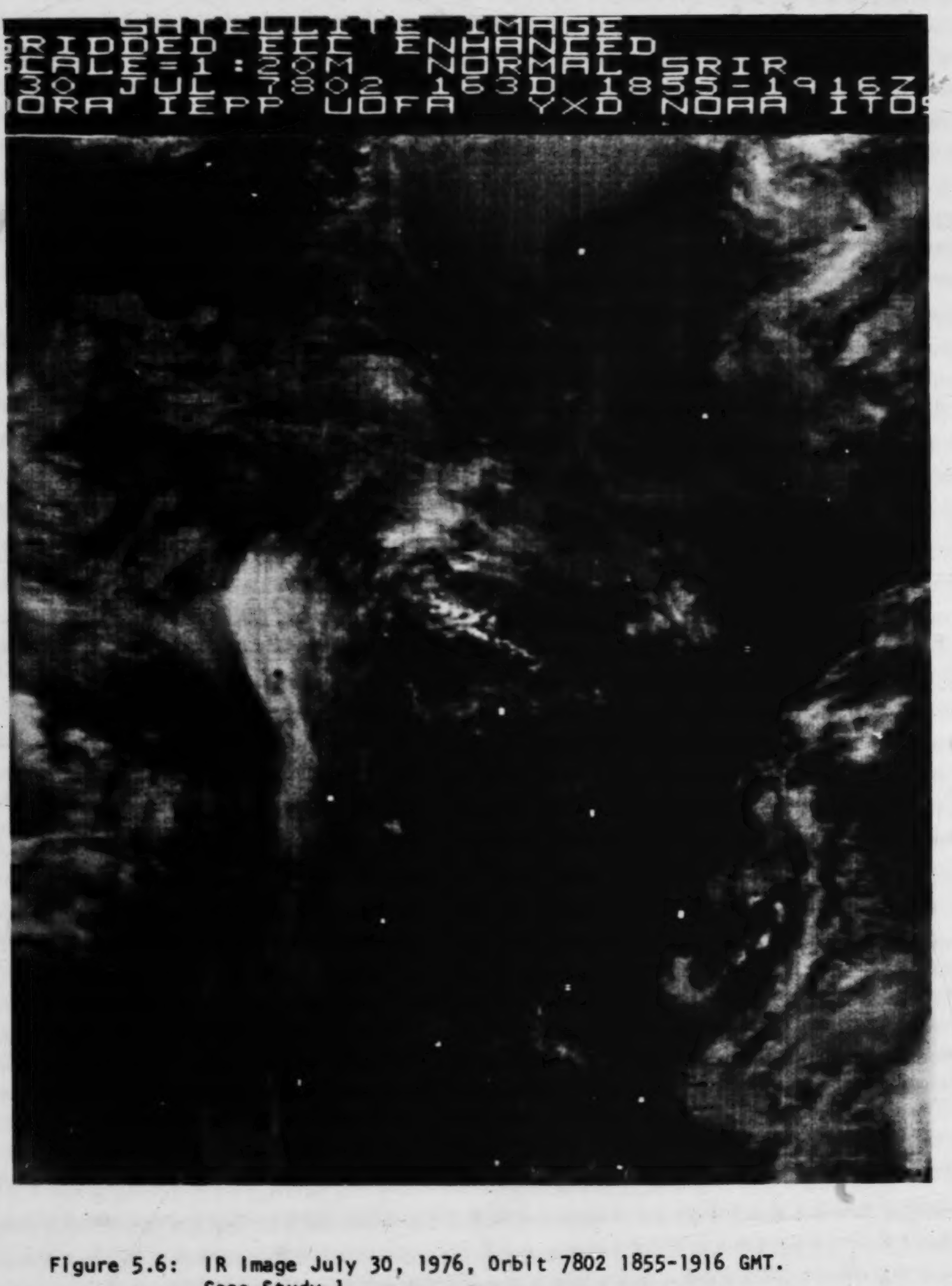
SATELLITE IMAGE
GRIDDED ECC ENHANCED
SCALE=1:20M NORMAL SRIR
30 JUL 7802 163D 1855-1916Z
DORA IEPP UOFA YXD NOAA ITOS

Figure 5.6: IR Image July 30, 1976, Orbit 7802 1855-1916 GMT.
Case Study 1.

With virtually no cyclonic circulation indicated by the cloud pattern, the surface depression seems to have little upper-air support. The main cloud area appears to consist mostly of jet-stream cirrus skirting the upper ridge.

The IR imagery clearly shows the dark land masses and the lighter gray of the Beaufort Sea. Considering previous temperature analyses of IR data, there appears to be a large temperature gradient along the north coast of Alaska and Canada. By comparing the visible and IR images, the open water along the north coast of the mainland and to west of Banks Island is readily discernible. The satellite imagery shows the low to have favoured the areas of open water.

This small depression appears to have been a low-level disturbance producing a weak, cyclonic circulation at the surface, but little else. The motion of the system was interesting in that it was generally northeastward, rather than easterly - the direction of the prevailing upper flow.

(ii) Case 2

This example of a short-lived, small cyclonic system, similar to Case 1, is found on the BAB charts of August 16, 1976. The 1200 GMT 500-mb chart of August 16 appears in Chapter 2 (Figure 2.20). The flow over the Beaufort Sea is quite light from a southwesterly to southerly direction. There are no indications at 500 mb of any organized system in the vicinity of the Mackenzie Delta.

The 0300 to 2100 GMT surface maps of August 16, and 0300 GMT map of August 17 are displayed in Figures 5.7 to 5.12. As in Case 1, the disturbance began as a trough in northern Alaska. On the 0600 GMT surface map (Figure 5.8) a closed, flat low is shown near 150°W longitude on the Alaskan coast. On this and some of the following analyses a frontal wave is carried along with the low. However, considering the nature of this depression, the frontal analysis is highly suspect.

By 1200 GMT (Figure 5.9) the system is shown to have moved out over the water. Lack of information may have hampered the analysis in this area. Three hours later, at 1500 GMT (Figure 5.10) the low is still shown to be close to the coast near the Mackenzie Delta. The central pressure was estimated at about 1001 mb. The cyclonic circulation is not indicated to be very strong at this point.

A significant change took place over the next 6 hours. The 2100 GMT map (Figure 5.11) shows the low has moved northeastward and its central pressure has dropped by 3 or 4 mb. A considerably stronger circulation is now in evidence around the low. Ship reports in the area provided support for this analysis.

The 0300 GMT map of August 17 (Figure 5.12) shows a continued northeastward motion of the disturbance. The system has begun to fill as central pressures are now higher. The low subsequently continued to weaken and drifted towards the west coast of Banks Island.

The satellite imagery available on this day is incomplete because of computer difficulties; the IR and visible images from orbit 8016, 2102 to 2119 GMT are displayed without grid markings.

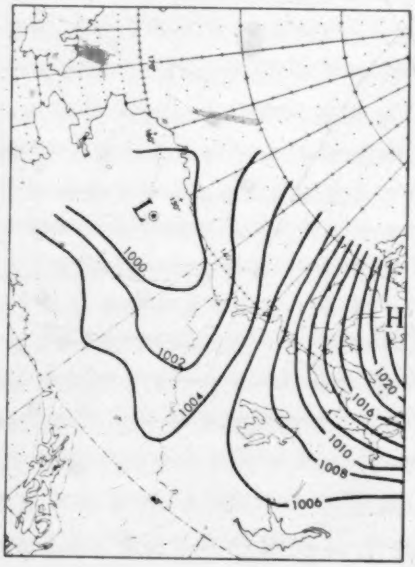
L
H
1000
1002
1004
1006
1008
1010
1016
1020

Figure 5.7: BAB Surface Map
0300 GMT
August 16, 1976

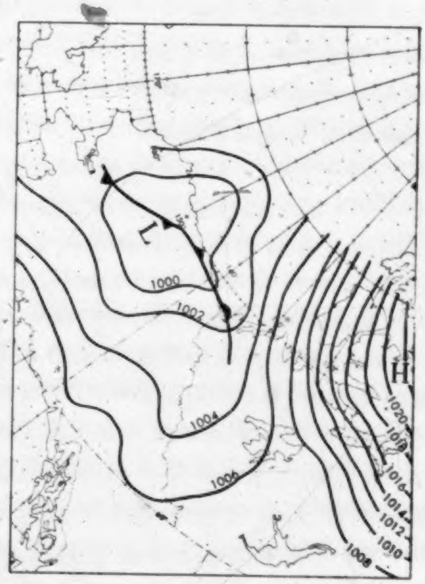
L
H
1000
1002
1004
1006
1008
1010
1012
1014
1016
1018
1020

Figure 5.8: BAB Surface Map
0600 GMT
August 16, 1976

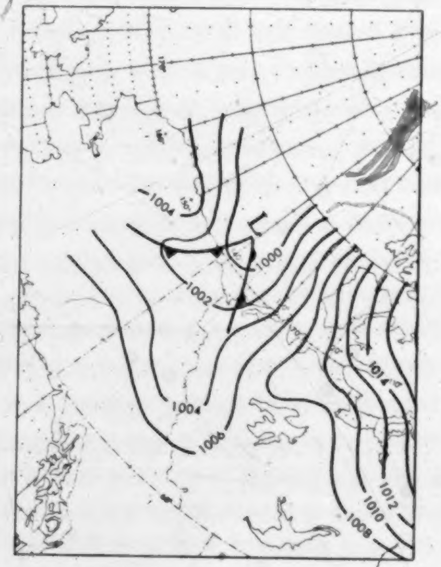
L
1000
1002
1004
1006
1008
1010
1012
1014

Figure 5.9: BAB Surface Map
1200 GMT
August 16, 1976

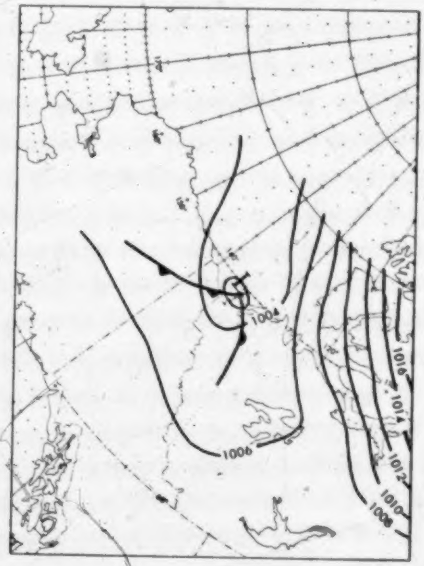
L
1004
1006
1008
1010
1012
1014
1016

Figure 5.10: BAB Surface Map
1500 GMT
August 16, 1976

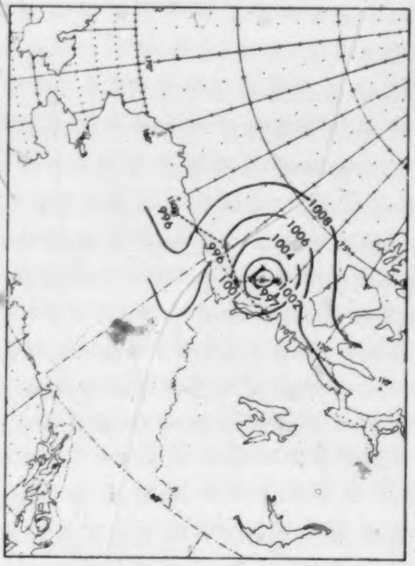
996
1008
1006
1004
1002
1000
L

Figure 5.11: BAB Surface Map
2100 GMT
August 16, 1976

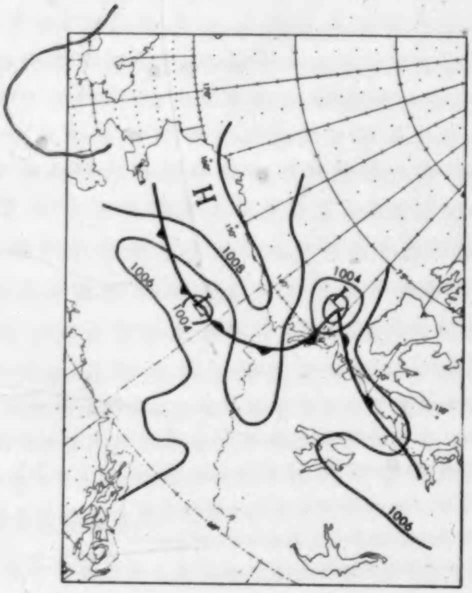
H
1008
1006
1004
1004
1006

Figure 5.12: BAB Surface Map
0300 GMT
August 17, 1976

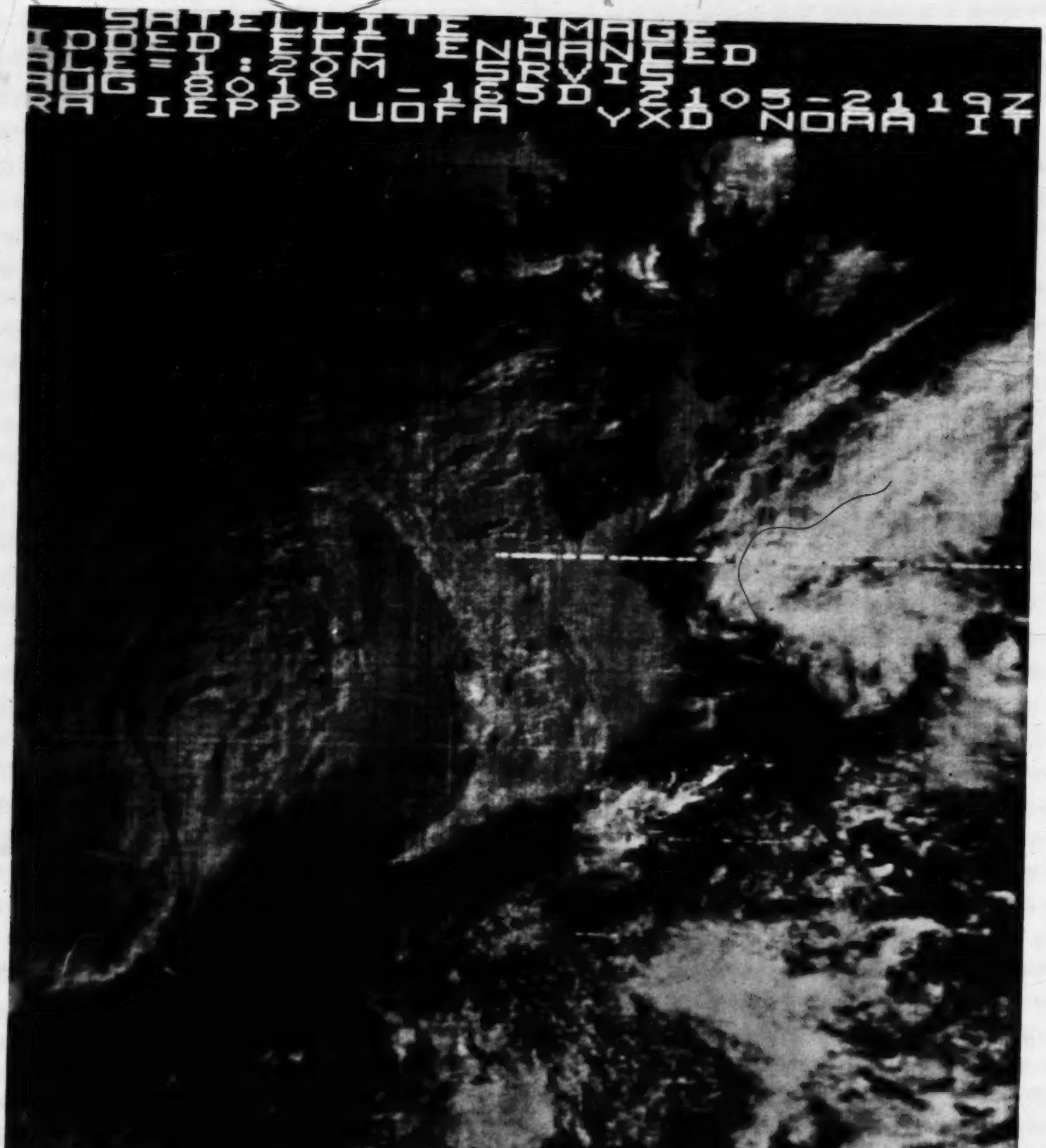
SATELLITE IMAGE
IDDED ECC ENHANCED
ALE=1:20M SRVIS
AUG 8016 -165D 2105-2119Z
RA IEPP UOFA YXD NOAA IT

Figure 5.13: Visible Range Image August 16, 1976, Orbit 8016 2105-2119 GMT. Case Study 2.

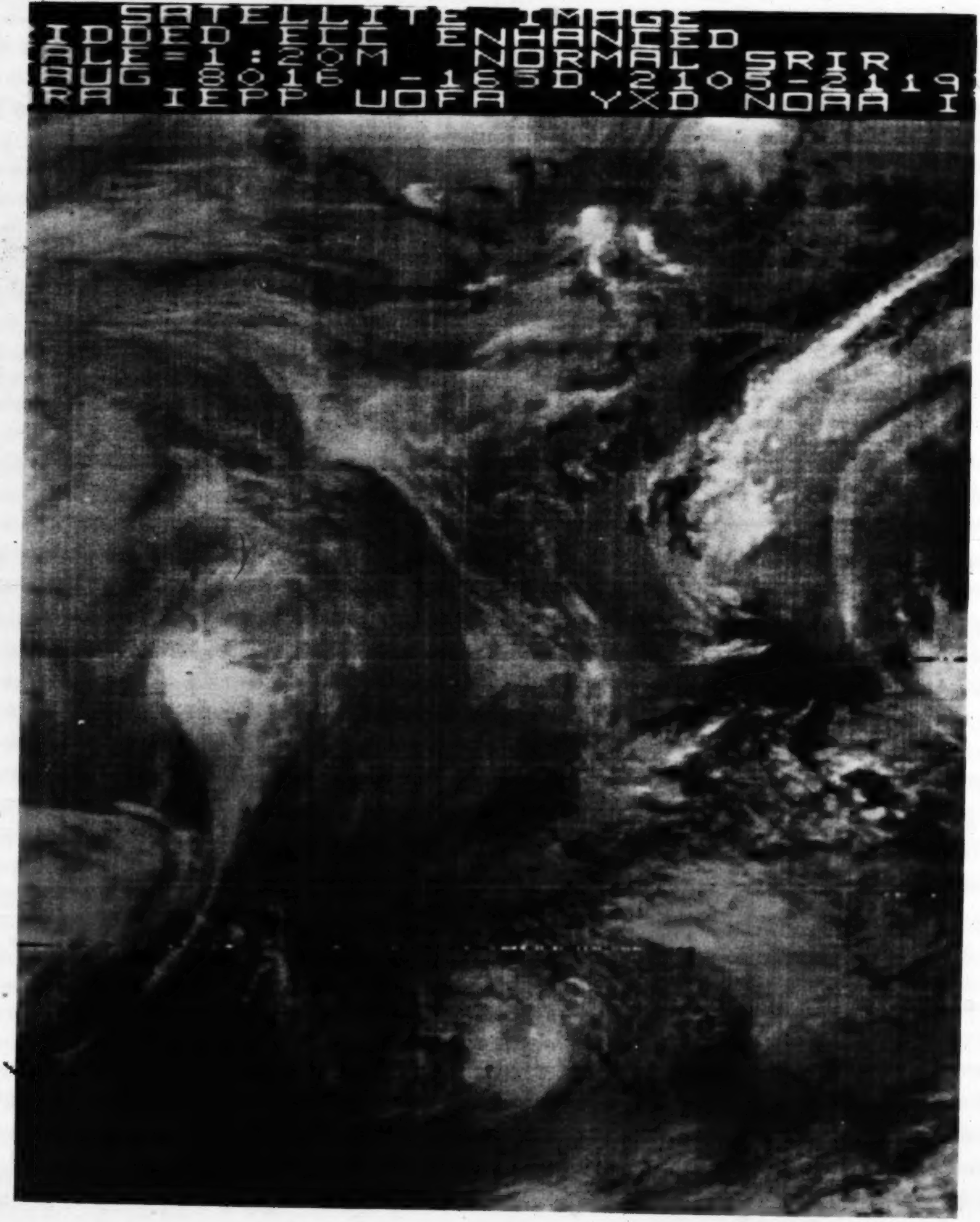
SATELLITE IMAGE
IDDED ELC ENHANCED
ALE=1:20M NORMAL SRIR
AUG 8016 -165D 2105-2119
RA IEPP UOFA YXD NOAA I

Figure 5.14: IR Image August 16, 1976, Orbit 8016 2105-2119 GMT. Case Study 2.

Melville and Prince Patrick islands are quite easily identified near the right-hand central part of the pictures in Figures 5.13 and 5.14. Banks and Victoria islands are considerably obscured by cloud. However, the shoreline along the north coast of the mainland is generally well defined.

Inspection of the satellite imagery in the vicinity of the low, as analyzed on the 2100 GMT surface map (Figure 5.11), yields little evidence of a cyclonic circulation in the cloud patterns. In fact, there seems to be no cloud that could be directly associated with the disturbance. Again this would suggest that the system is shallow and without upper-air support. The IR image confirms, however, the existence of a strong temperature gradient between the mainland and the Beaufort Sea.

The evolution of this small, synoptic-scale low was interesting in that it underwent intensification as it moved northeastward, away from the strong baroclinic zone along the Arctic coast. This disturbance, though also restricted to the lower levels of the atmosphere, produced a marked increase in cyclonic circulation at the surface.

(iii) Case 3

Less than two days after the system described in Case 2, another small disturbance appeared in the same area on August 18. The pertinent surface maps (1200 to 2100 GMT inclusive) are reproduced in Figures 5.15 to 5.18.

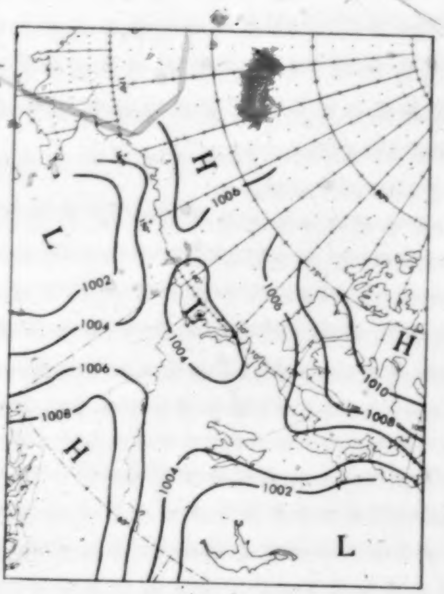
H
L
1006
1002
1004
1006
1008
H
L
1004
1006
1010
1008
H
1004
1002
L

Figure 5.15: BAB Surface Map
1200 GMT
August 18, 1976

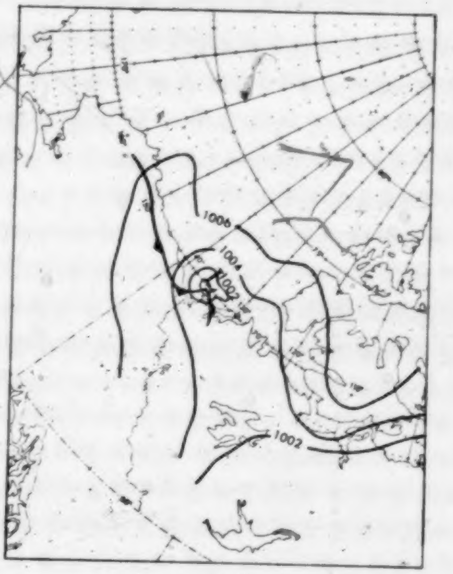
1006
1004
1002
1002

Figure 5.16: BAB Surface Map
1500 GMT
August 18, 1976

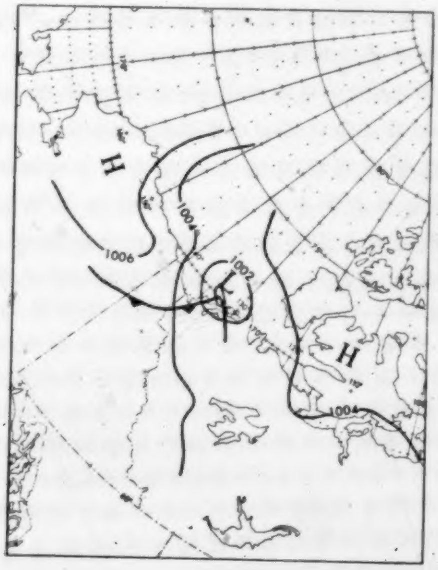
H
1006
1004
1002
L
H
1004

Figure 5.17: BAB Surface Map
1800 GMT
August 18, 1976

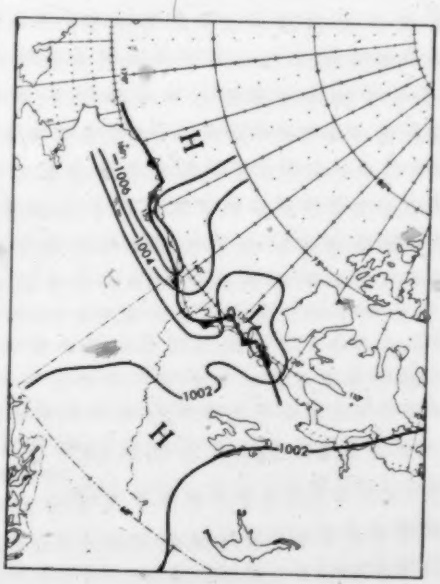
H
1006
1004
L
1002
H
1002

Figure 5.18: BAB Surface Map
2100 GMT
August 18, 1976

The 0000 GMT 500-mb chart of August 19 is included in the circulation summary of Chapter 2 (Figure 2.21). The upper flow showed little change from 1200 GMT August 16. The winds are still light southwesterly over the region, from near the mouth of the Mackenzie River towards Banks Island. The upper-level structure does not seem especially favourable for the development of a surface low in this region.

The 1200 GMT surface map of August 18 (Figure 5.15) shows a flat low-pressure area near Mackenzie Bay. The pressure at the centre of this system was estimated at 1002 mb. The isobars indicate a weak, cyclonic circulation.

By 1500 GMT (Figure 5.16), the low has intensified while remaining in nearly the same position. Its central pressure is now less than 1000 mb, and the cyclonic flow around the centre is more pronounced. Again, the frontal structure indicated on the original working charts is open to doubt.

By 1800 GMT (Figure 5.17), the system has acquired an easterly motion while maintaining its central pressure; a weaker pressure gradient is indicated north of the low. The easterly trend continued to 2100 GMT (Figure 5.18), with the disturbance seeming to move along the coastline. A second low-pressure centre is now located farther east along the coast. A trough has begun to form along the west coast of Banks Island, extending northward from both low-pressure centres. The cyclonic pressure gradient appears to be weakening at this time.

The system did not develop any further. The trough to the west of Banks Island filled slowly over the next few hours.

The earliest satellite imagery available for this region on August 18 was based on the IR and visible data from Orbit 8039, 1713 to 1734 GMT. Inspection of Figures 5.19 and 5.20 show that there was considerable cloud cover over Banks Island and the Beaufort Sea. The most striking feature is the apparent lack of cloud in the immediate vicinity of the surface low. The main cloud mass seems to be associated with the upper trough further to the west. It is again difficult to locate any cloud pattern on the satellite images which could be ascribed to the low-pressure centre shown on the 1800 GMT surface map.

The Arctic coast is barely visible in the satellite pictures. Where the coast is not completely covered by the high cloud, it is obscured by what appears to be stratus or fog. However, the darker shades of gray in the IR image do suggest a large temperature difference between the land and water, and the presence of a strong baroclinic zone along the shores of the Beaufort Sea.

This third example of a small synoptic-scale depression moving along the southern shore of the Beaufort Sea exhibited characteristics similar to those of the other two cases examined. The low began with a weak, cyclonic circulation over the land, and then intensified in the baroclinic zone along the coastline. This low preferred to track along the baroclinic zone, rather than drift northeastward like the first two systems. However, in this case a trough developed over the open water west of Banks Island.

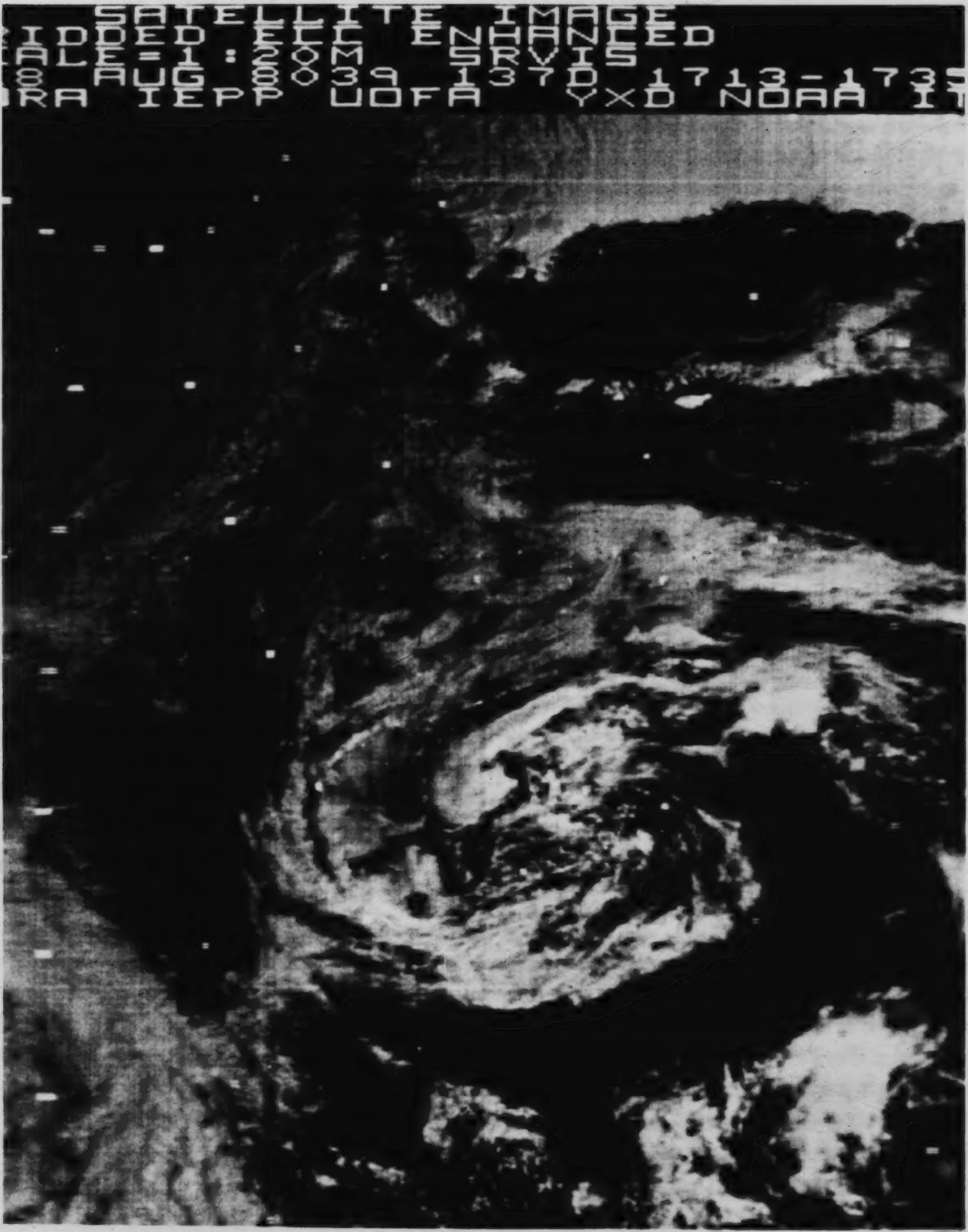
SATELLITE IMAGE
IDDED ELC ENHANCED
ALE=1:20M SRVIS
8 AUG 8039 137D 1713-173
RA IEPP UOFA YXD NOAA I

Figure 5.19: Visible Range Image August 18, 1976, Orbit 8039 1713-1735 GMT. Case Study 3.

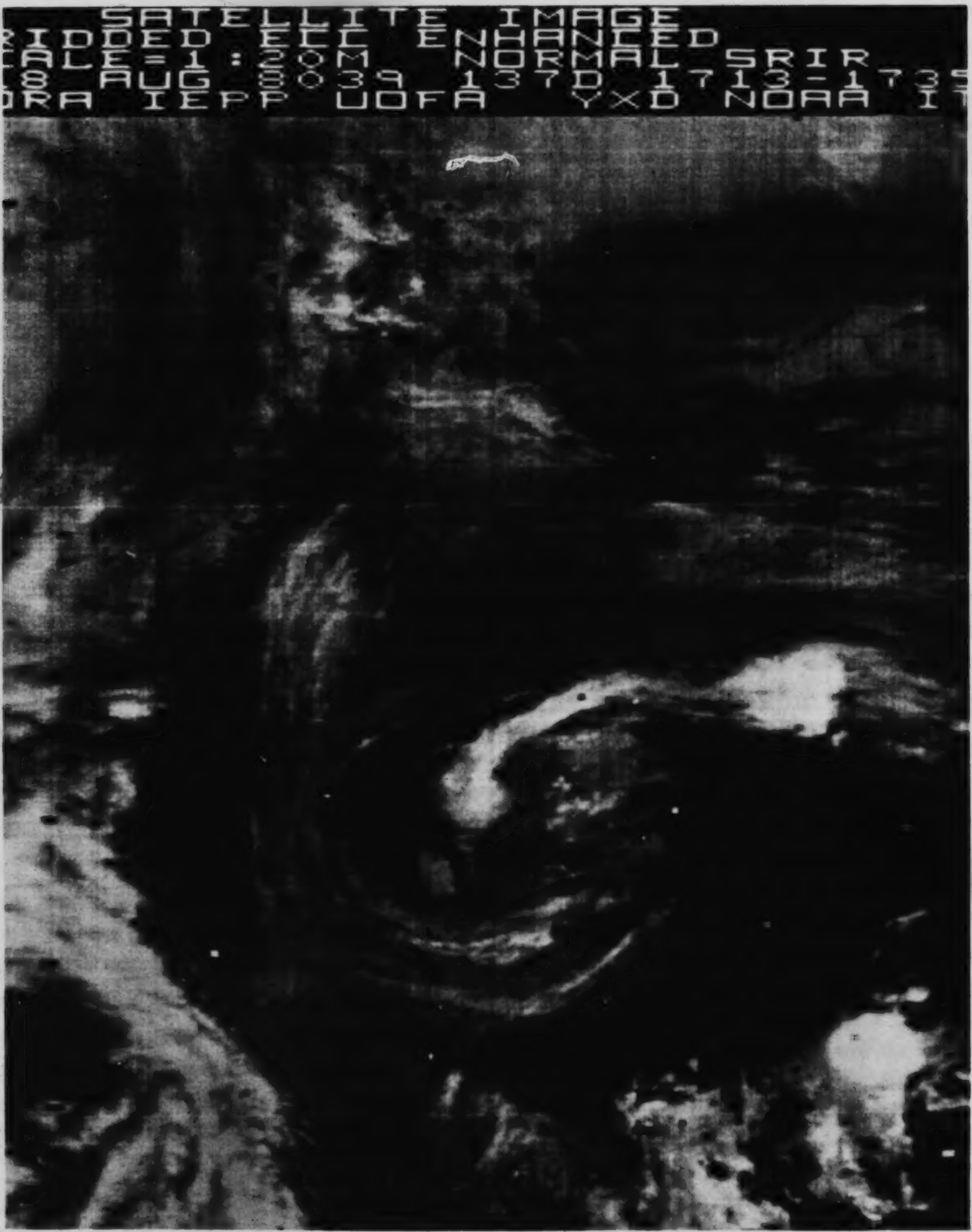
SATELLITE IMAGE
RIDDED ECC ENHANCED
ALE=1:20M NORMAL SRIR
18 AUG 8039 137D 1713-173
DRA IEPP UOFA YXD NOAA IT

Figure 5.20: IR Image August 18, 1976, Orbit 8039 1713-1735 GMT.
Case Study 3.

The main concern when forecasting for drilling ships would be surface winds strengthening suddenly as a cyclone undergoes rapid intensification - a difficult task at best. Fortunately, in the present case, the system soon weakened, and decayed in the next few hours. As before, this low seems to have been essentially a shallow system without a discernible upper-air structure. This conclusion follows readily from an examination of the 500-mb charts and the satellite imagery.

5.3 Local Circulation Over Heated Islands

Small-scale, subsynoptic circulations that are principally the result of local thermal patterns over the Arctic islands are also of considerable practical interest. These local, thermally-driven circulations are sometimes referred to in the literature (e.g., Willet, 1944) as tertiary circulations.

The analysis of IR satellite imagery reveals that, under relatively clear sky conditions, the islands in the Arctic Ocean will be significantly heated by solar radiation. A typical example is provided by the isotherm analysis of 22 July 1976 IR data reproduced earlier in Figure 4.15. This analysis shows surface temperatures of over 20°C in the interior of Banks and Victoria islands, which are comparable to temperatures on the mainland. The thermal contrast between temperatures in the interior of an island and the near-freezing temperatures of the surrounding Arctic waters must exert a considerable influence on local circulations.

Perhaps the best-known thermally-driven circulations are sea and land breezes which are observed in coastal areas everywhere in the world. A description of the sea breeze can be found in many books and papers, e.g., in Wexler (1946). He classified sea breezes into two basic types. When the prevailing gradient wind is very light, the sea breeze develops as a weak circulation in the immediate vicinity of the shore. The circulation gradually increases, vertically and horizontally, both landward and seaward. When the gradient wind is blowing offshore, the initial development of the circulation takes place further out at sea. The sea breeze reaches the coast later in the afternoon and advances slowly inland, much like a cold front, with its wind shift and drop in temperature.

The sea breeze circulation consists of a landward current near the Earth's surface and a much weaker but deeper seaward flow aloft. The top of the landward current ranges from a few hundred meters near the large lakes and temperate-latitude sea coasts, to approximately two kilometers in the Tropics. The landward extent of the sea breeze varies with the land-sea temperature gradient and the synoptic situation. In middle latitudes the sea breeze is often felt 30 to 50 km inland, while tropical breezes will reach points 100 to 200 km from shore.

Sea breezes normally attain velocities 5 to 10 m/sec, but gusts of up to about 15 m/sec may be observed immediately after the passage of a sea-breeze front. The winds associated with an established sea-breeze circulation usually have fairly constant velocities with little oscillation in direction. The sea breeze attains its greatest intensity shortly after maximum temperatures are reached, and decreases as sunset approaches. The land breeze that develops later is much weaker in intensity and smaller in extent. When the sea temperature is too low, the land breeze may be suppressed entirely.

Very little is known about the intensity, distribution and frequency of the Arctic sea breeze. At present, no adequate observational network of any kind is available for examining the structure of sea-breeze circulations in even moderate detail. It may well be, however, that the Arctic sea breeze though similar in structure, is more intense than the sea breeze in temperate latitudes because of the larger temperature contrast between land and sea.

There is a lack of observational data on island sea breezes, especially in the Arctic. The sea breeze over a heated island may be quite different from that at a mainland coast. Depending on the size of the island, the prevailing gradient wind will have a large influence on the local, tertiary circulation. Wind direction and speed are both important, since the sea breeze circulation would likely be affected in diverse ways in different parts of an island. On the synoptic scale, calm conditions or light winds are necessary for establishing a pure sea-breeze circulation.

Some theoretical work has been done on heated island circulations. Malkus and Stern (1953) studied the flow of a stable air mass over a small heated island some 10 km wide. They found that the island had an "equivalent mountain" effect on the flow, creating lee-wave type of disturbances downstream.

Smith (1955) used the equations of motion, continuity, and a heat function to model the circulation over a land mass 200 km wide. He obtained vertical velocities over the island centre of 2-3 cm/sec. Neumann and Mahrer (1974) considered sea breezes for circular islands in a numerical model. For an island of radius 51.25 km they found a well-developed sea breeze front, a better-defined circulation than for a straight coastline, with strong horizontal convergence ahead of the front and divergence behind, to an altitude of 400-500 m. The reverse of this circulation existed aloft. Maximum vertical velocities near the front were 50 cm/sec.

Banks and Victoria islands were selected for the study of sea breeze effects in the Arctic islands, since they had been included in previous temperature analyses. Both islands are quite large, Banks being roughly 150 km by 350 km in size, and Victoria about 500 km by 600 km. These land masses are large enough for sea breezes to be established under appropriate conditions.

Sachs Harbour, located on the west coast of Banks Island, is the only meteorological station in the region. There are no weather stations whatsoever on Victoria Island, a major gap in the network. The map in Figure 5.21 shows the location of the observational site at Sachs Harbour. Being situated on the north side of an inlet, one might expect a sea breeze to have a southerly as well as a westerly component.

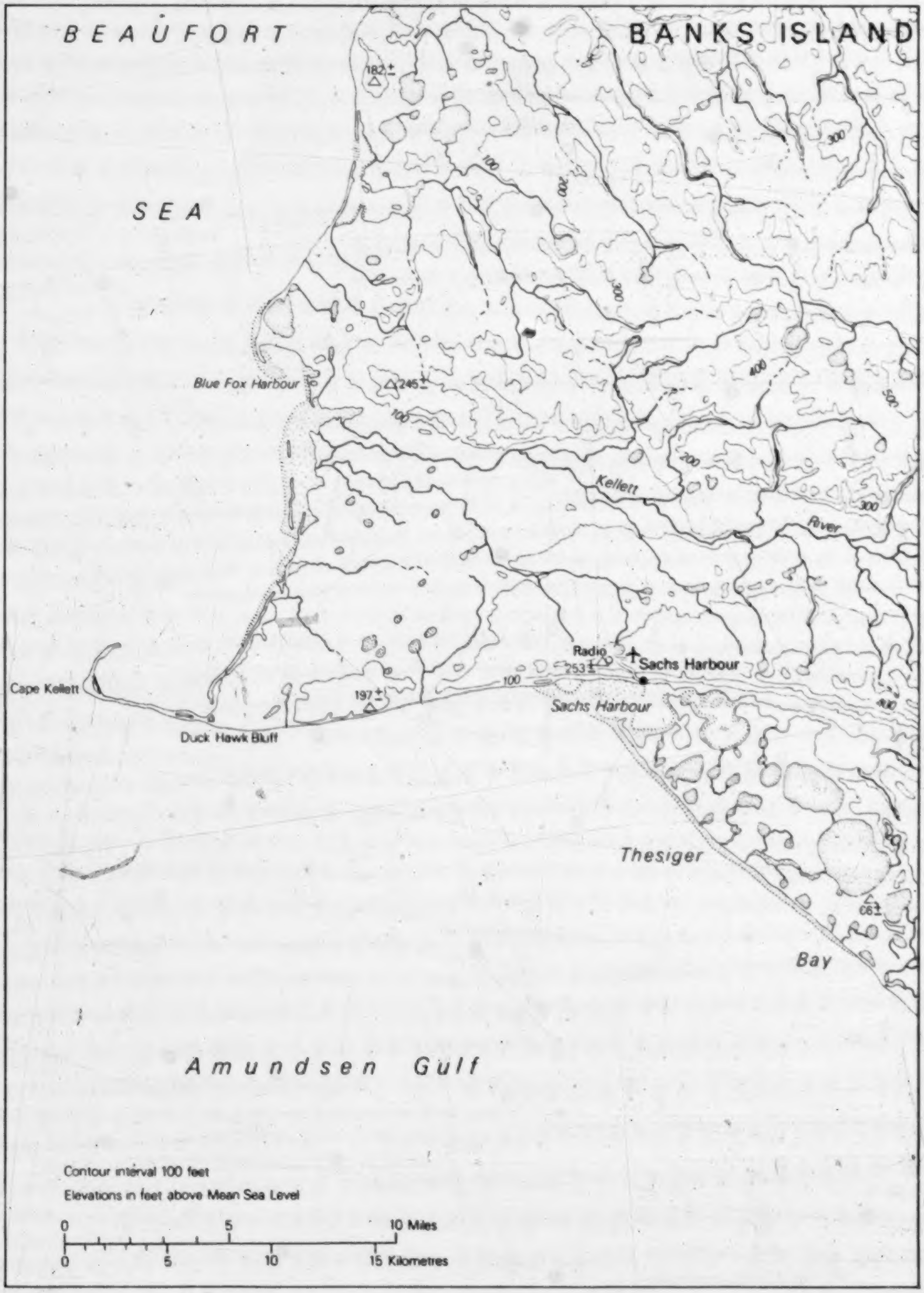
BEAUFORT
BANKS ISLAND
SEA
182±
300
100
200
300
245±
Blue Fox Harbour
400
500
100
200
Kellett
River
300
Radio
253±
Sachs Harbour
Cape Kellett
100
197±
Sachs Harbour
400
Duck Hawk Bluff
Thesiger
66±
Bay
Amundsen Gulf
Contour interval 100 feet
Elevations in feet above Mean Sea Level
0
5
10 Miles
0
5
10
15 Kilometres

Figure 5.21: Map of Sachs Harbour Region

Since heating through insolation plays the major role in sea-breeze circulations, consideration must be given to sunrise and sunset times. The Arctic has long periods of continuous daylight during much of the summer. At Sachs Harbour (latitude 71°59'N) on July 1, at local solar noon, the sun's elevation above the horizon is about 41°. At midnight, the sun's minimum elevation is 5°. By August 1, the maximum elevation has decreased to 36° and at midnight the sun first begins to dip below the horizon. On the first day of September the noon elevation is 27° and the minimum at night is 9° below the horizon. Thus Sachs Harbour experiences continuous daylight throughout July and for most of August.

However, in any given 24-hour day, the sun's elevation above the northern horizon is so low that its rays barely graze the ground, and only effect negligible heating for a significant part of the time. The surface temperature will, therefore, also undergo diurnal changes in the Arctic summer, with a maximum one or two hours after local noon, and a minimum in the early morning.

Daily weather reports and satellite imagery were used to select reasonably cloud-free days in July and August. Synoptic situations were also required with predominantly light gradient winds. Four cases in each month were chosen as being representative of sea breeze circulations at Sachs Harbour. The wind records of July 12, 1976 (the first of the eight days sampled) taken at Sachs Harbour, Cape Parry, Nicholson Point and Clinton Point, are listed below, in Table 5.1. The winds recorded on the other seven days are included in Appendix C. Cape Parry, Nicholson and Clinton Point are located

Table 5.1

WIND ABSTRACTS

DATE: July 12, 1976

Hour (GMT)		Station			
		YSY	ZUE	YUC	YUH
12 July	06	030/08	020/03	070/15	320/07
	07		350/05		300/10
	08	020/06	350/07		300/05
	09	080/10	360/06	090/10	350/05
	10	080/10	020/04		280/05
	11	080/10	010/05		260/05
	12	090/08	040/01	090/10	calm
	13	080/07	100/03		320/01
	14	100/04	110/05		calm
	15	calm	080/05	090/10	020/02
	16	230/05	100/09		020/03
	17	240/06	110/08		030/03
	18	230/07	090/09	090/14	040/02
	19	230/08	080/12		090/03
	20	220/10	080/12		
	21	230/10	090/13	060/16	140/05
	22	240/12	090/14		140/05
	23	240/11	100/17		
13 July	00	320/04	080/17	080/19	140/10
	01		090/13		120/03
	02	030/05	090/19		050/04
	03	020/05	090/18	090/17	150/04
	04	340/07	100/15		150/05
	05	030/08	100/14		180/02

on the Arctic coast, south of Banks Island; the records at these sites were used primarily as indicators of synoptic wind conditions.

The sea breeze appeared to favour directions from the south-southwesterly sector, 180° to 240°. In most cases the wind underwent a gradual veering change over a few hours, with the sea breeze usually established by 1800 GMT. There were some exceptions. On July 12 the wind shifted dramatically from east at 1400 GMT to southwest at 1600 GMT. Moreover, the sea breeze came to an early and sudden end that day. The southwest wind at 2300 GMT became a northwest wind by 0000 GMT, and northeasterly by 0200 GMT. On other sea breeze days the wind tended to back gradually after about 2300 GMT.

The sea breeze circulation seemed late to develop on August 9 with no definite wind shift reported until 2100 GMT. The speed of the sea breeze was usually less than ten knots, and rarely greater than twelve knots. Moderately strong winds were reported late in the day on August 3, but these were caused by a changing synoptic situation.

On days with light gradient winds the sea breeze at Sachs Harbour favours a southerly to southwesterly direction at speeds of five to ten knots. In July and August the sea-breeze circulation is generally established by 1800 GMT and begins to dissipate after 2300 GMT. Usually the wind shifts are gradual, at least on the days with light prevailing winds considered here.

A circulation similar to that found at Sachs Harbour may be assumed to be characteristic of Banks Island as a whole. The extent to which a general sea breeze circulation will affect the entire island will depend on the prevailing wind and local temperature gradients at the surface. During the warm part of the day one would expect a net convergence of air from the coast towards the center of the island. With air temperatures at the coast only a few degrees above freezing, and surface temperatures in the interior of the island above 20°C, the landward moving airmass will undergo rapid modification from below. A rough estimate of the rate of this modification may be obtained from the isotherm analysis for July 22, a date with a good sea breeze at Sachs Harbour.

Consider the temperature gradient along the west coast of Banks Island. A good estimate of the temperature of the air arriving at the coast from the Beaufort Sea might be 3°C. The major temperature gradient, as the air advances inland, ends at about 20°C. This represents a change of approximately 17°C in an average distance of about 15 nautical miles, or around 1.1°C per nautical mile. If the sea breeze has a speed of 10 knots, then the air is being subjected to 11°C of warming per hour while traversing this zone of intense temperature gradient.

As the air near the surface is rapidly warmed and existing inversions "burn off", considerable vertical velocities should develop as the bubbles of heated air rise. The upward motion might be expected to generate a line of convective cloud, especially ahead of the advancing sea breeze front. This has often been observed in more southerly latitudes. However, satellite imagery fails to reveal this type of cloud with any regularity for sea breeze days over Banks Island. The limiting factor here would seem to be the moisture content of the air.

Along with a coastal air temperature of $3^{\circ}C$, it is not unreasonable to assume a dew point of about $2^{\circ}C$. Then, since the landward moving air will have little opportunity to acquire additional moisture from the barren ground, the moisture content of the air should change very little as it warms to near $20^{\circ}C$. Simple extrapolation on a tephigram shows that convective cloud is not likely to develop below an altitude of 8000 feet under these temperature and moisture conditions.

If sufficient moisture is injected into the warm, rising air, cloud should form. Attention is again drawn to the imagery of July 22, (Figures 4.2 and 4.3), where a patch of what appears to be convective cloud is found over central Victoria Island. Reference was made to this cloud earlier, in section 4.4. It was then concluded that the cloud was low and of little vertical extent. The air would seem to have been moist enough to initiate cloud development, but conditions aloft were apparently not conducive to much vertical development.

CHAPTER 6

SUMMARY AND CONCLUSIONS

6.1 Outline

The main purpose of this study was to investigate the temperature structure near the Earth's surface in the Canadian Western Arctic with the aid of satellite data. In addition, it was intended to identify those characteristics of the Arctic circulation in summer which may be directly linked to the complex, thermal patterns that were observed.

This work is presented basically as it evolved - in two interdependent parts. First a method was devised to deduce temperatures from the diverse, gray hues of IR satellite imagery. The resulting analyses indicated certain anomalies in the thermal pattern that led quite naturally to the second part of the investigation, so-called secondary and tertiary circulations, found in the Arctic in summer, which seemed to be strongly influenced by the surface temperature regime. These circulations included small synoptic-scale lows, found along the northern coasts of Alaska and Canada, and the thermal lows and sea breezes associated with the Arctic islands.

6.2 Thermal Structure from IR Satellite Imagery

The quickest and most common method of satellite data display involves the production of a photographic image in varying shades of gray. This approach has the advantage of putting the visible and IR satellite data into an easily recognizable form. However, from a quantitative point of view, interpretations based on levels-of-gray discrimination are not very satisfactory in practice.

In the course of this work it was decided to attempt a more quantitative display of the IR data by converting the digitized radiation levels into estimates of equivalent blackbody temperatures. While only estimates of absolute temperature were justified in principle, the method could be used with confidence for the determination of temperature differences. Moreover, the estimates could be improved by calibration against reference surfaces, with known temperature characteristics, such as the water and ice which were in a near-freezing state.

Isotherm analyses were performed on the derived temperatures for two satellite passes on different days, July 22, 1976 and June 17, 1977. The analyses revealed a very complex thermal pattern in the Western Arctic. The sharp contrast in temperature between the land and sea was clearly recognizable.

The temperature gradient was very strong along the coasts of Alaska and Canada bordering on the Beaufort Sea. This dense "packing" of isotherms is similar to that found in baroclinic zones associated with fronts in mid-latitudes.

The temperature analysis revealed that the interior regions of the Arctic islands, which were free of snow and ice, attained surface temperatures comparable to those found on the mainland. These heated islands were judged to have a pronounced influence on local circulations, evidence of which was later found.

Since surface-based inversions are a common phenomenon in the Arctic, it was hoped that the satellite imagery could be used as a means of mapping these inversions. However, little success was achieved in this area. It was found that, in the absence of low cloud to mark an inversion layer, the radiation originating from the Earth's surface would mask the temperature anomalies existing in the air above. The APT imagery was more useful in delineating those areas where an inversion would not be found.

6.3 Secondary and Tertiary Circulations

The presence of a baroclinic zone, or "quasi-front", along the borders between the land and water areas is expected to have an effect on local circulation patterns. This was investigated by considering three case studies involving small, synoptic-scale depressions.

The three situations bore similarities to each other. The disturbances were spawned near the Arctic coast of Alaska and northwestern Canada. The initial impetus to cyclogenesis could have been provided by the remains of a lee trough, aided by a southwesterly upper flow over Alaska. Thermally-generated low pressure could also have been a factor, the result of strong heating over the land surface.

The case studies described how relatively weak lows intensified and then decayed, over a period of a few hours, while moving eastward along the coast and over the waters of the Beaufort Sea. Once over the open sea, the motion of the low pressure systems showed a tendency to favour the warmest water, as identified in the satellite imagery. The evidence indicated that these small depressions were low-level systems. The main meteorological effect was an increased cyclonic circulation in the immediate vicinity of the lows. The lows examined in the three case studies demonstrated characteristics which are often associated with cyclogenesis along a middle-latitude baroclinic zone. In these examples the "front" was, in Petterssen's terminology, "geographically bound" in nature, fixed along the northern coastline of the mainland.

Sources and sinks of vorticity in polar regions are discussed by Petterssen (1956). In a summer situation, the main export of cyclogenic vorticity is from sea to land, or from cold to warm ocean currents. This suggests that once a low has moved from the land to the water, the tendency would be for the low pressure to be maintained over the warmest water. This was generally borne out by the present work.

The final aspect of secondary circulations was concerned with the sea breeze effect over the heated Arctic islands. Under favourable conditions of light gradient winds and clear skies, there was evidence that a sea breeze, blowing from a southerly to southwesterly direction, became established at Sachs Harbour. The expected strong convergence of coastal air towards the center of the islands, and associated vertical motion of the air mass was not, in general, supported by observations of convective cloud. However, due to the extreme modification of the air moving inland, it may well have been that there was not sufficient moisture present for the formation of cloud. In spite of this, there were instances where small amounts of convective cloud were observed. Considering the amount of surface heating revealed by the analysis, it can only be concluded that these Arctic "heat islands" must have a significant effect on the Arctic circulation in summer.

6.4 Suggestions for Future Work

The present study has only provided a preliminary look at several quite varied aspects of Arctic circulations. Practically all of the topics discussed require further investigation as more data become available. Of particular interest should be the local circulations over the Arctic islands. Much of the critical weather, from a forecasting point of view that affects the Arctic, is caused by low-level phenomena such as stratus and fog. It is these elements that are particularly dependent on local wind conditions.

REFERENCES

Anderson, R.K., and A.H. Smith, 1971: Application of meteorological satellite data in analysis and forecasting. ESSA Technical Report, NESC 51, Supp. 1, 61 pp.

Anderson, R.K., 1973: The use of satellite pictures in weather analysis and forecasting. W.M.O. Technical Note, No. 124, 275 pp.

Belmont, A.D., 1956: Lower tropospheric inversions at ice-island T-3. Arctic Meteor. Res. Group, Pub. Meteor. No. 4, McGill University, Montreal, 21 pp.

Bilello, M.A., 1966: Survey of arctic and subarctic temperature inversions. Tech. Report 161, Cold Regions Res. and Eng. Lab., Hanover, N.H., 35 pp.

Feuerherdt, W.R., 1977: A study of recorded winds and Beaufort Sea storms during the 1976 drill season. Unpublished, Arctic Weather Centre, Edmonton, 62 pp.

Fraser, D.B., 1973: Synoptic weather patterns in the arctic. Unpublished, Arctic Weather Centre, Edmonton, 26 pp.

Gerson, D., 1975: Computer estimation of the presence of sea ice in satellite pictures. NASA Tech. Report 366, Washington, D.C., 96 pp.

Keegan, T.J., 1958: Arctic synoptic activity in winter. J. Meteor., 15, pp. 513-521.

Klein, W.H., 1956: Principal tracks of cyclones and anticyclones in the northern hemisphere. U.S. Weather Bureau Res. Paper No. 40.

Kunkel, B.A., 1959: A synoptic-climatological study of the arctic circulation in summer. Dept. of Meteor. and Climatol., Scientific Report No. 7, University of Washington, 50 pp.

Maddin, R., H. Miller, M. Polifka, and T. Vonder Haar, 1972: Computer programs for direct read-out satellite use. Atmos. Science Tech. Report, Colorado State University, Fort Collins, 95 pp.

Maddin, R. and C. Parsons, 1973: A technique for real-time, quantitative display of APT scanning radiometer data. J. Appl. Meteor., 12, pp. 381-385.

Malkus, J.S. and M.E. Stern, 1953: The flow of a stable atmosphere over a heated island, Part I. J. Meteor., 10, pp. 30-41.

McClain, E.P., 1972: Special displays of satellite infra-red data for sea ice monitoring. In: Earth Resource Program Review, 4th Annual, Houston, Texas, Manned Space Craft Center, Jan. 17-21, 1972, (Papers), Vol. 4, Sect. 87, Washington, D.C., 11 pp.

Munn, R.E., J. Tomlain and R.L. Titus, 1970: A preliminary climatology of ground-based inversions in Canada. Atmosphere, 8, pp. 52-68.

Neumann, J. and Y. Mahrer, 1974: A theoretical study of the sea and land breezes of circular islands. J. Atmos. Sci., 31, pp. 2027-2039.

Petterssen, S., 1950: Some aspects of the general circulation of the atmosphere. Centenary Proceedings of the Royal Meteorological Society. London, pp. 120-155.

Petterssen, S., 1956: Weather Analysis and Forecasting, Volumes I and II, 2nd ed. McGraw-Hill Book Co., N.Y., 428 pp and 266 pp.

Reinelt, E.R., P. Hof, D. Oracheski and J. Broszkowski, 1975: Research studies of numerical enhancement of APT scanning radiometer data for application to arctic weather and ice prediction. Final Report, DDS(AES) Contract OSV4-0183, University of Alberta, Edmonton, 204 pp.

Rao, P.K., 1970: Estimating cloud amount and height from satellite infrared radiation data. ESSA Technical Report NESC 54, 11 pp.

Schwalb, A., 1972: Modified version of the improved TIROS operational satellite (ITOS D-G). NOAA Technical Mem. NESS 35, Washington, D.C., 48 pp.

Smith, W.L., P.K. Rao, R. Koffler and W.R. Curtis, 1970: The determination of sea surface temperature from satellite high resolution infrared window radiation measurements. Mon. Wea. Rev., 98, pp. 604-611.

Struebing, K., 1972: Satellite pictures and sea ice reconnaissance: A methodical attempt for the Baltic Sea. Trans., [NLL-M-20841], National Lending Library, Boston, Mass., 37 pp.

Thompson, A.H., 1972: The polar inversion: A review and some recent studies in northwest North America. Paper presented at the Sixth Annual Congress of the Canadian Meteorological Society.

Vowinckel, E., 1965: The inversion over the polar ocean. Arctic Meteor. Res. Group, Scientific Report 14, McGill University, Montreal, 21 pp.

Wexler, H., 1936: Cooling in the lower atmosphere and the structure of polar continental air. Mon. Wea. Rev., 64, pp. 122-136.

Wexler, R., 1946: Theory and observation of land and sea breezes. Bull. Amer. Meteor. Soc., 27, pp. 272-287.

Willet, H.C., 1944: Descriptive Meteorology. Academic Press, Inc., N.Y., 310 pp.

APPENDIX A

Table A.1a Observed Inversion Classes - Sachs Harbour

Day	1	2	3	4	5	6	7	8	9	10	11	12	13	14	15	16	17	18	19	20	21	22	23	24	25	26	27	28	29	30	31
JULY																															
0000 GMT	3B	4	3B	4	4	3B	3B	4	4	4	4	4	4	3B	4	3C	4	4	3C	2	2	4	2	4	4	4	3B	4	2	3B	3B
1200 GMT	3B	3B	3B	3B	3B	3B	4	3B	4	4	4	4	3B	3C	2	3B	3A	3B	3B	2	3C	3B	2	3B	3B	3C	3B	3B	2	1	3B
AUGUST																															
0000 GMT	3B	3B	3B	3B	3B	4	3B	4	3B	3B	4	3B	4	4	3B	3B	3B	M	3B	3B	4	4	4	3B	3B	4	3B	3B	3B	4	2
1200 GMT	3B	3B	2	1	3B	3B	4	3B	3B	3B	3B	2	3B	3B	3B	3B	3B	3A	M	4	3B	4	3B	3B	3B	3A	3B	3B	2	2	2
SEPTEMBER																															
0000 GMT	2	4	4	3B	4	3B	4	4	4	4	4	4	4	4	3A	4	3B	3B	3B	3B	4	3A	2	3B	3B	4	3B	3B	3B	3B	
1200 GMT	3C	3B	3B	M	3B	3B	3B	3B	3B	3C	4	3B	3A	3B	3A	4	3B	4	3B	2	2	2	3B	3B	3B	3B	3B	4	3B	4	

M - Missing Report

Table A.1b Observed Inversion Classes - Inuvik

Day	1	2	3	4	5	6	7	8	9	10	11	12	13	14	15	16	17	18	19	20	21	22	23	24	25	26	27	28	29	30	31
JULY																															
0000 GMT	4	4	4	4	4	4	4	4	3B	3B	4	4	4	4	4	4	4	4	4	4	4	4	4	4	4	4	4	4	4	4	3B
1200 GMT	3C	3A	4	3C	4	4	3B	3B	3A	3B	3C	3B	4	3C	3C	3B	3C	3C	3C	3C	3C	3C	2	3B	3A	3C	4	2	3C	2	3B
AUGUST																															
0000 GMT	4	4	4	4	4	4	4	4	4	4	4	4	3B	4	4	4	4	4	4	4	4	4	4	4	4	4	4	4	4	4	4
1200 GMT	3B	3B	3C	3A	4	4	4	3B	4	3B	2	3C	3A	3B	M	3B	3B	M	3B	4	3B	4	3B	3B	3B	2	2	2	3C	3B	3C
SEPTEMBER																															
0000 GMT	4	4	4	4	4	4	4	4	4	4	4	4	4	4	4	3B	4	4	4	4	3C	3A	2	3C	3B	3A	3B	4	3B	3B	
1200 GMT	4	3B	2	3B	4	3C	3B	2	3C	4	3B	3C	3C	3B	3B	3B	3B	3B	2	3C	2	2	3B	3B	2	2	3B	3A	M	4	

M - Missing Report

Table A.1c Observed Inversion Classes - Norman Wells

Day	1	2	3	4	5	6	7	8	9	10	11	12	13	14	15	16	17	18	19	20	21	22	23	24	25	26	27	28	29	30	31
JULY																															
0000 GMT	4	4	3C	4	4	4	4	4	4	3C	4	4	4	4	M	4	4	4	4	4	4	4	4	4	4	4	4	4	4	4	4
1200 GMT	4	2	3B	3C	2	3C	3C	3B	3B	3B	4	4	4	3B	4	3C	2	2	2	3B	2	3B	2	2	3B	2	3B	1	3B	2	2
AUGUST																															
0000 GMT	4	4	4	4	4	4	4	4	4	4	4	4	4	4	4	4	M	4	4	4	4	4	4	4	4	4	4	4	4	4	4
1200 GMT	4	3C	M	2	3B	4	2	3B	3B	3B	3B	3C	3B	4	3B	4	M	4	3B	4	4	4	3B	3C	3B	2	2	2	3B	3B	4
SEPTEMBER																															
0000 GMT	4	4	4	4	4	4	4	4	4	4	4	4	4	4	4	4	4	4	4	4	4	4	4	4	4	4	3B	3C	3B	4	
1200 GMT	3B	3B	2	2	4	M	2	3B	2	4	4	4	3B	M	3B	M	1	1	3B	1	3B	2	3B	2	3B	M	3C	4	3B	4	

M - Missing Report

Table A.1d Observed Inversion Classes - Barter Island

Day	1	2	3	4	5	6	7	8	9	10	11	12	13	14	15	16	17	18	19	20	21	22	23	24	25	26	27	28	29	30	31
JULY																															
0000 GMT	1	3B	3B	2	1	3C	3B	3B	M	3B	3A	M	2	1	1	3A	2	2	2	2	1	M	1	1	2	2	2	2	3B	2	3C
1200 GMT	2	3B	2	1	2	3B	3B	3B	M	3B	2	1	1	1	2	2	1	1	3B	2	1	1	1	1	2	2	2	2	1	1	3B
AUGUST																															
0000 GMT	4	1	1	1	3B	3C	3B	3B	3B	2	2	2	3B	3A	1	2	3B	3A	3C	3B	3B	4	3C	M	2	1	M	1	1	2	2
1200 GMT	2	2	1	3B	3C	3B	3B	3B	3B	M	2	3A	3B	1	1	2	3B	3B	3C	3B	2	4	2	1	1	1	1	1	1	1	2
SEPTEMBER																															
0000 GMT	2	M	2	3B	4	4	3B	2	2	3B	3B	3B	3C	2	2	3B	4	4	2	2	2	M	3B	3B	3B	2	M	3B	3B	M	
1200 GMT	2	2	3B	3B	3C	3B	2	1	3B	4	3B	3A	2	2	2	3B	3B	3A	2	2	1	M	3B	3B	3A	2	3A	3B	3B	4	

M - Missing Report

Table A.1e Observed Inversion Classes - Point Barrow

Day	1	2	3	4	5	6	7	8	9	10	11	12	13	14	15	16	17	18	19	20	21	22	23	24	25	26	27	28	29	30	31
JULY																															
0000 GMT	4	M	M	M	M	4	4	3B	3B	3B	3A	2	2	2	2	2	2	M	3B	M	M	M	1	2	1	3B	3A	3A	2	3C	3C
1200 GMT	M	M	M	M	M	3B	3B	3B	3B	3B	3A	1	1	2	2	2	1	M	M	M	M	M	1	1	1	2	2	3B	3C	3B	3A
AUGUST																															
0000 GMT	4	3A	3B	3B	3B	3C	3B	3B	M	2	3B	3B	3B	3A	1	2	3B	4	3B	4	3B	3B	4	2	3A	2	1	1	2	2	2
1200 GMT	M	2	1	3B	3B	2	3B	3B	M	M	3B	3B	3B	2	1	M	3B	3B	3B	3B	3B	3B	3B	2	1	2	1	1	1	2	3B
SEPTEMBER																															
0000 GMT	3C	3A	3B	4	4	4	4	4	2	4	4	4	3A	3A	M	3B	4	3B	3A	M	2	3B	4	3A	3B	3B	M	3B	3A	4	
1200 GMT	2	3B	3B	4	2	4	3C	M	3B	4	3C	2	2	3B	M	3B	3C	3B	3A	2	M	4	3B	3B	3B	3B	3B	3A	3B	4	

M - Missing Report

APPENDIX B

QUANTITATIVE DISPLAY OF APT INFRARED SCANNING RADIOMETER DATA

1. Introduction

Conventional automatic picture transmission (APT) displays the scanning radiometer (SR) data by means of varying shades of gray. Since the eye has only a limited ability to discriminate between small differences in a scale of grays, it is often desirable to refer to the digitized numerical values corresponding to certain shades of gray. In the case of infrared (IR) data, the numerical values are representative of equivalent blackbody (EBB) temperatures. In this way, a quantitative measure of temperature and temperature gradients contained in the IR data can be obtained.

A computer program package for the quantitative display of IR or visible data from a scanning radiometer was developed at Colorado State University (Madden et al., 1972). Programs and data input were designed for a CDC 6400 computer. The SR data with a superimposed longitude-latitude grid can be output on a standard line printer. Each line or scan of SR data is analyzed for specified latitude and longitude crossings. The algorithm for computing the intersections of scan lines with lines of latitude and longitude of given increments is described by Madden and Parsons (1973). This algorithm was modified to include a more general solution given by Reinelt et al. (1975). The modified method was required for the gridding procedure applied to the APT scanning radiometer data received at the University of Alberta Satellite Laboratory.

Since the Colorado State University (CSU) program package was based on the algorithm by Madden and Parsons, it was necessary to adapt the program to the modified algorithm before it could be used on the University of Alberta data. A number of other adjustments were required also to make the program compatible with the Amdahl 470 computer at the University of Alberta.

2. Scan-by-Scan Gridding

The various latitude and longitude crossings are calculated in terms of scan angles which are then located in the data array. Since the same basic procedure is repeated for each scan line, the method is sometimes called scan-by-scan gridding.

The laws of spherical trigonometry provide the basis for the gridding technique. This requires that certain assumptions be made about satellite orientation and behaviour. It is assumed that (1) satellite yaw, roll and pitch are negligible; (2) the scan plane of the SR is perpendicular to the spacecraft heading line; and (3) the satellite orbit is very nearly circular. From these assumptions it follows that the scan line describes a great circle through the satellite subpoint.

The program called SRGRID was used from the CSU program package. This program contained the Madden and Parsons gridding algorithm (MPGA) which had to be modified. The fundamental weakness of the MPGA was that it failed to allow for the ambiguities that may arise with SR data taken at high latitudes. When a receiving station is located at a high enough latitude it is possible to access the satellite signal when the spacecraft is "seen" to be travelling both north and south in the same orbit, that is, when one of the poles is included in the area from which SR data are received. Part of the same problem was that the MPGA did not allow for the possibility of a scan line crossing the same latitude line twice, a quite common occurrence at high latitudes. These difficulties were overcome by employing the algorithm for scan-by-scan gridding described by Reinelt et al. (1975). In this algorithm the arcsine function is replaced by the arctangent to remove the ambiguities, and a simpler solution is used for calculating the arc length from the satellite subpoint to an arbitrary latitude. The revised form of the program SRGRID, called SRGRID-2, is able to construct a latitude-longitude grid in the SR data array of polar regions.

The main steps of the gridding procedure used in SRGRID-2 are reviewed below:

(a) Input:

It is assumed that certain information is available concerning the satellite's characteristics in orbit, and the operation of the SR. In particular, the following is required:

(i) average height H of the satellite, in km

(ii) orbital displacement L to west, in degrees

(iii) orbital period P, in minutes

(iv) orbit inclination i, in degrees

(v) equator crossing θ_s, (ascending node) in degrees
(Note: θ_s is measured 0° to 360° counter-clockwise from the prime meridian for the northern hemisphere.)

(vi) time of ascending node, in hours

(vii) SR revolutions per minute, SRPM

(viii) time of the first scan line, in hours

The SR data are made available in a digitized form. The exact nature and format of the data will be discussed later.

(b) Determination of the latitude ϕ_{sp} and longitude θ_{sp} of the satellite subpoint:

The computation of ϕ_{sp} is straightforward from Figure B.1

i_{sp} - azimuth of heading line

S - angular distance from equator travelled by satellite in time t

if $S = \frac{2\pi}{P} t = \frac{360}{P} t$

then
$$\phi_{sp} = \sin^{-1}(\cos i \sin s) \qquad (1)$$

and
$$\Delta\theta = \tan^{-1}\left(\frac{\sin i \sin s}{\cos s}\right) \qquad (2)$$

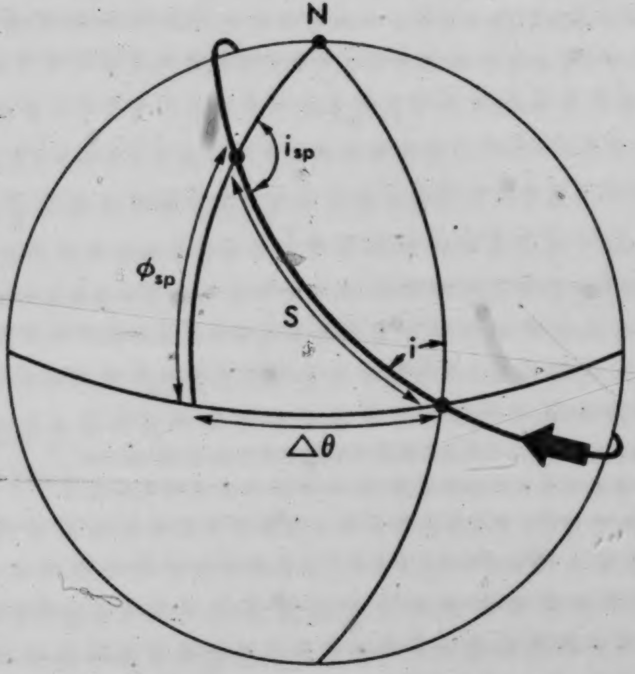

Figure B.1: Inclination of Satellite in Polar Orbit

If the earth rotates θ_E degrees in time t, then

$$\theta_{sp} = \theta_s - \Delta\theta - \theta_E \tag{3}$$

is the satellite's longitude.

(c) Determination of the scan angles for first (σ_1) and second (σ_2) horizons:

The scan angles are measured from the top of the scan, as indicated below in Figure B.2.

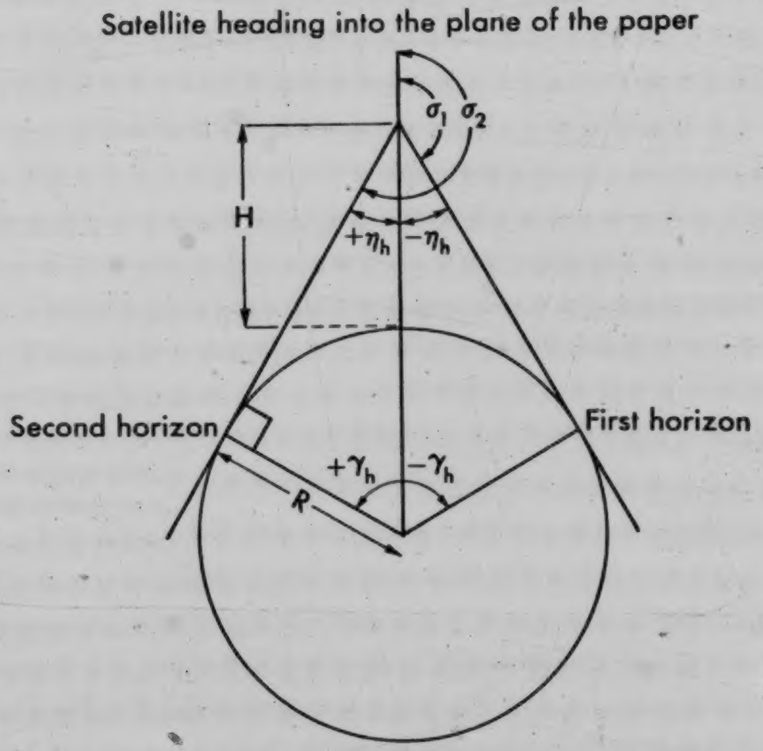
Satellite heading into the plane of the paper
σ1 σ2
H
+ηh −ηh
Second horizon
First horizon
+γh −γh
R

Figure B.2: Geometry of Satellite Horizon

The relationship between the great circle arc lengths to the first and second horizons (γ_h) and scan angles σ_1 and σ_2 is given in Figure B.2.

From Figure B.2

$$\gamma_h = \sin^{-1}\left(\frac{R}{R + H}\right) \qquad (4)$$

then

$$\sigma_1 = 180 - \eta_L$$

$$\sigma_2 = 180 + \eta_L$$

(d) Determination of the azimuth of the heading line (i_{sp}) at the satellite subpoint:

The angle i_{sp} is measured from the satellite's track (in the direction from which the satellite has travelled), counter-clockwise to the line of longitude which passes through the satellite subpoint.

Therefore from Figure B.1,

$$i_{sp} = \tan^{-1}\left(\frac{\sin i / \cos i}{- \cos s}\right) \qquad (5)$$

using spherical trigonometry.

(e) Determination of latitude/longitude of first (ϕ_{h_1} / θ_{h_1}) and second (ϕ_{h_2} / θ_{h_2}) horizons:

From Figure B.2

$$\gamma_h = \cos^{-1}\left(\frac{R}{R + H}\right) \qquad (6)$$

where γ_h is the great-circle arc length from the subpoint to the horizon.

It can then be shown, using spherical trigonometry (Madden and Parsons, 1973; Reinelt et al., 1975) that

$$\phi_{h_1} = \sin^{-1}(\sin \phi_{sp} \cos \gamma_h + \cos \phi_{sp} \sin \gamma_h \sin i_{sp}) \qquad (7)$$

$$\theta_{h_1} = \theta_{sp} - \tan^{-1}\left(\frac{\sin \gamma_h \cos i_{sp} \cos \phi_{sp}}{\cos \gamma_h - \sin \phi_{h_1} \sin \phi_{sp}}\right) \qquad (8)$$

$$\phi_{h_2} = \sin^{-1}(\sin \phi_{sp} \cos \gamma_h - \cos \phi_{sp} \sin \gamma_h \sin i_{sp}) \qquad (9)$$

$$\theta_{h_2} = \theta_{sp} - \tan^{-1}\left(\frac{- \sin \gamma_h \cos i_{sp} \cos \phi_{sp}}{\cos \gamma_h - \sin \phi_{h_2} \sin \phi_{sp}}\right) \qquad (10)$$

Now before proceeding to the next step in constructing the grid, the latitudes crossed by the scan line must be determined.

In the northern hemisphere we are concerned with the maximum latitude ϕ_m crossed by the scan line. The arc length from the satellite subpoint to ϕ_m is γ_m and if $\gamma_m < \gamma_h$, then the scan line will cross some latitudes twice.

From Reinelt et al. (1975) it can be shown that

$$\gamma_m = \tan^{-1}\left(\frac{\sin i}{\sin \phi_{sp}}\right) \qquad (11)$$

and

$$\phi_m = \sin^{-1}\left(\frac{\sin \phi_{sp}}{\cos \gamma_m}\right), \qquad (12)$$

where $\phi_{sp} \neq 0$.

Also, if

$$\phi_{sp} = 0, \quad \phi_m = i.$$

(f) Determination of great-circle arc lengths (γ) to given latitudes (ϕ_γ):

Once the maximum latitude is known, the next step is to identify the latitudes to be marked on the scan. The desired latitude ϕ_γ is chosen and the arc length γ from the satellite subpoint to ϕ_γ is calculated. Figure B.3 shows how the case where the scan line crosses a latitude twice is accounted for by this method.

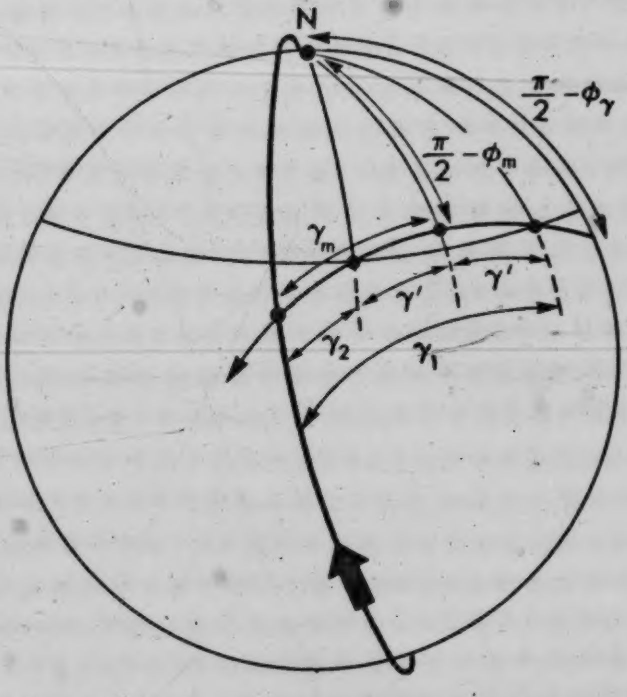
N
$\frac{\pi}{2} - \phi_\gamma$
$\frac{\pi}{2} - \phi_m$
γ_m
γ'
γ'
γ_2
γ_1

Figure B.3: Westward Shift of Equator Crossings

From Figure B.3,

$$\gamma' = \cos^{-1}\left(\frac{\sin\phi_\gamma}{\sin\phi_m}\right) \qquad (13)$$

Then in the northern hemisphere for that part of the scan from ϕ_{h_1} to ϕ_m, $\gamma_1 = -\gamma' - \gamma_m$

and from ϕ_m to ϕ_{h_2}

$$\gamma_2 = \gamma' - \gamma_m .$$

This procedure works even for $\gamma_m > \gamma_h$ since solutions where $\gamma > \gamma_h$ may be discarded, leaving only the correct latitude crossing.

(g) Determination of the great circle arc lengths (γ) to given longitudes (θ):

In Figure B.4 α is measured counterclockwise from the direction of the scan to a longitude.

From Figure B.4,

$$\cos\alpha = \sin i_{sp}\cos(\theta_{sp} - \theta) - \cos i_{sp}\sin(\theta_{sp} - \theta)\sin\phi_{sp} .$$

The value of sin α will be required, so we write

$$\sin\alpha = \sqrt{1 - \cos^2\alpha} . \qquad (14)$$

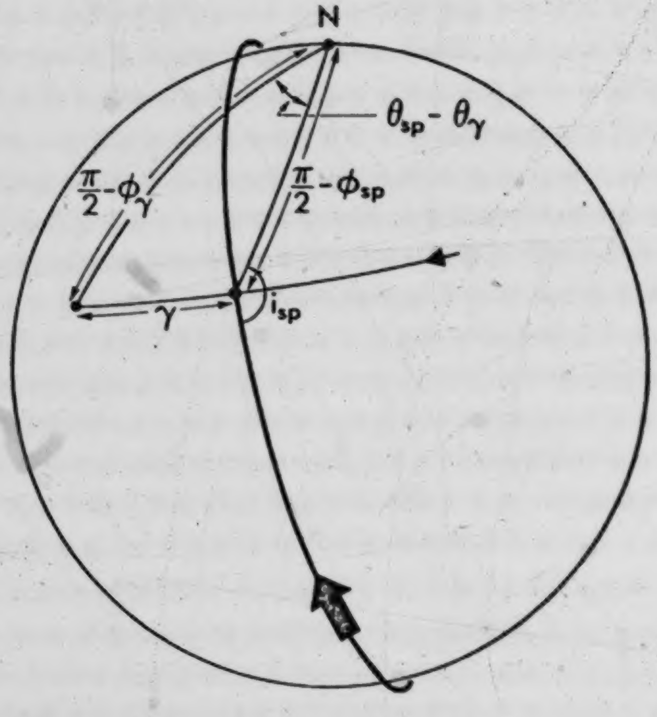
N
$\theta_{sp} - \theta_\gamma$
$\frac{\pi}{2} - \phi_\gamma$
$\frac{\pi}{2} - \phi_{sp}$
γ
i_{sp}

Figure B.4: Geometry of Trans-polar Orbit

However, this will not distinguish between $+\alpha$ and $-\alpha$. Since from Figure B.4

$$\sin \alpha = \frac{-\cos i_{sp} \cos \phi_{sp}}{\cos \phi_\gamma} , \qquad (15)$$

the sign of $\sin \alpha$ will depend on the sign of $- \cos i_{sp}$ only as $\cos \phi_{sp} > 0$ and $\cos \phi_\gamma \geq 0$. From Equation (5) it can be seen that the sign of $- \cos i_{sp}$ is the same as the sign of $\cos s$. Therefore, if

$$\mathrm{SIGN}(\chi) = +1 \quad \text{for} \quad \chi \geq 0$$

and

$$\mathrm{SIGN}(\chi) = -1 \quad \text{for} \quad \chi < 0$$

the corrected form of Equation (14) is

$$\sin\alpha = \mathrm{SIGN}(\cos s) \times \sqrt{1 - \cos^2\alpha} \qquad (16)$$

This value of sin α can then be substituted in another relation obtained from Figure B.4,

$$\gamma = \sin^{-1}\left(\frac{\sin(\theta_{sp} - \theta)\cos\phi_{sp}}{\sin\alpha}\right) . \qquad (17)$$

We now have calculated the great circle arc lengths from the satellite subpoint to specified lines of latitude and longitude which intersect with the scan. It remains to calculate where the scan should be altered to indicate these intersections. To do this, the scan must be looked at from the satellite's frame of reference.

(h) Determination of the scan angle (σ_γ) for a given great circle arc length (γ):

Using Figure B.2, the following relation may be obtained,

$$\eta_\gamma = \tan^{-1}\left[(R\sin\gamma) / (H + R(1 - \cos\gamma))\right] \qquad (18)$$

So when γ is negative, η_γ will also be negative and we can write for the scan angle,

$$\sigma_\gamma = 180 + \eta_\gamma .$$

The array containing the scan line data is altered at the point where the scan angle is equal to the calculated σ_γ.

3. Slicing the Data

The SR data at the University of Alberta are recorded on magnetic tape. The data are stored in an array in digitized form, ready to be accessed, scan by scan, by the gridding program. Each digitized value is stored as an unsigned (8-bit) byte. Each byte represents a range of values from 0 to 255. The digitizing frequency is 2400 Hz. The input analog signal level is adjusted at the start of the satellite pass to give maximum values of 245 to 250. Any negative values which occur are stored as zeroes (0) and values greater than 255 are stored as 255. The input analog circuit did not have automatic gain control, so digitized values will increase by about 10 percent during the pass.

The IR digitized values represent equivalent blackbody temperatures, the lowest values representing the highest temperatures. For display purposes it is convenient to replace a particular set of digital values by an appropriate symbol. The letters of the alphabet are convenient for this purpose. One method involves using all 26 letters to cover the entire range of digital values, starting with "A" for values 0 to 9, etc.

D

Another method involves assignment of letters to a certain temperature range represented by the IR data. This resembles a "slicing" of the data at specified digital increments. The assigned letters can then be used to delineate isotherms in the IR data display. For example, a digital value could be chosen to approximate a temperature of 0°C. Then the letters A, B, C, etc. would represent temperature ranges higher than 0°C; the size of the ranges would depend on the digital increment selected. Temperature ranges lower than 0°C could be denoted by starting at the opposite end of the alphabet and proceeding backwards, e.g., Z, Y, X, etc. Using this approach, a particular temperature regime can be displayed in great detail.

Since automatic gain control was not in effect at the time data for the present study, the IR data will not give exact equivalent blackbody temperatures. However, relative temperature differences and temperature gradients can be represented with confidence, and in a realistic manner.

4. Output

The gridding program SRGRID-2 is designed such that the output is suitable for a standard line printer. The output takes the form of an array of letters of the alphabet as the SR data are printed scan by scan. The array also contains symbols indicating the lines of latitude and longitude. A facility of the SLICE subroutine enables the user to replace alternate letters by blanks, producing a so-called "zebra" pattern. This pattern allows selected features to be emphasized for ease in interpretation and further study.

Table B.1

```
C     PROGRAM SPGRID-2
C
C ***** ***************************************************************
C ***** IT CAN BE USED WITH VIS OR IR DATA
C *****  D            =1   NORTH TO SOUTH
C *****  D            =2 SOUTH TO NORTH
C *****  KF           START POSITION TO OUTPUT FOR FIRST SEGMENT
C *****  KL           END   POSITION TO OUTPUT FOR FIRST SEGMENT
C *****  SSCAN        SCAN TO START PRINTING
C *****  ESCAN        SCAN TO END PRINTING
C *****  H            HEIGHT
C *****  NDY          DAY OF MESSAGE
C *****  NMO          MONTH OF MESSAGE
C *****  PL           ORBITAL DISPLACEMENT TO WEST
C *****  PMIN         ORBITAL PERIOD
C *****  PSEC         ORBITAL PERIOD (SEC)
C *****  ORBIT        ORBIT NUMBER
C *****  ORIN         ORBIT INCLINATION
C *****  RDY          REFERENCE DAY OF ASCENDING NODE
C *****  RHR          REFERENCE HOUR OF ASCENDING NODE
C *****  RL           REF LONGITUDE IN DEGREES
C *****  RMIN         REFERENCE MIN  OF ASCENDING NODE
C *****  RO           REFERENCE ORBIT NO.
C *****  RQ           QUADRANT OF ASCENDING NODE
C *****  RQ           =0   NORTH HEM. 0 TO 90 DEGREES WEST
C *****  RQ           =1   NORTH HEM. 90 TO 180 DEGREES WEST
C *****  RQ           =2   NORTH HEM. 90 TO 180 DEGREES EAST
C *****  RQ           =3   NORTH HEM. 0 TO 90 DEGREES EAST
C *****  RSEC         REFERENCE SEC  OF ASCENDING NODE
C *****  SAT          IDENTIFIER 04 = NOAA 4
C *****  SRPM         FIRST SCAN RPM
C *****  TMULP        A FACTOR TO MULTIPLY POSITIONS OF LAT AND LON BY
C *****               (CONVERTS SCAN ANGLE TO POSITION IN ARRAY)
C *****  TMULP        =8.3333333333 FOR IR DATA
C *****  TSRH         FIRST SCAN HOUR
C *****  TSRM         FIRST SCAN MIN
C *****  TSRS         FIRST SCAN SEC
C *****  MSTOP        =1 TO PRINT LAT AND LONG OF HORIZONS AND SUBPOINT
C *****  NSTOP        =1 FOR NO EXECUTION ONLY CHECK INPUT DATA
C *****               =2 TO PRINT POSITION OF SECOND HORIZON AND LAT
C *****               AND LONG LINES IN ARRAY
C *****  KEND         NUMBER OF SEGMENTS OF WIDTH 120 TO PRINT
C ***** ***************************************************************
      REAL*8 TMULP
      INTEGER RYR
      LOGICAL*1 STAR/1H*/,BLANK/1H /,SLASH/1H//,SLASH2/1H%/,ISC(64)
      LOGICAL*1 LA(906),A(1000)
      REAL*8 IR,VISIBL,IROV
      DATA IR/8H  IR    /,VISIBL/8H VISIBLE/
      DATA ISC/1H ,1H!,1H",1H#,1H$,1H%,1H&,1H',1H(,1H),1H*,1H+,1H,,1H-,
     11H.,1H/,1H0,1H1,1H2,1H3,1H4,1H5,1H6,1H7,1H8,1H9,1H:,1H;,1H.,1H=,
     21H>,1H?,1H@,1HA,1HB,1HC,1HD,1HE,1HF,1HG,1HH,1HI,1HJ,1HK,1HL,1HM,
     31HN,1HO,1HP,1HQ,1HR,1HS,1HT,1HU,1HV,1HW,1HX,1HY,1HZ,
     41H(,1H/,1H),1H|,1H_/
```

```
C      USEFUL CONSTANTS
      TMULP=8.3333333333
      READ(4,1122) RYR,NSTOP,MSTOP,KF2,KL2,KEND
 1122 FORMAT(I4,2I2,3I4)
      READ(4,1002) KF,KL,SSCAN,ESCAN
      WRITE(6,1002) KF,KL,SSCAN,ESCAN
 1002 FORMAT(2I5,F10.2,F10.2)
      PI=3.1416
C *****  RADIUS OF EARTH
      R=6368.
C *****  DEGREES TO RADIANS
      C1=0.0174533
C *****  RADIANS TO DEGREES
      C2=1.0/C1
      KTIME=0
      JTIME=0
C        READ INCREMENTS OF LAT(DELP) AND LONG(DEL) LINES
      READ(4,1330) DELP,DEL
 1330 FORMAT(2F2.0)
      RDELP=DELP*C1
C     READ IN ORBITAL INFORMATION
    1 CONTINUE
      READ(4,100) NMO,NDY,SAT,RO,RDY,RHR,RMIN,RSEC,RQ,RL,PMIN,PSEC,
     1PL,H
      WRITE(6,1002) NMO,NDY
  100 FORMAT(I2,I2,F2.0,F5.0,1X,2F2.0,1X,2F2.0,F1.0,F4.2,1X,F2.0,
     1F4.2,1X,F4.2,F4.0)
C      PUT TIME INTO DECIMAL FORM AND PUT REF ORBIT IN CORRECT LONG DEG
      DT = PMIN + 100. + PSEC/60.
      IF(PMIN.GT.50.)DT=DT-100.
      DT=DT/60.
      REFTIM=RHR+RMIN/60.+RSEC/3600.
      IF(RQ.EQ.2..AND.RL.LT.90.)RL=RL+100.
      IF(RQ.EQ.1..AND.RL.LT.90.)RL=360.-RL-100.
      IF(RQ.EQ.0..OR.RQ.EQ.5.)RL=360.-RL
      IF(RQ.EQ.7..AND.RL.LT.90.)RL=RL+100.
      IF(RQ.EQ.6..AND.RL.LT.90.)RL=360.-RL-100.
C      READ IN ORBIT HR,MN,SEC OF FIRST SCAN,RPM OF SR,ORBIT INCLINATION
      READ(4,101) ORBIT,TSRH,TSRM,TSRS,SRPM,ORIN
      WRITE(6,1011) ORBIT
  101 FORMAT(F5.0,3F2.0,F3.0,F5.0)
 1011 FORMAT('0',F5.0)
      DTSR=1.0/SRPM/60.
      TSR=TSRH+TSRM/60.+TSRS/3600.
      RI = C1*ORIN
    3 CONTINUE
C      ADJUST REFTIM FROM RO TO ORBIT
      IF(RO.EQ.ORBIT) GO TO 10
      RO=RO+1.
      REFTIM=REFTIM+DT
      IF(REFTIM.LT.24.)GO TO 21
      RDY=RDY+1.
      REFTIM=REFTIM-24.
   21 CONTINUE
      RL=RL-PL
      IF(RL.LT.0.)RL=360.+RL
      GO TO 3
   10 CONTINUE
      IF(REFTIM.GT.TSR) TSR=TSR+24.
      CALL DATEF(NMO,RYR,RDY)
      TR=TSR-REFTIM
      TR=TR-DTSR
      SCAN=0.
      RRL=RL*C1
C        CHECK INPUT DATA
      WRITE(6,521) REFTIM,TSR,TR,DTSR,DT
      WRITE(6,531) NMO,NDY,SAT,RO,RDY,RHR,RMIN,RSEC,RQ,RL,PMIN,PSEC,PL,
     1H,ORBIT,TSRH,TSRM,TSRS,SRPM,ORIN
521   FORMAT('1','REFTIM',F10.6,'TSR',F10.6,'TR',F10.6,'DTSR',F10.7,
     1'DT',F10.6)
531   FORMAT('-',10X,'NMO',I3,4X,'NDY',I3,4X,'SAT',F3.0,4X,
     1'RO',F6.0,2X,'RDY',F4.0,3X,'RHR',F4.0,//' ','RMIN',F3.0,3X,
     2'RSEC',F4.0,2X,'RQ',F3.0,5X,'RL',F6.2,2X,'PMIN',F4.0,2X,'PSEC',
     3F5.2,1X,'PL',F6.2,2X,//' ','H',F6.0,3X,'ORBIT',F5.0,' TSRH',
     4F4.0,1X,'TSRM',F4.0,2X,'TSRS',F4.0,2X,'SRPM',F4.0,2X,'ORIN',F7.1)
      IF(NSTOP.EQ.1)STOP
      JTMP=0
      KF3=KF2+120
      KL3=KL2+120
      KF4=KF3+120
      KL4=KL3+120
      KF5=KF4+120
      KL5=KL4+120
      KF6=KF5+120
      KL6=KL5+120
      KF7=KF6+120
      KL7=KL6+120
C       READ IN VALUES FOR SLICING OPERATION
      READ(4,80) KZERO,INC,KMAX,KMIN,IZEB
   80 FORMAT(5I4)
C
C*** START PROCESSING SAT DATA SCAN BY SCAN ***
C
    2 CONTINUE
      IF(DEL.LT.0) DEL=-DEL
      TR=TR+DTSR
      SCAN=SCAN+1.
C        READ IN DIGITIZED SR DATA
C     *******************************************************************
      IF(SCAN.GT.1..AND.SCAN.LE.SSCAN)GO TO 1004
      DO 1003 I=1,1000
      A(I) = BLANK
 1003 CONTINUE
 1004 CONTINUE
C ***** READ IN ONE SCAN OF DATA
      READ(3) (LA(I),I=1,906)
 1305 FORMAT(120A1)
      IF(SCAN.LT.SSCAN)GO TO 2
C        CHANGE DIGITAL VALUE INTO A SYMBOL ACCORDING TO SPECIFIED
C                      SLICING PROCEDURE
      CALL SLICE(ISC,A,LA,KZERO,INC,KMAX,KMIN,IZEB)
C      1. DETERMINE THE LATITUDE (PHI) AND LONGITUDE (THET) OF SUBPOINT
      DEGAM=TR/DT*360.
      RDEGAM=DEGAM*C1
      RPHI=ARSIN(SIN(RDEGAM)*COS(RI))
      X1=SIN(RI)*SIN(RDEGAM)
      X2=COS(RDEGAM)
      RDLONG=ATAN2(X1,X2)
C       ADJUST LONGITUDE (THET) TO ROTATING EARTH
      RTHET=RRL-RDLONG-15.*TR*C1
      IF(RTHET.LT.0.)RTHET=2.*PI+RTHET
      PHI=RPHI*C2
      THET=RTHET*C2
C      2. DETERMINE SCAN ANGLES FOR FIRST (SIGH) AND SECOND (SIGH2)
C         HORIZONS
      RETAH=ARSIN(R/(R+H))
      ETAH=RETAH*C2
      RGAMH=PI*.5-RETAH
      GAMH=90.-ETAH
      SIGH=180.-ETAH
      SIGH2=180.+ETAH
C      SIMULATE OUTER SPACE PAST SECOND HORIZON WITH STARS
      JJ2 = (SIGH2-1)*TMULP +1.5 -1046.
      JJJ2 = JJ2+20
      IF(NSTOP.NE.2)GO TO 1310
      WRITE(6,1301)JJ2,JJJ2
 1301 FORMAT('0','JJ2=',I4,'JJJ2=',I4)
 1310 DO 2001 I=JJ2,JJJ2
      A(I) = STAR
 2001 CONTINUE
C        ************************************************************
C      3. DETERMINE AZIMUTH OF HEADING LINE (RIS) AT SUBPOINT
      X1=SIN(RI)/COS(RI)
      X2=-COS(RDEGAM)
      RIS=ATAN2(X1,X2)
C      DETERMINE WHETHER SAT IS SOUTH(D=1) OR NORTH(D=2) BOUND
      D=1.
      RT=PI/2.
      IF(RIS.GT.RT)D=2.
C      4. DETERMINE LAT/LON OF FIRST (PHIH/THETH) AND SECOND (PHIH2/
C         THETH2) HORIZONS
      RIST=RIS
      RPHIH=ARSIN(SIN(RPHI)*COS(RGAMH)+COS(RPHI)*SIN(RGAMH)*SIN(RIST))
      X1=SIN(RGAMH)*COS(RIS)*COS(RPHI)
      X2=COS(RGAMH)-SIN(RPHIH)*SIN(RPHI)
      FUD=ATAN2(X1,X2)
      RTHETH=RTHET-FUD
      PHIH=RPHIH*C2
      THETH=RTHETH*C2
C      DETERMINE LAT/LON OF SECOND HORIZON
      RIST2=RIS
      RPHIH2=ARSIN(SIN(RPHI)*COS(RGAMH)-COS(RPHI)*SIN(RGAMH)*SIN(RIST2))
      X1=-X1
      X2=COS(RGAMH)-SIN(RPHIH2)*SIN(RPHI)
      FUD=ATAN2(X1,X2)
      RTHEH2=RTHET-FUD
      PHIH2=RPHIH2*C2
      THETH2=RTHEH2*C2
      IF(MSTOP.NE.1)GO TO 1340
      WRITE(6,1341)PHIH,THETH,PHIH2,THETH2,PHI,THET
 1341 FORMAT('0','FIRST HORIZON',4X,'LAT ',F6.2,3X,'LONG ',F6.2,/' ',
     1'SECOND HORIZON',3X,'LAT ',F6.2,3X,'LONG ',F6.2,/' ','SUBPOINT',
     29X,'LAT ',F6.2,3X,'LONG ',F6.2)
C        DETERMINE LATITUDE CROSSINGS
C        FIRST LAT TO BE PLOTTED NEAREST 'DELP' DEGREE TO HORIZON
 1340 KTWO=1
      J85=990
      K85=999
      RGAMM=ATAN(SIN(RI)/SIN(RPHI))
C        DETERMINE IF SCAN CROSSES SAME LATITUDE TWICE
```

```
      IF(RGAMM.LT.RGAMH)KTWO=2
      RPHIM=ARSIN(SIN(RPHI)/COS(RGAMM))
      PHIM=RPHIM*C2
      IF(KTWO.EQ.1)GO TO 62
      KTEMP=PHIM
      PHIG=KTEMP
   64 KTEMP=PHIG/DELP
      PTEMP=KTEMP*DELP
      IF(PTEMP.EQ.PHIG)GO TO 63
      PHIG=PHIG-1.
      GO TO 64
   62 KTEMP=PHIH
      PHIG=KTEMP
      GO TO 64
C      5. DETERMINE GREAT CIRCLE ARC LENGTHS (GAMG) TO GIVEN LATITUDES
   63 RPHIG=PHIG*C1
      RGAMP=ARCOS(SIN(RPHIG)/SIN(RPHIM))
      RGAMG1=-RGAMP-RGAMM
      RGAMG2=RGAMP-RGAMM
      IF(ABS(RGAMG1).GT.RGAMH)GO TO 65
      RGAMG=RGAMG1
      KCHK=1
      GO TO 66
   65 IF(ABS(RGAMG2).GT.RGAMH)GO TO 43
      RGAMG=RGAMG2
      KCHK=2
C      6. DETERMINE SCAN ANGLE (SIGG) FOR A GIVEN GREAT CIRCLE ARC
C          LENGTH
   66 RETAG=ATAN(R*SIN(RGAMG)/(H+R*(1.-COS(RGAMG))))
      ETAG=RETAG*C2
      SIGG=180.+ETAG
      IF(D.NE.1.)GO TO 41
      TEST=SIGG-SIGH
      IF(TEST.GT.1.)GO TO 42
C       LABEL LATITUDE
      KPHIG=PHIG
      J=SIGG*TMULP-1046.
      IF(J.LT.1)J=1
      NCHAR=2
      CALL SNUM(A,J,NCHAR,KPHIG)
      GO TO 1561
   41 CONTINUE
      TEST=SIGH2-SIGG
      IF(TEST.GT.1.)GO TO 42
C       LABEL LATITUDE
      KPHIG=PHIG
      J=SIGG*TMULP-1046.
      NCHAR=2
      CALL SNUM(A,J,NCHAP,KPHIG)
      GO TO 1561
   42 CONTINUE
      JSIG=SIGG*TMULP +.5 -1046.
      IF(NSTOP.NE.2)GO TO 1312
      WRITE(6,1303)JSIG,PHIG
 1303 FORMAT(' ','JSIG2=',I4,3X,'LAT',F5.1,' DEG.')
 1312 A(JSIG) = SLASH2
C       FIND IF SCAN CROSSES 85 DEG. LATITUDE CIRCLE
      IF(PHIG.NE.85.)GO TO 1561
      IF(J85.NE.990)GO TO 1571
      J85=JSIG
      GO TO 1561
 1571 K85=JSIG
 1561 IF(KCHK.EQ.2)GO TO 43
      GO TO 65
   43 CONTINUE
      PHIG = PHIG - DELP
       RPHIG=PHIG*C1
      IF(D.NE.1..AND.TEST.LE.0.) GO TO 49
      IF(RPHIG.GT.RPHIH2)GO TO 63
   49 CONTINUE
C   COME IN FROM HORIZON 'DEL' DEGREES AND DETERMINE LONGITUDE CROSSINGS
      JLMIN=MIN0(J85,K85)
      JLMAX=MAX0(J85,K85)
      IF(D.NE.1.)DEL=-DEL
      RDEL=DEL*C1
      TEMP=THETH+DEL
      KTEMP=TEMP
      THETG=KTEMP
   75 KTEMP=THETG/DEL
      TTEMP=KTEMP*DEL
      IF(TTEMP.EQ.THETG)GO TO 76
      T1=1.
      IF(THETH.GT.THET)T1=-T1
      THETG=THETG-T1
      GO TO 75
   76 RTHETG=THETG*C1
   30 CONTINUE
C       7. DETERMINE GREAT CIRCLE ARC LENGTHS (GAMG) TO GIVEN LONGITUDES
C          (THETG)
      RDTHET=RTHET-RTHETG
      CSALFA=SIN(RIS)*COS(RDTHET)-COS(RIS)*SIN(RDTHET)*SIN(RPHI)
      X=COS(RDEGAM)
      SNALFA=SIGN(1.,X)*SQRT(1.-CSALFA*CSALFA)
      RGAMG=ARSIN(SIN(RDTHET)*COS(RPHI)/SNALFA)
C       8. DETERMINE SCAN ANGLE (SIGG) FOR A GIVEN GREAT CIRCLE ARC
C          LENGTH
      RETAG=ATAN(R*SIN(RGAMG)/(H+R*(1.-COS(RGAMG))))
      ETAG=RETAG*C2
      SIGG=180.+ETAG
      JSIG=SIGG *TMULP +.5 -1046.
      IF(NSTOP.NE.2)GO TO 1311
      WRITE(6,1302)JSIG,THETG
 1302 FORMAT(' ','JSIG1=',I4,3X,'LONG',F6.1,' DEG.')
 1311 IF(KTIME.EQ.1)GO TO 35
C       FIRST LABEL LONGITUDES
      KTHG=THETG
      IF(KTHG.GT.360)KTHG=KTHG-360
      IF(JSIG-JTMP.LT.5)GO TO 37
      J=JSIG-2
      IF(J.LT.1)J=1
      IF(J.GT.903)J=903
      NCHAR=3
      CALL SNUM(A,J,NCHAR,KTHG)
      JTMP=JSIG
      GO TO 37
   35 CONTINUE
C        ALTER DATA ARRAY AT SCAN ANGLE SIGG
      IF(JSIG.LT.1)JSIG=1
      IF(JSIG.LE.JLMIN.OR.JSIG.GE.JLMAX)GO TO 1580
      KTMP=THETG/90.
      THG=KTMP*90
      IF(THG.NE.THETG)GO TO 37
 1580 A(JSIG) = SLASH
   37 CONTINUE
      THETG=THETG+DEL
      RTHETG=THETG*C1
      IF(D.NE.1..AND.RTHETG.GT.RTHEH2)GO TO 30
      IF(D.EQ.1..AND.RTHETG.LT.RTHEH2)GO TO 30
C
C ***    OUTPUT GRIDDED SR DATA
C
      IF(KTIME.EQ.1)GO TO 45
      IROV =  IR
C     IF(IRORVIS.EQ.2) IROV = VISIBL
      MDY=RDY
      DEL=ABS(DEL)
      WRITE(6,103)IROV,ORBIT,TSRH,TSRM,TSRS,NMO,MDY,RYR,DEL,DELP
  103 FORMAT(1H1,A8,' DATA FROM ORBIT',F7.0,'.   TIME OF FIRST SCAN IS
     1',3(1X,F3.0),'   DATA   ',I2,'/',I2,'/',I4,
     1           //,' LONGITUDE AND LATITUDE LINES DRAWN IN AT ',F3.0,
     2' AND ',F3.0,' DEGREES RESPECTIVELY                    XXXXXXXXXXX
     3X',16X,'SCAN')
      KTIME=1
   45 CONTINUE
      IF(JTIME.EQ.1)GO TO 1590
      JTIME=1
C      USE KF,KL,KF2,KL2, TO SPECIFY WHICH PART OF SCAN IS TO BE PRINTED
C                         AT 120 DATA POINTS PER SEGMENT
      KSEG=KF/120+1
      WRITE(7,105)ORBIT,KZERO,INC,KMAX,KMIN,IZEB,KSEG
      KSEG=KSEG+1
  105 FORMAT('1',5X,'ORBIT ',F5.0,3X,'KZERO',I4,3X,'INC',I3,3X,'KMAX',I3
     1,3X,'KMIN',I4,3X,'IZEB',I2,10X,'SEGMENT NUMBER',I2)
      IF(KEND.EQ.1)GO TO 1590
      WRITE(8,105)ORBIT,KZERO,INC,KMAX,KMIN,IZEB,KSEG
      KSEG=KSEG+1
      IF(KEND.EQ.2)GO TO 1590
      WRITE(9,105)ORBIT,KZERO,INC,KMAX,KMIN,IZEB,KSEG
      KSEG=KSEG+1
      IF(KEND.EQ.3)GO TO 1590
      WRITE(10,105)ORBIT,KZERO,INC,KMAX,KMIN,IZEB,KSEG
      KSEG=KSEG+1
      IF(KEND.EQ.4)GO TO 1590
      WRITE(11,105)ORBIT,KZERO,INC,KMAX,KMIN,IZEB,KSEG
      KSEG=KSEG+1
      IF(KEND.EQ.5)GO TO 1590
      WRITE(12,105)ORBIT,KZERO,INC,KMAX,KMIN,IZEB,KSEG
      KSEG=KSEG+1
      IF(KEND.EQ.6)GO TO 1590
      WRITE(13,105)ORBIT,KZERO,INC,KMAX,KMIN,IZEB,KSEG
      KSEG=KSEG+1
      IF(KEND.EQ.7)GO TO 1590
      WRITE(14,105)ORBIT,KZERO,INC,KMAX,KMIN,IZEB,KSEG
 1590 WRITE(7,102)(A(I),I=KF,KL),SCAN
  102 FORMAT('9',120A1,F4.0)
      IF(KEND.EQ.1)GO TO 1555
      WRITE(8,102)(A(I),I=KF2,KL2),SCAN
      IF(KEND.EQ.2)GO TO 1555
      WRITE(9,102)(A(I),I=KF3,KL3),SCAN
      IF(KEND.EQ.3)GO TO 1555
      WRITE(10,102) (A(I),I=KF4,KL4),SCAN
      IF(KEND.EQ.4)GO TO 1555
      WRITE(11,102) (A(I),I=KF5,KL5),SCAN
      IF(KEND.EQ.5)GO TO 1555
      WRITE(12,102) (A(I),I=KF6,KL6),SCAN
      IF(KEND.EQ.6)GO TO 1555
      WRITE(13,102) (A(I),I=KF7,KL7),SCAN
      IF(KEND.EQ.7)GO TO 1555
      WRITE(14,102) (A(I),I=841,960),SCAN
 1555 IF(SCAN.LE.ESCAN) GO TO 2
      STOP
      END
```

```
      SUBROUTINE DATEF(NMO,RYR,RDY)
      DIMENSION MONTH(12)
      INTEGER RYR
      DATA MONTH/31,28,31,30,31,30,31,31,30,31,30,31/
      IY = RYR/4. + .0001
      IY = RYR-IY*4
      MONTH(2) = 28
      IF(IY.EQ.0) MONTH(2) = 29
    5 CONTINUE
      DO 10 I=NMO,12
      RDY = RDY - MONTH(I)
      IF(RDY.LE.C.) GO TO 20
      NMO = NMO +1
   10 CONTINUE
      NMO = 1
      GO TO 5
   20 CONTINUE
      RDY = RDY + MONTH(I)
      RETURN
      END
```

```
      SUBROUTINE SLICE(ISC,AD,LA,KZERO,INC,KMAX,KMIN,IZEB)
C ***********************************************************************
C *****  KZERO    MIDPOINT DIGITAL VALUE, KZERO=0 BYPASSES SLICING
C *****  INC      DIGITAL INCREMENT BETWEEN SLICES
C *****  KMAX     MAX NUMBER OF SLICES ABOVE KZERO
C *****  KMIN     MAX NUMBER OF SLICES BELOW KZERO (NEGATIVE NUMBER)
C *****  IZEB     =0 FOR NO BLANKS
C *****           =1 EVERY SECOND LETTER BLANKED
C *****           =2 EVERY THIRD LETTER BLANKED
C ***********************************************************************
C
C      FOR IR DATA: WHEN KZERO IS GIVEN A NON-ZERO VALUE,
C      DIGITAL VALUES LESS THAN KZERO(WARMER TEMPERATURES)
C      ARE INDICATED BY LETTERS BEGINNING WITH A,B,C,D,....
C      AND SO ON.  HIGHER DIGITAL VALUES THAN KZERO(COLDER
C      TEMPERATURES) START WITH THE LETTERS IN REVERSE ORDER,
C      Z,Y,X,W,.... AND SO ON.
C
```

```
      LOGICAL*1 LA(906),ISC(64),AD(1000)
      INTEGER*2 ID(906)
C
C        IF SLICING IS BYPASSED ALL 26 LETTERS ARE USED TO
C        REPRESENT RANGES OF TEN DIGITAL VALUES (EXCEPT FOR LAST
C        RANGE ABOVE 250).  LETTER 'A' INDICATES LOWEST VALUES.
C
      IF(KZERO.EQ.0)GO TO 705
      DO 25 J=3,906
      ID(J)=IBYTE(LA(J))
      ID(J)=ID(J)-KZERO
      IF(ID(J).GT.0)ID(J)=ID(J)+INC
      K=ID(J)/INC
      IF(K.LE.0)GO TO 620
      IF(K.LE.KMAX)GO TO 630
      K=14
      GO TO 660
  630 K=60-K
      GO TO 640
  620 IF(K.GE.KMIN)GO TO 650
      K=12
      GO TO 660
  650 K=34-K
  640 IF(K.LT.34)K=K+26
      IF(K.GT.59)K=K-26
C        ESTABLISH BLANKING PROCEDURE
      IF(IZEB.EQ.0)GO TO 660
      IF(IZEB.EQ.1)GO TO 670
      KTEMP=K/3.
      KTEMP=KTEMP*3
      IF(KTEMP.EQ.K)K=1
      GO TO 660
  670 KTEMP=K/2.
      KTEMP=KTEMP*2
      IF(KTEMP.NE.K)K=1
  660 AD(J)=ISC(K)
   25 CONTINUE
      RETURN
  705 DO 22 J=1,906
      ID(J)=IBYTE(LA(J))
  700 K=ID(J)/10.+.5
      K=K+34
      AD(J)=ISC(K)
   22 CONTINUE
      RETURN
      END
      FUNCTION IBYTE(NUM)
C
C        CONVERTS ONE BYTE NUMBER INTO TWO BYTES
C
      LOGICAL*1 NUM,INT(2)
      INTEGER*2 I/0/
      EQUIVALENCE (I,INT)
      INT(2)=NUM
      IBYTE=I
      RETURN
      END
      SUBROUTINE SNUM(LDATA,ICOL,NCHAR,INT)
C *********************************************************************
C     LABELS LINES OF LAT AND LONG BY DEGREES
C             LDATA   SCAN LINE WHERE LABEL IS WRITTEN
C             ICOL    COLUMN WHERE LABEL BEGINS IN SCAN
C             NCHAR   NUMBER OF NON-BLANK CHARACTERS IN LABEL
C             INT     LAT OR LONG DEGREE
C     LABEL IS PADDED WITH A BLANK ON EITHER SIDE
C *********************************************************************
C
      LOGICAL*1 LDATA(1000)
      IF(ICOL.LT.1.OR.ICOL.GT.906-NCHAR) RETURN
      IF(NCHAR.LE.0) RETURN
      IF(INT.LT.0) RETURN
      ICOLE=ICOL+NCHAR+1
      DO 10 I=ICOL,ICOLE
      CALL SBYTE(LDATA,I,64)
10    CONTINUE
      I=INT
      DO 20 ILOOP=1,NCHAR
      IR=240+MOD(I,10)
      I=I/10
      CALL SBYTE(LDATA,ICOL+NCHAR-ILOOP+1,IR)
      IF(I.EQ.0)GO TO 30
20    CONTINUE
30    RETURN
      END
```

```
      SUBROUTINE SBYTE(LDATA,I,KNUM)
C*********  LDATA(I)=KNUM
      LOGICAL*1 LDATA(1000),LNUM(4)
      EQUIVALENCE (LNUM,INUM)
      INUM=KNUM
      LDATA(I)=LNUM(4)
      RETURN
      END
```

SAMPLE DATA FOR SRGRID-2

Parameter	Value	Parameter	Value
RYR	1977	NSTOP	0
MSTOP	0	KF2	121
KL2	240	KEND	8
KF	1	KL	120
SSCAN	1	ESCAN	300
DELP	5	DEL	5
NMO	6	NDY	17
SAT	5	RO	3999
RDY	17	RHR	18
RMIN	5	RSEC	12
RQ	3	RL	38.58
PMIN	16	PSEC	20.19
PL	29.08	H	1525
ORBIT	3999	TSRH	18
TSRM	35	TSRS	57
SRPM	48	ORIN	12.1
KZERO	151	INC	2
KMAX	7	KMIN	-19
IZEB	2		

APPENDIX C

Table C.1

WIND ABSTRACTS

DATE: July 17, 1976

Hour (GMT)		Station			
		YSY	ZUE	YUC	YUH
17 July	06	030/12G17	050/10	060/19	calm
	07	040/16	060/11		calm
	08		060/13		calm
	09	050/11	060/13	050/17	080/01
	10	050/10	060/14		330/02
	11	060/12	060/13		350/02
	12	060/12	070/14	050/15	calm
	13		070/10		calm
	14	060/08	080/10		calm
	15	050/07	070/11	080/12	calm
	16	070/09	070/10		calm
	17	070/08	070/12		calm
	18	080/09	070/12	070/14	calm
	19	190/06	070/12		110/03
	20	210/08	070/13		
	21	230/08	060/13		100/03
	22	230/07	060/12	110/03	
	23	250/09	060/10		120/03
18 July	00	220/06	060/14	080/21	090/03
	01	210/06	060/13		130/11
	02	130/01	060/13		130/04
	03	180/02	070/13	090/17	130/03
	04		080/13		
	05	140/06	070/14		calm

WIND ABSTRACTS

DATE: July 18, 1976

		Station			
Hour (GMT)		YSY	ZUE	YUC	YUH
18 July	06	170/08	070/14	090/19	calm
	07	160/09	070/15		calm
	08	170/06	080/15		calm
	09	calm	080/15	080/16	
	10	calm	090/16		090/04
	11	060/05	090/15		090/02
	12	040/05	090/15	080/12	calm
	13	040/06	090/12		calm
	14	120/06	090/10		
	15	150/08	100/11	090/08	calm
	16	160/06	100/09		calm
	17	180/06	100/12		
	18	170/03	100/09	080/06	calm
	19		100/13		calm
	20	210/08	100/14		calm
	21	190/07	100/13	060/06	090/02
	22	210/09	110/13		100/03
	23	200/08	090/13		120/06
19 July	00	180/10	100/13	080/07	130/05
	01	170/08	090/14		140/03
	02	180/08	090/14		150/06
	03	160/06	100/12G19	100/09	140/07
	04	190/07	100/14		140/03
	05	200/04	100/15		150/06

WIND ABSTRACTS

DATE: July 22, 1976

Hour (GMT)	Station			
	YSY	ZUE	YUC	YUH
22 July 06	130/10	060/03	060/09	170/05
07	130/11	070/06		calm
08	120/13	070/04		calm
09	120/14	040/02	180/08	160/05
10	120/14	050/03		calm
11	130/11	030/02		150/06
12	150/10	080/03	140/04	calm
13	160/08	calm		180/02
14	160/11	170/03		130/10
15	170/14	130/02	140/04	120/06
16	190/05	030/04		130/06
17	190/07	060/04		120/08
18	190/07	060/03	130/06	140/03
19	160/10	030/02		
20	190/10	070/02		080/04
21	170/11	070/08	010/04	150/06
22	170/12	030/06		140/06
23	170/10	040/04		120/04
23 July 00		060/05	030/07	150/05
01		060/06		150/05
02	170/12	360/06		120/02
03	170/11	030/05	040/10	calm
04	170/10	010/06		120/02
05	160/08	010/06		calm

WIND ABSTRACTS

DATE: August 3, 1976

Hour (GMT)		Station YSY	ZUE	YUC	YUH
3 August	06	010/14	010/06	080/22	310/10
	07	360/09	010/07		330/03
	08	040/07	350/04		290/03
	09	020/07	360/04	110/18	290/05
	10	010/06	010/04		280/04
	11	360/04	calm		calm
	12	040/06			
	13		calm		320/03
	14	040/07	calm		030/02
	15	020/07	calm	090/20	030/03
	16	040/06	calm		010/05
	17	160/07	calm		020/05
	18	180/07	120/03	110/12	030/04
	19	180/09	100/05		calm
	20	190/10	120/		090/03
	21	190/09	120/07		100/03
	22	150/16	130/07		120/06
	23		110/12		120/06
4 August	00	170/14	110/11	140/07	340/06
	01	160/14	110/13		110/09
	02	160/14	110/14		120/10
	03	160/17	110/12		
	04		110/09		110/10
	05	160/18	110/13		140/10

WIND ABSTRACTS

DATE: August 9, 1976

		Station			
Hour (GMT)		YSY	ZUE	YUC	YUH
9 August	06	350/06	050/05	070/13	230/04
	07	330/05	060/04		250/04
	08	340/06	060/03		calm
	09	340/05	050/03	090/14	calm
	10	010/04	050/04		calm
	11	020/04	020/03		calm
	12	020/06	030/04	090/18	calm
	13	050/06	040/03		210/03
	14	070/06			210/03
	15	060/05	090/03	090/18	140/02
	16	080/09	090/06		110/04
	17	050/11	100/08		090/03
	18	110/05	110/09	070/16	090/03
	19	030/08	100/08		090/04
	20	070/08	090/12		090/03
	21	210/07	080/15	070/18	100/04
	22	170/11	100/15		110/05
	23	160/10	100/13G18		120/05
10 August	00	160/11	100/20	090/16	100/05
	01	170/11	090/22		110/05
	02	160/12	090/17		
	03	170/09	100/17		
	04	170/05	100/16		090/04
	05	150/05	090/12		080/03

WIND ABSTRACTS

DATE: August 17, 1976

Hour (GMT)		Station			
		YSY	ZUE	YUC	YUH
17 August	06	120/06	120/04	300/13	290/01
	07				310/06
	08	080/08	090/03		320/05
	09	170/06		250/12	310/10
	10	100/09	080/07		320/08
	11	130/08	110/06		310/06
	12	120/09	090/05	270/14	300/07
	13	130/10	080/08		calm
	14	120/06	100/07		030/02
	15	150/07	130/03	270/14	300/03
	16	170/07	110/04		350/04
	17	210/07	140/02		110/03
	18	170/05	120/04	240/13	120/01
	19		080/04		calm
	20	190/06	100/04		090/02
	21	210/09	100/07	210/10	040/03
	22	210/09	100/05		040/02
	23	200/06	110/05		calm
18 August	00	170/07	110/05	270/09	calm
	01	180/10	110/06		100/02
	02		100/05		calm
	03	140/08	100/06	270/08	calm
	04	150/07	070/05		160/02
	05	150/07	100/03		calm

WIND ABSTRACTS

DATE: August 25, 1976

Hour (GMT)		Station			
		YSY	ZUE	YUC	YUH
25 August	06		070/02	090/14	300/04
	07	050/09	calm		270/03
	08	060/07	130/03		260/03
	09	070/05	100/02		
	10		calm		calm
	11	110/04	130/03		
	12	090/08		120/12	calm
	13	090/06			calm
	14	090/07			
	15	070/05	090/06	120/12	130/05
	16	100/09	100/10		120/08
	17	130/08	110/08		110/07
	18	130/09	110/08	120/12	130/10
	19		100/09		100/06
	20	170/12	100/11		
	21	170/10	100/13	070/10	120/10
	22	170/10	090/15		100/10
	23	180/09	090/15		110/10
26 August	00	180/09	100/16	090/10	110/10
	01	160/08	100/19		110/10
	02	140/09	100/20		110/11
	03	160/08	090/21		
	04	160/08	090/19G24		100/10
	05	160/11	100/18G23		100/10